Pavol Jozef Šafárik University in Košice
Faculty of Science

BOOK OF ABSTRACTS

The 6th International Conference on Nanomaterials: Fundamentals and Applications

October 16-19, 2022
Organized by:

Department of Physical Chemistry
Faculty of Science
Pavol Jozef Šafárik University in Košice
&
Slovak Chemical Society
Bratislava

Košice 2022

The 6th International Conference on Nanomaterials: Fundamentals and Applications
Book of Abstracts

Edited by:
RNDr. Jana Shepa, PhD., *Pavol Jozef Šafárik University in Košice, Institute of Chemistry, Moyzesova 11, 040 01 Košice, Slovakia, jana.shepa@upjs.sk*

Reviewed by:
Ing. Erika Múdra, PhD., *Intitute of Materials Research, Slovak Academy of Sciences, Watsonova 47, 040 01 Košice, Slovakia, emudra@saske.sk*
Mgr. Ivan Shepa, PhD. *Intitute of Materials Research, Slovak Academy of Sciences, Watsonova 47, 040 01 Košice, Slovakia, ishepa@saske.sk*

Available at: https://unibook.upjs.sk
Publication date: 12.10.2022

ISBN 978-80-574-0127-8 (e-publication)

LIST OF CONTENTS

LIST OF AUTHORS

Preface

On behalf of the NFA 2022 Organizing Committees, we introduce with pleasure these proceedings devoted to contributions from the 6th NFA Nanomaterials: Fundamentals and Applications conference held in Štrbské pleso, High Tatras, Slovakia. The conference is organized by the Faculty of Science Pavol Jozef Šafárik Uninversity in Košice and Slovak Chemical Society. The conference program provides an opportunity for researchers interested in various applications of nanomaterials to discuss their latest results and exchange ideas on the new trends. The main objective of the conference umbrella is to encourage discussion on a broad range of related topics and to stimulate new collaborations among the participants.

The proceedings contain all papers of both: oral and poster presentations. We hope that these proceedings will give readers an excellent overview of important and diversity topics discussed at the conference. We thank all authors for submitting their latest work, thus contributing to the excellent technical contents of the Conference. Especially, we would like to thank the organizators that worked diligently to make this conference a success, and to the recenzents for the thorough and careful review of the papers.

We wish all attendees of NFA 2022 an enjoyable scientific gathering in High Tatras, Slovakia. I wish all participants enjoy this scientific meeting to collect new information form nanoscience.

Ivana Šišoláková

This is not just a potentiostat

µStat-i Multi16

Introducing µStat-i MultiX by Metrohm DropSens

Enhanced possibilities for electrochemical research based on an efficient, versatile and reliable user experience are at hand with the newly launched µStat-i MultiX. This multi-channel bipotentiostat, galvanostat and impedance analyzer (with MultiplEIS® technology for performing dual-channel Electrochemical Impedance Spectroscopy) is suitable for multi-user and multi-disciplinary work.

Choose the number of channels that you need (with optional floating mode), benefit from having several users working with the same instrument at the same time, work remotely and support your research with an easy to use software.

Electrochemistry has proven its high potential to solve real-life analytical problems. µStat-i MultiX simplifies analytical research and transforms daily work.

Discover more about µStat-i MultiX by visiting: www.metrohm.com

PEOPLE
YOU
CAN
TRUST

FIND OUT MORE

Metrohm

Invited Lectures

Material Aspects of the Energy Conversion Devices Based on Hydrogen as an Energy Vector

K. Bouzek[a]*, M. Paidar[a]

[a]Department of Inorganic Technology, University of Chemistry and Technology, Prague
*bouzekk@vscht.cz

Fuel cells and water electrolysis as a core of the hydrogen technologies experience recently very rapid increase of interest. Despite the fact, however, the fuel cell technology itself is known since 1842, i.e. for 180 years, it did not yet reach full commercial implementation. It has several reasons, the main two of them being (i) high energy content and easy availability of the carbon based fossil fuels and (ii) production costs and lifetime of the currently available fuel cells and water electrolysers. Although it is quite clear, that fossil fuels availability and properties represent a primary reason for the very slow penetration of the hydrogen technologies on the market, focus of the present contribution is on the second aspect, i.e. production costs and time stability.

The first version of the fuel cell invented by William Grove (or Christian Friedrich Schönbein) was working with the massive platinum electrodes in acidic environment. Although the principle was known, energy density of the process was far too low for a practical application. This was mainly due to the low active surface of the electrodes and to significant ohmic losses on the electrolyte. Therefore, no significant progress was happening over the next 90 years, until in 1932 Francis Thomas Bacon developed alkaline fuel cell. Why as long time and why alkaline? Why environment on the opposite side of the pH scale? The main reason were the materials available. To facilitate efficiently electrode reaction of the gaseous reactant (hydrogen and oxygen) at the solid electrode surface, gas diffusion electrode (GDE) had to be developed. GDE is characterised by high specific area of the electrochemically active surface achieved by its porous structure. At the same time, it needs to be partly flooded by the electrolyte in order to form so-called three phases interface (gaseous reactant, electron conductive electrode and ionically conductive electrolyte). Fine tuning of the electrode properties allowing high occurrence of the three phases interface and at the same time high stability of the system requires availability of the corresponding materials. Corrosiveness of the acidic environment has turned to be a decisive point. Less corrosive alkaline environment has offered easier way to the final result. This was an important step, which has provided proof of feasibility of the fuel cell technology as such, with final verification within the framework of the Apollo program of the USA.

With an alkaline fuel cell technology successful validation, the attention has turned back to the acidic environment. Due to the high proton mobility in an acidic environment, and due to the rapid kinetics of a hydrogen oxidation in an acidic environment, this approach is much more promising regarding higher process intensity and flexibility. The main issue remains materials stability under acidic fuel cells operational conditions. Obvious solution was utilising proton selective polymer electrolyte, instead of a liquid acid solution. Unfortunately, materials existing at this time have turned to be unstable under harsh conditions of an operating fuel cell. This concerns especially cathode with its high redox potential, presence of oxygen, peroxides and under certain conditions even hydroxyl radicals. Situation has changed with discovery of a perfluorinated sulphonated acids in a form of polymeric membranes discovered in 1960. This material possess unique properties given by its molecular structure determining, beside others, internal structure of the membrane and its resistance to the fuel cell conditions. It, thus, offers new options in the fuel cells design. Presence of circulating liquid electrolyte is eliminated making the fuel cell construction and operation significantly easier. Much attention has therefore focused in this direction with promise of rapid solution of the existing problems and penetration to the market. Alkaline technology was to a certain extend abandoned. Main issue, however, still represents the material side of the cell construction.

In parallel to this development, second line focusing on the development of processes compatible with possible direct combustion of natural gas instead of hydrogen was opened. Combustion of carbon containing species required high operational temperature avoiding poisoning of the catalyst. High temperature at the same time allowed to speed-up

electrode reaction kinetics to the level, that platinum group metals were no more needed to catalyse the electrode reactions. Two types of the cells were developed allowing work at corresponding temperatures. Molten carbonate fuel cell and solid oxide fuel cell. Due to the operational temperature between 500 and 1 000 °C, construction materials differ significantly from the low temperature alternative moving much more to ceramics and composites of metals and ceramics. Here the material issues are even more severe than at the low temperature. With elevated temperatures reactivity of the individual system components increases endangering their stability. At the same time, system becomes susceptible to the thermal shocks leading to mechanical damage of the cell. It limits significantly not only flexibility of the cell, but also size of the cells produced.

Historically, the focus in the field of hydrogen technologies was only on the fuel cells as electric power sources. This was primarily motivated by an increased efficiency of the energy production and by a general reduction of the exhalations, especially in the large agglomerations. With an increasing share of the renewable power sources in the electricity distribution grid a new challenge appeared. Water electrolysis as a stabilising element was an obvious solution. At the same time, produced hydrogen can be further used in energy production, or in another economy sector. Acidic process seemed to be the ideal candidate for this purpose due to its high flexibility and energy density. Initial idea was, that development of the modern water electrolysis process will be easy, based predominantly on the fuel cells know-how. Unfortunately, similarly to previous cases, this assumption turned unrealistic. Once more, due to the materials reason. In this case, it concerns primarily oxygen side of the cell. Due to the sluggish kinetics of the oxygen evolution reaction, anode potential is highly oxidative causing instability of the materials used for its construction. Changing construction materials brings about number of new, unexpected issues. This finding boosted unexpectedly research in the field of alkaline processes. Here, in contrast to the acidic environment, main obstacle represents absence of generally accepted alkaline polymer electrolyte, which would help to increase flexibility and efficiency of the current alkaline electrolyser utilising porous separator and concentrated KOH as an electrolyte. In the case of the high temperature processes, situation does not differ significantly. Water electrolysis process is studied for the solid oxide cell and predominantly materials developed for the fuel cells technology are used to the date also in the electrolysis application.

This very short and general description does not aim to clarify the problem of materials in the fuel and water electrolysis cells design and construction. It is just trying to point out the fact, that all advancements in these technologies are primarily connected with development of new materials satisfying demanding conditions of operating cells. Also currently available technologies still suffer from important issues connected to the properties of materials used. To avoid these troubles, new approaches are intensively searched in order to improve technology and its competitiveness on the market. Presentation will try to provide cleared and more specific examples.

Acknowledgement
The work was supported from European Regional Development Fund-Project "Fuel Cells with Low Platinum Content" (No. CZ.02.1.01/0.0/0.0/16_025/0007414).

Two-Dimensional Nanomaterials and Hybrids for Advanced Applications

M. Omastová[a]*

[a]Polymer Institute SAS, Dúbravská cesta 9, 845 41 Bratislava, Slovakia
*maria.omastova@savba.sk

Introduction

The current intense interest about two-dimensional (2D) materials is due to their unique properties resulting from their structure. They offer highly specific surface area as well as electronic structures that can achieve new interesting properties. Graphene was the first 2D material isolated in 2004 and extensively studied [1]. Graphene oxide (GO) and reduced graphene oxide (rGO) are nowadays studied for many application [2]. GO has a hexagonal carbon structure similar to graphene and contains oxygenated groups (hydroxy, alkoxy, carbonyl, etc.) which confer GO a hydrophilicity and possibility for surface functionalization [3], and therefore increasing possibility of its application in many areas, including biomedical field. The fast-growing family of 2D nanomaterials are MXenes. MXenes are a new class of 2D inorganic materials, first described in 2011 by researchers from Drexel University [4]. Different MXenes are prepared from different MAX phases of the formula $M_{n+1}AXn$, where M is the most common transition metal, A is an element of the 13 or 14 group of the periodic table of elements, and X is usually C and/or N. By etching of the A layers from MAX phase, MXene are formed with the formula $M_{n+1}X_nT_x$ where T is a functional group e.g., -O, -F, or -OH. Metal organic frameworks (MOFs) with two dimensional (2D) nanosheets due to their exceptional large surface area and high surface-to-volume atom ratios are attracted for supercapacitor application. Because of their poor electrical conductivity, they are combined with conducting materials as graphene or conducting polymers as polypyrrole or polyaniline. Supercapacitors, as one of most promising emerging energy storage devices, 2D nanomaterials, including MOFs and conducting polymers have been explored to providing huge potential for the development of flexible supercapacitors with higher electrochemical performance [5].

Hybrid nanomaterials usually contain two or more different components, typically inorganic and organic components. In the last decade, new functional nanostructured hybrids based on graphene, graphene oxide and carbon nanotubes (CNTs) have been developed with promising electrical, mechanical and thermal properties. Combination of 2D and 1D particles in polymeric composites provides interesting 3D structures and properties, which is why they have been intensively studied in recent years [6].

Materials and Methods

GO platforms were prepared by a modified Hummers method from exfoliated graphite after several cycles of centrifugation and ultrasonication. Subsequently, GO platforms were characterized in terms of oxidation, nanoparticle size and exfoliation, using various physical and chemical methods. Magnetic nanoparticles (MNps) were prepared by the chemical precipitation method and their surface-was modified by D, L-lysine (DLL) or with other compounds.

MAX phase Ti_3AlC_2, with particle size 40 μm, was used for MXene preparation by etching process. After delamination of MXene to individual layers, various methods were used for particles characterization including SEM, X-ray photoelectron spectroscopy system (Thermo Fisher Scientific, UK), etc. Additionally, the wettability of prepared layers was deeply investigated [7].

In our study, hybrids were created by combining 2D nanosheets with 1D nanoparticles such as CNTs.

Results and discussion

2D particles graphene oxide were used for preparation of a new type of graphene-oxide multifunctional nanoplatform (GO-MFN) for the detection of tumor cells. CA IX-specific antibody was attached via an amide bond to a modified magnetic nanoparticle that was conjugated to the GO platform again via an amide bond. After performing toxicological

tests on the B16-F0 cell line, no effect of the cytotoxicity of the multifunctional GO platforms was found. The immunofluorescence assay indirectly confirmed binding between graphene oxide and monoclonal antibody (Mab)conjugated magnetic nanoparticles. The selectivity of GO-MNps-MAb platforms to target tumor cells has been demonstrated. These results have provided promising evidence of tumor cell targeting with a wide potential for visualization and future tumor treatment [3,8].

Benzendicarboxylic acid based metal–organic frameworks (MOFs) have been widely utilized in various applications, including supercapacitor electrode materials. Manganese and copper have solid diamond frames formed with BDC linkers among transition metals chosen for MOF formation. They have shown the possibility to enlarge capacitance at different combinations of MOFs and polyaniline (PANI). Reduced graphene oxide (rGO) was used as the matrix to fabricate electrochemical double-layer supercapacitors. PANI and Mn/Cu-MOF's effect on the properties of electrode materials was investigated through electrochemical analysis. As a result, the highest specific capacitance of about 276 F/g at a current density of 0.5 A/g was obtained for rGO/Cu-MOF@PANI composite [9].

2D MXene nanoparticles was developed. A $Ti_3C_2T_z$ MXene was prepared from Ti_3AlC_2 MAX phase using hydrochloric acid and lithium fluoride etching. XPS analysis confirmed etching the aluminium layer out of the Ti_3AlC_2 MAX phase. The intensity of Al signal decreased from 12.9 at.% to 0.0 at.%. Results also showed cleaning MXene from oxidized parts, which are in precursor MAX phase in a larger amount, and in prepared MXene this signal decreased significantly. Ageing of MXene was checked by XPS in two forms of samples, aged in air atmosphere and under argon, within few months by combined XPS and TEM/SAED study. Epoxy and glass fibre–reinforced composites were spray-coated using an MXene water solution. The electromechanical response of the MXene coating was investigated under tensile loading and cyclic loading conditions [9]. The surface energies of MXene nanofillers critically affect the mechanical properties and durability of any polymer-based devices and composites to which these fillers are applied [10]. The wettability properties were found to depend on the number of coating layers and the liquids used. Additionally, the coating roughness was evaluated by using atomic force microscopy. The effectiveness of MXenes as a reinforcing nanofiller for polymer matrix was investigated by utilising an epoxy resin. The work of adhesion between the MXene and epoxy was calculated to be up to 123.6 mJ/m^2. The prediction of a high adhesion was also confirmed with the use of scanning electron microscopy images to examine the fractured surface of the MXene–epoxy specimens [11].

Hybrids were created by combining 2D nanosheets with zero-dimensional nanoparticles such as quantum dots or 1D nanoparticles such as CNTs. Due to the metallic conductivity, high mechanical strength and hydrophilic character of MXenes, they are regarded as one of the most promising materials for supercapacitor electrodes or in solar cells.

Composites, where poly(methyl methacrylate)- PMMA was used as matrix and MXenes and CNTs as conducting fillers, were prepared and studied in the next step. The range of fillers in PMMA/CNT, PMMA/MXenes and PMMA/MXenes/CNTs composites varied from 0.5 to 10 wt.%. Composites were prepared by solvent casting method. The higher the MXene amount, the higher the final conductivity of polymeric composites, but the highest conductivity value was about 10^{-5} S/cm. Much higher conductivity was achieved for composites with hybrid 2D and 1D nanofillers. PMMA/2.5% MXene/3% CNTs reached a conductivity of about 30 S/cm. Synergistic 1D-2D nanostructures are the reason for better electrical properties compared to composites containing only 2D or 1D fillers.

Conclusions

During recent years, nanotechnology has been widely explored for studies in medical science. 2D nanomaterials in combination with magnetic nanoparticles belong to the group of materials with an impact in nanomedicine. Our results confirmed the specific binding of antibody-conjugated functionalized magnetic nanoparticles to CA IX protein and graphene oxide are promising materials for cancer therapy.

The high electrical conductivity and mobility of MXene can accelerate the charge transfer, what opened opportunities for the use of MXene as potential materials for solar cell applications and in the field of supercapacitors. Incorporating MXenes or hybrid nanofillers into polymeric matrices will result in a number of advanced applications, such as

lightweight and flexible electromagnetic interference (EMI) shielding materials, damage-tolerant in-situ sensors, components of structural composites with additional functionalities (e.g. de-icing, electrostatic discharge) and many others. Lithium-ion battery and supercapacitor hybrid devices combine the advantages of high-energy battery and high-power supercapacitor electrodes together to achieve high performance. Cathode materials developing for supercapacitors on the base of hybrids containing conducting polymers 2D nanomaterials are extensively studied.

Acknowledgements
This work has received funding from the European Union's Horizon 2020 research and innovation programme under the Marie Skłodowska-Curie grant agreement No 777810, from projects APVV 19-0465 (Slovakia). The research was partially funded by grants No. M-ERA.NET 2/2019/966/LiBASED from Slovak Academy of Sciences.

References

[1] K. S. Novoselov et al., Nature. **490** (2012) 192–200.
[2] Y. Zhu, S. Murali, W. Cai, X. Li, .J. W. Suk, J.R. Potts, R. S. Ruoff, Advanced Materials. **22** (2010) 5226-5226.
[3] N. Bugárová, Z. Špitálsky, M. Mičušík, Matej, et al., Cancers. **11** (2019) art. no. 753.
[4] M. Naguib, M. Kurtoglu, V. Presser, J. Lu, J. Niu, M. Heon, L. Hultman, Y. Gogotsi, M.W. Barsoum, Adv. Mat. **23 (**2011) 4248- 4253.
[5] L. Q. Bao, et al., Electrochimica Acta. **367** (2021) art. no. 137563, [13] p.
[6] Y. Sun, D. Xu, S. Li, L. Cui, Lele, et al., J. Membrane Sci. **623** (2021) 119075.
[7] P. Machata, M. Hofbauerová, Ya. Soyka, A. Stepura, D. Truchan, Yu. Halahovets, M. Mičušík, P. Šiffalovič, E. Majková, M. Omastová, J. Colloid Interface Sci. **622** (2022) 759-768.
[8] I. Antal, M. Koneracká, et al. Colloids and Surfaces B – Biointerfaces. **205** (2021) art.no. 111893.
[9] L. Q. Bao, et. al. Scientific Reports. **12** (2022) art.no. 664 [13] p.
[10] G. Monastyreckis, A. Stepura, Ya. Soyka, et al., Sensors. **21** (2021) art. no. 2378.
[11] K. Zukiene G. Monastyreckis, S. Kilikevicius, M. Prochazka, M. Micusik, M. Omastova, A. Aniskevich, D. Zeleniakiene, Mat. Chem. Phys. **257** (2021) art. no.123820.

Size-dependent Electronic Properties of Strongly Confined Graphene Quantum Dots

M. Sýkora[a*], Z. Ji[b], M. R. G. Raj[a], P. Tisovský[a], L. F. Pašteka[c]

[a]Laboratory for Advanced Materials, Faculty of Natural Sciences, Comenius University, 842 15 Bratislava, Slovakia
[b]Los Alamos National Laboratory, Los Alamos, NM 87544, USA
[c]Department of Physical and Theoretical Chemistry, Faculty of Natural Sciences, Comenius University, 842 15 Bratislava, Slovakia
*sykoram@uniba.sk

Thanks to its remarkable properties, graphene has been described as the electronic material of the future. However, the absence of an electronic band gap in bulk graphene presents a barrier to its effective utilization in many electronic and optoelectronic applications. One way an electronic band gap can be introduced into graphene is through the exploitation of reduced dimensionality effects. Graphene Quantum Dots (GQDs) are nanometer-size graphene fragments, which retain many of the remarkable properties of bulk graphene, but unlike bulk graphene, they possess a size dependent, nonzero electronic band gap. According to theory, the size dependence of graphene electronic properties is a consequence of quantum confinement (QC) effects similar to those observed in inorganic nanocrystals but with different scaling laws, sensitivity to its shape, edge structure, and functionalization. Systematic experimental studies of the QC on the electronic structure of GQDs is an important step toward their utilization in practical applications. To date, quantitative experimental studies of effects in GQDs have so far been limited. This is, in part, due to the difficulties with the reproducible preparation of structurally uniform GQDs and challenges with their experimental characterization.

Recently, we have developed new methods for preparation of uniform ensembles of small (<2 nm) GQDs, using a systematic bottom-up step-wise synthesis. The new approach facilitates quantitative investigation of the effect of the QC effect on the electronic structure of the GQDs using readily accessible ensemble level techniques, such as optical spectroscopy, electrochemistry and spectro-electrochemistry. Using a spectro-electrochemistry approach developed in our laboratory, we were able to determine how charging of the GQDs affects their physical and electronic structure and optical properties. We demonstrate how the electronic characteristics important for development of applications, such as bandgap, valence and conduction band offsets, exciton binding energies and densities of states systematically vary with the GQD sizes. We also show that the models of solid-state physics used to describe electronic structure of bulk graphene (e.g, Dirac fermion model, tight binding approximation) do not adequately describe the electronic properties of GQDs in the strongly confined regime. This is attributed to stronger carrier-carrier interactions in GQDs compared to the bulk graphene. Finally, I will discuss few examples of proof-of-concept applications of GQDs developed in our laboratory.

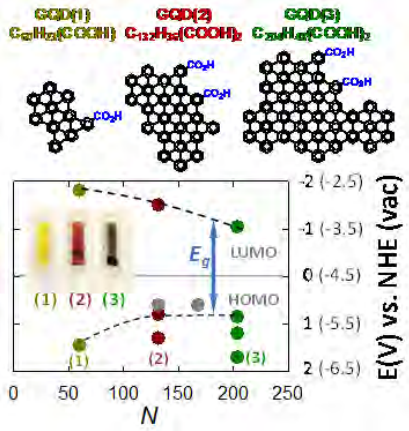

Figure 1: Examples of the strongly confined GQDs prepared by a new "bottom up" synthesis approach and the experimentally determined dependence of the electronic structure on their size.

Acknowledgements
This work was financially supported by the European Union's Horizon 2020 research and innovation programme under grant agreement No. 810701, Slovak Research and Development Agency under grant agreement No. APVV-19-410 and Slovak Ministry of education under grant agreement No. 1/0892/21.

References
[1] Z. Ji, E. Dervishi, S. K. Doorn, M. Sykora, J. Phys. Chem. Lett. **10** (2019) 953-959.
[2] E. Dervishi, Z. Ji, H. Htoon, M. Sykora, S. K. Doorn, Nanoscale 11 (2019) 16571-16581.
[3] Z. Ji, S. K. Doorn, M. Sykora, ACS Nano **9** (2015) 4043-4049.
[4] Z. Ji, R. Wu, L. Adamska, K. A. Velizhanin, S. K. Doorn, M. Sykora, ACS Appl. Mater. Interfaces **6** (2014) 20473-20478.

Surface Functionalization of Carbon for Lithium-Sulphur Battery Cathodes

N. Hoffmann[a]*, M. Ortiz[a,b], A. Visintin[a]

[a] Instituto de Investigaciones Fisicoquímicas Teóricas y Aplicadas (INIFTA), Facultad de Ciencias Exactas (UNLP), CONICET, Diag. 113 y 64, La Plata, Argentina
[b] Centro de Investigación y Desarrollo en Ciencia y Tecnología de Materiales (CITEMA), Universidad Tecnológica Nacional - CICPBA, 60 y 124, 1923, Berisso, Argentina
*nhoffmann@inifta.unlp.edu.ar

Abstract

In this presentation there will be a review of the development that is being developed in the INIFTA of the National University of La Plata, on the subject of active materials for lithium batteries and a special subject of this work lithium-sulphur batteries.

The lithium-sulphur cell is one of the chemical systems expected to deliver capabilities beyond those of the lithium-ion battery, thus allowing for more efficient portable electric supplies and making practical a number of long-desired applications [1]. However, the system has a number of phenomena during cycling that degrade its capacity, and must be addressed in order to make such a cell practical. The most complex of those drawbacks is the "polysulfide shuttle" effect, in which the polysulfides inherent to the cell's functioning dissolve in the electrolyte, reducing the amount of active material available to the cathode, and react with the anode, creating a blocking layer of lithium sulphide [2].

One of the possible strategies for mitigation of the polysulfide shuttle is the use of surface moieties on carbon, which interact with the strongly polar polysulfides after they dissolve; the attractive forces between the sulfides and a normal carbon surface are minimal, while the polar functions can react strongly, anchoring the polysulfides and thus both their availability on the cathode and reducing their transport to the anode, thus reducing the capacity loss over time [3].

In this work, several modifications have been tested out in carbon, looking to improve the anchoring of the polysulfides [4,5,6]. This results in carbons with modified surfaces, the discharge capacities of which are altered, as is their charging and discharging behaviour. Cyclic voltammetry for fresh cells is shown in Fig. 1, while full charge-discharge curves for later cycles are shown in Figure 2.

Narrower, sharper peaks are visible for all the modified carbons over the unmodified carbon in the voltammetry for fresh (uncycled) cells. It is clear that all of the modified carbons show a more stable discharge at their 100th cycle, with the nitric-modified carbon in particular showing a more stable voltage during its lower voltage discharge plateau. The ammonia-modified carbon shows the least stable cycling, with its initial voltages varying widely as the cycling progresses.

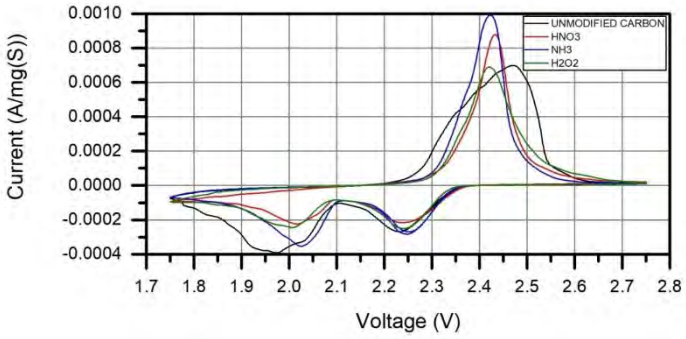

Figure 1: Cyclical voltammetry of uncycled samples at 0.05 mV/sec starting from open circuit voltage.

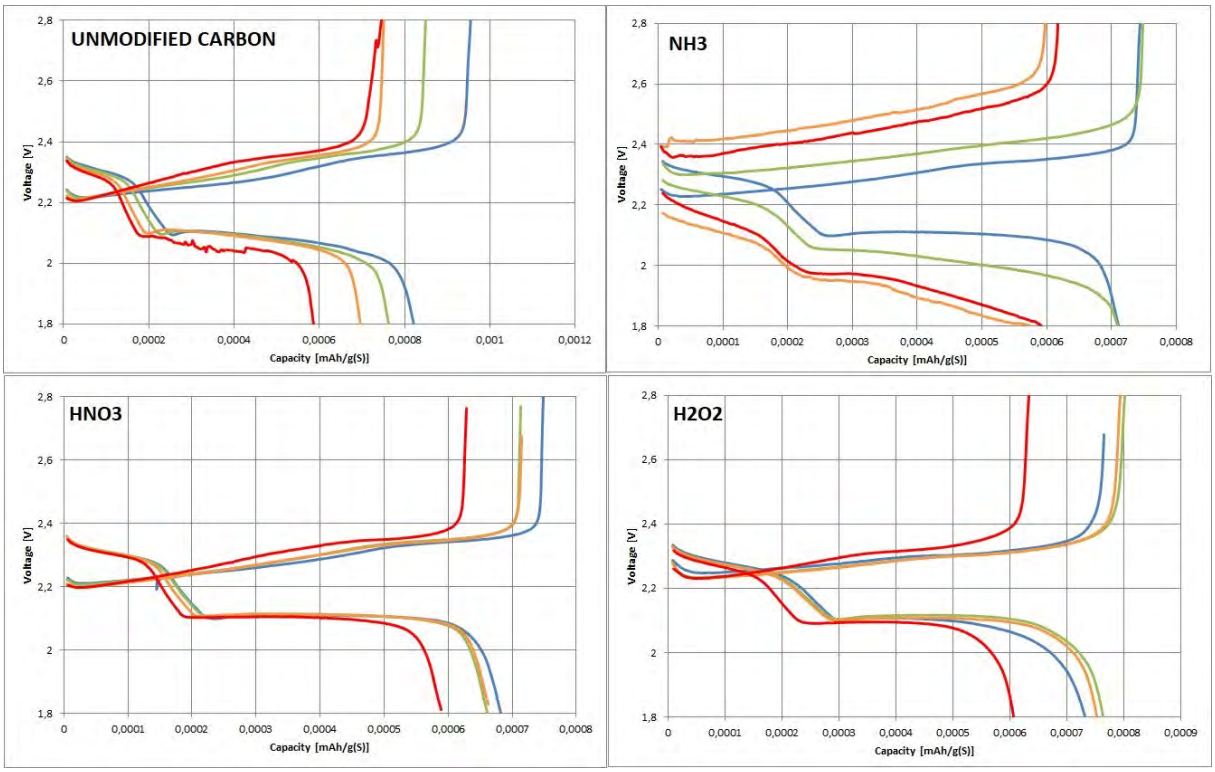

Figure 2: Discharge curves of cathodes with different chemical treatments, at C/10 rate (Blue: 5th cycle. Green: 20th cycle. Yellow: 50th cycle. Red: 100th cycle).

References

[1] P. Bruce, S. Freunberger, L. Hardwick, J. Tarascon, Nature Materials **11** (2011) 19-29.

[2] Zheng, D., Wang, G., Liu, D., Si, J., Ding, T., Qu, D.Yang, X., Qu, D. Advanced Materials Technologies **3** (2018) 1700233.

[3] X. Yang, X. Li, K. Adair, H. Zhang, X. Sun, Electrochemical Energy Reviews **1** (2018) 239-293.

[4] G. Jin, Z. Mingang, Y. Shijian, Y. Xiaoyan, W. Shiwei. Ionics **24** (2017) 2219.

[5] D. Leistenschneider, K. Zürbes, C. Schneidermann, S. Grätz, S. Oswald, K. Wegner, B. Klemmed, L. Giebeler, A. Eychmüller, L. Borchardt. J. Carbon Research **14** (2018).
[6] R. Pongilat, S.Franger, K. Nallathamby. J. Phys. Chem. C **122** (2018) 5948.

High Entropy Alloys for Energy Storage

K. Saksl[a,b,c*]

[a] Institut of Materials Research, Slovak Academy of Sciences, Watsonova 47, 040 01 Košice, Slovak Republic
[b] Faculty of Materials Metallurgy and Recycling, Technical University of Košice, Letna 9, 042 00 Košice, Slovak Republic
[c] Faculty of Science, Institute of Physics, Pavol Jozef Šafárik University in Košice, Košice 041 80, Slovak Republic
*ksaksl@saske.sk

The emergence of high-entropy materials (HEMs) with their excellent mechanical properties, stability at high temperatures, and high chemical stability is poised to yield new advancement in the performance of energy storage and conversion technologies. Graphite has traditionally been used as an anode material in Li-ion batteries. Its intercalation mechanism makes it very stable, but it suffers from a low inherent capacity of 372 mAh/g. High entropy oxides (HEOs) for batteries have been used as anode materials owing to their ability to host lithium ions via a conversion-type reaction. These materials typically have a capacity much greater than graphite, but they have poor cycle stability.

In my contribution I will present our recent achievements in anode electrode tailoring, where the properly selected HEO/metals are not only characterized by a high specific energy density > 500 mAh/g, but also have the ability to regenerate and increase their capacity during charge/discharge cycles.

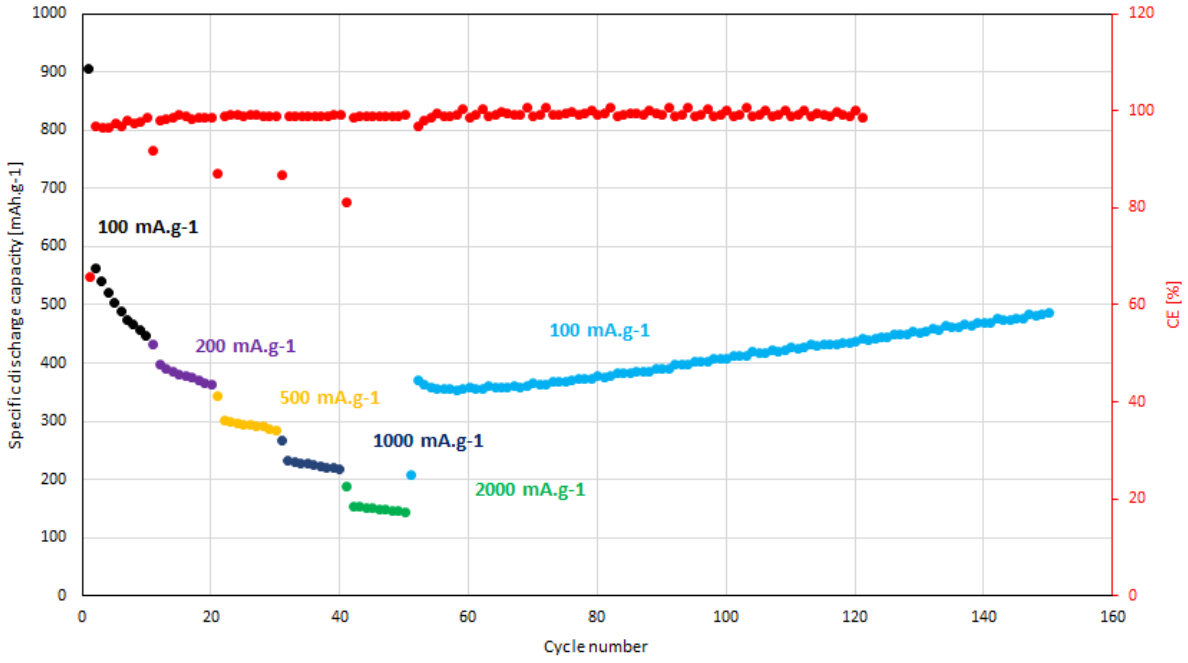

Acknowledgements

This work was supported by the Slovak Research and Development Agency under contract No. APVV-20-0205, APVV-20-0068, APVV-20-0138. Authors are grateful also to the Scientific Grant Agency of the Ministry of Education, Science, Research and Sport of the Slovak Republic and the Slovak Academy of Sciences (VEGA project No. 2/0039/22).

Abstracts

Novel Poly-L-Lysine Coated Nanoparticles in a Form of Magnetic Fluid Designed for Biomedical Applications

I. Antal[a]*, M. Kubovcikova[a], M. Koneracka[a], V. Zavisova[a], A. Jurikova[a], I. Khmara[a], R. Sobotova[a]

[a]Institute of Experimental Physics, Slovak Academy of Sciences, Watsonova 47, Kosice, Slovakia
*iryna.antal@saske.sk

In the last two decades, many publications related to a wide variety of coating compounds for magnetic nanoparticles (MNPs) and their use in biomedical applications have been published. Among them, the macromolecule poly-L-lysine (PLL) takes an important place [1-3]. PLL is a polymer composed of lysine amino acids, which displays excellent biocompatibility and biodegradability. It belongs to the group of cationic polyamino acids, and in alkaline media contains positively charged hydrophilic amino groups (pKa = 10.53) [4].

In our work, we describe a simple synthesis of poly-L-lysine (PLL) functionalized magnetite nanoparticles. The functionalization itself was preceded by the process of coating the surface of the magnetic particles with an oleate layer (OL).

The effect of PLL content on adsorption was studied ranging from 0 to 2.0 weight ratio of PLL:MNPs, and the optimal mass ratio of PLL:MNPs for MNP surface coating was found to be 0.5 (sample $PLL_{0.5}$-OL@MNPs). For confirmation of PLL conjugation on OL@MNP, the dynamic light scattering method (DLS) and electrophoretic mobility measurement were applied. While the hydrodynamic average size of $PLL_{0.5}$-OL@MNPs exhibited an average hydrodynamic size of 124 nm, in the case of nonfunctionalized OL@MNPs was 61 nm (Figure A). This increase in the average diameter of $PLL_{0.5}$-OL@MNPs confirms successful PLL conjugation on OL@MNPs. The values of ζ-potential, determined from electrophoretic mobilities, were -43 and +41 mV for OL@MNPs and $PLL_{0.5}$-OL@MNPs, respectively. The change of zeta potential also indicates PLL conjugation on OL@MNPs as well (Figure B).

Moreover, good colloidal stability of $PLL_{0.5}$-OL@MNPs at neutral pH was observed even after 6 months of the sample preparation. The influence of pH and the ionic strength of the solution on ζ-potential values was studied; $PLL_{0.5}$-OL@MNPs are stable up to 0.3 and 0.2 M NaCl in pH 4.7 and 7.4 solutions respectively.

These poly-L-lysine nanoparticles are suitable for biomedical applications due to their high positive effective surface charge and good colloidal stability in the conditions of physiological pH.

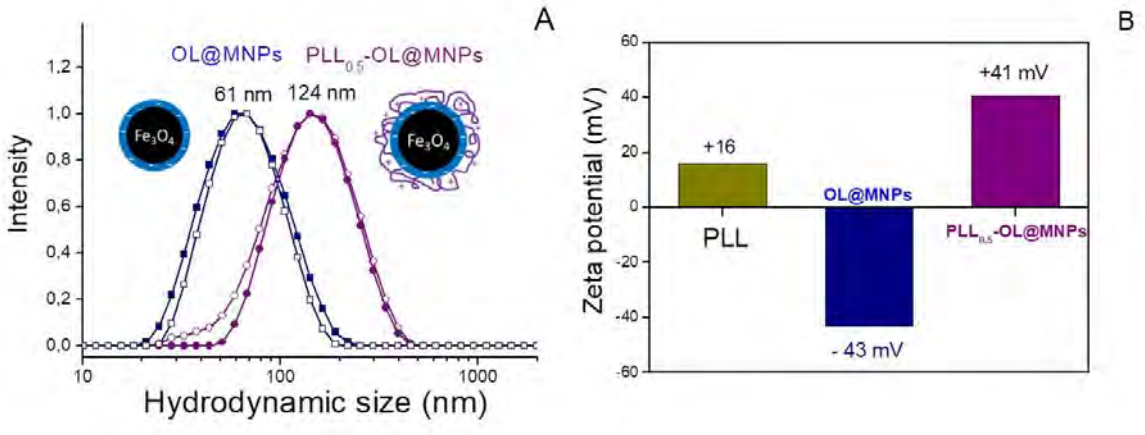

Figure 1: A) Hydrodynamic size of OL@MNPs and $PLL_{0.5}$-OL@MNPs samples after preparation (full symbols) and in 6 months (empty symbols). B) ζ-potential of pure PLL and OL@MNPs before and after their functionalization with PLL.

Acknowledgements

The work was supported by the Operational Programme Integrated Infrastructure, project "BIOVID", ITMS 313011AVG3 co-funded by ERDF.

References

[1] D. Horák, M. Babič, P. Jendelová et al, J. Magn. Magn. Mater. **321** (2009) 1539-1547.
[2] J.J. Xiang, X.M. Nie, J.Q. Tang et al, Chin. J. Oncol. **26** (2004) 71-74.
[3] Z. Li, C. Shuai, X. Li et al, J. Biomed. Mater. Res. Part A. **101A** (2013) 2846-2850.
[4] L. Marsich, A. Bonifacio, S. Mandal et al, Langmuir **28** (2012) 13166-13171.

Establishing the Concept of the Nanocellulose Information Processing Chip

E. Bencurova[a]*, T. Dandekar[a]

[a] Department of bioinformatics, University of Würzburg, Germany
*elena.bencurova@uni-wuerzburg.de

Natural polymers (biopolymers) have fascinated scientists and engineers over several decades. They can be derived from different sources, such as microbes, plants and animals. Nanocellulose is the most abundant polymer on Earth. It can be obtained from trees and plants *via* mechanical and/or chemical processing of the trunks, stems or leaves, or it can be sourced from several aerobic bacterial species, algae and tunicate. The most typical bacterium for the high-throughput production of nanocellulose is *Komagataeibacter xylinus*, however, it can be secreted by various genera, such as *Acetobacter* and *Agrobacterium* [1]. The potential significance of nanocellulose as a structural biopolymer with desirable properties has stimulated interest in recent years as a result of its potential use as an alternative to petrochemically-derived polymers since it represents a renewable, biodegradable resource.

Our concept replaces conventional computer chips with nanocellulose composites. Nanocellulose composites integrate processing enzymes and DNA well and react fast to modifications, electronic signals, surface treatment, and insertion of pores or even use of transparent nanocellulose for display.

Furthermore, electronics can be replaced with light and transistors with light-operated proteins which according to a specific light signal become active: this can be synthesis, deletion or transfer of a certain nucleotide and the output achieved and its activity is monitored by light. For such applications, we can use various natural molecules, such as BLUF and LOV domains, which can activate the protein in presence of light with a specific wavelength. The operation can be achieved by various sets of enzymes including polymerases (e.g. template-free polymerase Cid*I*) for the read-in and exonucleases for read-out. The information is stored in form of DNA, which is then produced or processed according to the activation of light-gated proteins [2]. In our experiments, we explored the full potential of this concept [2]: Nanocellulose is used as a matrix, however, it will also protect the DNA against enzymatic degradation and physical damage. The potential for fast or even ultrafast operation is huge (petahertz chip) as known from fast enzyme catalysis. However, nanocellulose can also accommodate now conventional electronic parts such as transistors, light-emitting diodes [3] and miniaturized transistors (e.g. single electron organic transistors [4]). Moreover, nanocellulose after treatment with conductive substances such as iodine, may become electric itself and provide a capacitor or resistor. Figure 1 summarizes how the nanocellulose chip integrates novel components with classical chip technology. We emphasize that we currently probe only the high potential of the nanocellulose chip technology, giving only proof of concept data. To deliver the full potential technically solid will require years of development as each component (Fig. 1) has to be developed to be (i) highly performant, (ii) truly digital. However, the combination, i.e. the nanocellulose chip, is very powerful in its emergent potential for new information processing technology, it is robust and environmentally friendly and nanocellulose composites incorporate well also conventional electronics to stimulate the performance of the novel components (Fig. 1).

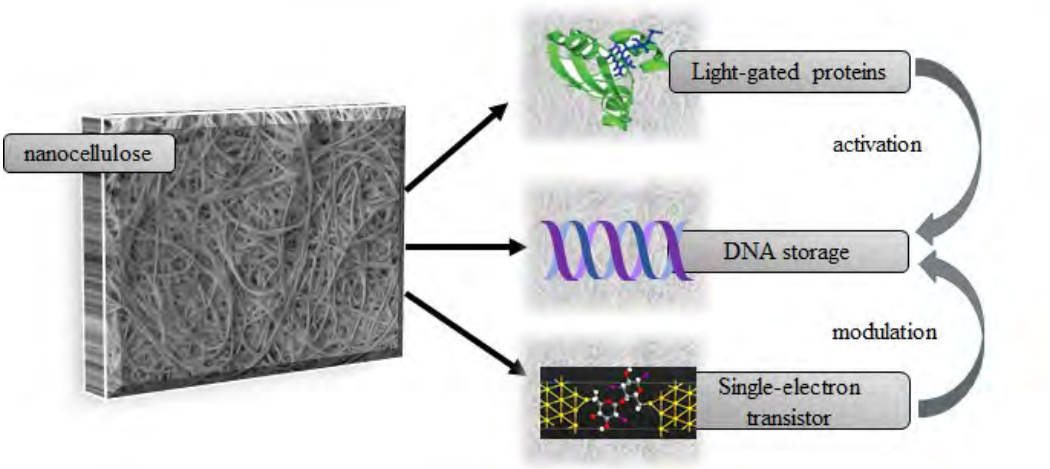

Figure 1: Nanocellulose as support, chassis and protection for DNA storage. Upon stimulation with light, proteins attached to the nanocellulose allow the information stored on the nanocellulose to be read. Subsequently, the read-out proteins process and analyse the DNA anchored on the nanocellulose. The signal can be modulated with additional elements, such as single-electron transistors or DNA wires.

Acknowledgment:
We thank Land Bavaria for support (including its contribution to DFG Project number 324392634 – TRR 221/INF).

References

[1] Qiu, K. and Netravali, A.N. Polymer Reviews. **54** (2014) 598-626.
[2] Bencurova, E., Shityakov, S., Schaack, D., Kaltdorf, M., Sarukhanyan, E., Hilgarth, A., Rath, C., Montenegro, S., Roth, G., Lopez, D., Dandekar, T. Front. Bioeng. Biotechnol. (2022, in press) doi: 10.3389/fbioe.2022.869111
[3] Jung, Y. H., Chang, T. H., Zhang, H., Yao, C., Zheng, Q., Yang, V. W., et al. Nat. Commun. **6** (2015) 1-11..
[4] Shityakov, S., Roewer, N., Förster, C., & Broscheit, J. A. Nanoscale research letters **12** (2017) 1-8.

Study of Synergistic Effects and Compositional Dependence of Hydrogen Evolution Reaction on Mo_xNi_y Alloy Thin Films in Alkaline Media

R. Bodnarova[a]*, M. Kozejova[a], V. Latyshev[a], S. Vorobiov[a], M. Lisnichuk[a], H. You[c], M. Gregor[d], V. Komanicky[a]

[a]Institute of Physics, Faculty of Science, P. J. Safarik University, Park Angelinum 9, 040 01, Kosice, Slovak Republic
[b]Institute of Materials Research, Slovak Academy of Sciences, Watsonova 47, 040 01, Kosice, Slovak Republic
[c]Argonne National Laboratory, 9700 S. Cass Avenue, Lemont, IL 60439
[d]Department of Experimental Physics, Faculty of Mathematics, Physics and Informatics, Comenius University in Bratislava, Mlynska dolina F2, 842 48 Bratislava, Slovak Republic
*renata.bodnarova@student.upjs.sk

In recent years, dependence on the use of fossil fuels is increasing. The combustion of fossil fuels leads to environmental pollution and climate change. It is necessary to find new solutions to the impending energy crisis that will be sustainable. One possible solution is to use hydrogen as a fuel [1]. Our research focused on the preparation of new catalysts for the hydrogen evolution reaction (HER). A good catalyst should have properties such as a low overpotential for HER, high electrical conductivity, and stability in an often harsh and corrosive environment [2]. It is well known that pure Ni has good catalytic performance [3]. Catalytic activity can be improved by alloying. By the preparation of an alloy of nickel with another metal, its dissolution in the electrolyte is slowed down, which increases the stability of the catalyst [2].

Mo-Ni alloys have been studied [4] as a promising catalyst for HER development in aqueous electrolytes. They show not only increased HER activity, but also better stability. We studied the dependence of the composition of Mo-Ni alloys on the catalytic activity in alkaline solution for HER using electrochemical methods (cyclic voltamperometry, impedance measurements). The composition ratio of the prepared alloys was determined by EDX analysis. The morphology of the surface of the thin film was investigated and confirmed by various methods of SEM, AFM, TEM, XRD, and XPS.

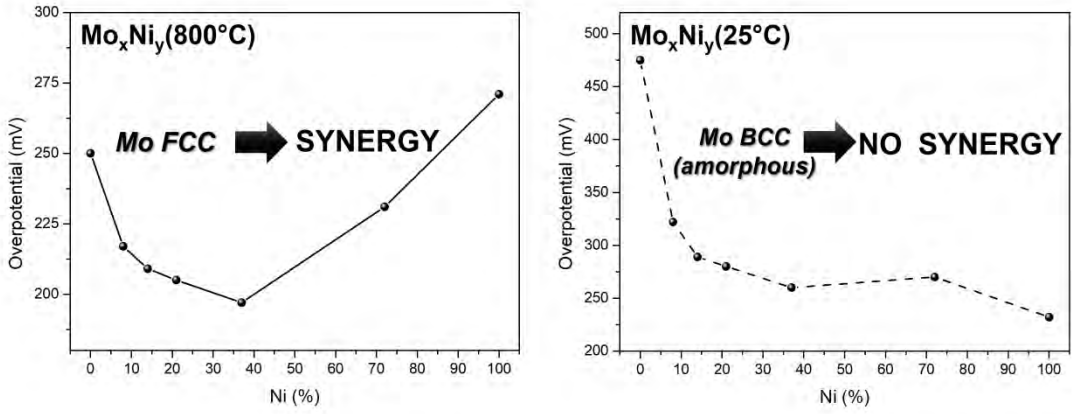

Figure 2: Study of synergistic effects and compositional dependence of hydrogen evolution reaction on MoxNiy alloy thin films in alkaline media.

Our research shows that structural effects play an important role in the activity of Mo_xNi_y alloys. The results indicate that synergistic effects exist only in Mo-Ni alloys prepared at a high temperature (800 °C), Figure 1a. Alloys prepared at room temperature show no synergy between Mo and Ni, Figure 1b. We observed the structures of the alloys by XRD analysis. The alloys prepared at 800 °C had an fcc crystal structure. Samples prepared at 25 °C had an amorphous or bcc structure. The fcc phase of transition metals, which usually occurs in the bcc phase, can be prepared by sputtering in the form of thin films at elevated temperatures [5]. The thin film geometry helps to preserve the crystal structure of fcc. This is due to the tension, which is related to the easier location of more densely arranged structures. We confirmed that by observing Mo-rich Mo-Ni alloys prepared at 800 °C. Mo_xNi_y samples with the fcc phase are stabilized in a thin film configuration. The fcc MoNi sample is stressed by 15% more, than what is expected for Mo to fit the fcc lattice (from Vegard's law). Internally strained lattices show high activities also in other electrocatalysts with the combined effect of electronic and crystallographic structures [6].

Acknowledgements
This work has been supported by grant 313011V334, Innovative Solutions for Propulsion, Power and Safety Components of Transport Vehicles, and grants of the Slovak Research and Development Agency under contract APVV-20-0324 and APVV-20-0528.

References

[1] X. Zou, Y. Zhang, Chemical Society Reviews **44.15** (2015) 5148-5180.
[2] M. Wang, Z. Wang, Z. Guo, Z. Li, Int. J. Hydrog. Energy **36.5** (2011) 3305-3312.
[3] R. K. Shervedani, A. H. Alinoori, A. R. Madram, J. New Mater. Electrochem. Syst. **11.4** (2008) 259-265.
[4] J. M. Jakšić, M. V. Vojnović, and N. V. Krstajić, , Electrochim. Acta **45.25-26** (2000) 4151-4158.
[5] K. L. Chopra, M. R. Randlett, R. H. Duff, Philos. Mag. **16.140** (1967) 261–273.
[6] P. Strasser, S. Koh, T. Anniyev, J. Greeley, K. More, Ch. Yu, Z. Liu, S. Kaya, D. Nordlund, H. Ogasawara, M. F. Toney, A. Nilsson, Nat. Chem. **2.6** (2010) 454-460.

Colloidal Gold and Silver Nanocrystals for Studies of Antimicrobial Activity

I. Božeková[a], M. Mazúrová[b], M. Horniačková[b], M. Sýkora[a]*

[a]Laboratory for Advanced Materials, Faculty of Natural Sciences, Comenius University, Ilkovičova 6, 842 15 Bratislava, Slovakia
[b]Department of Microbiology, Institute of Microbiology, Slovak Medical University in Bratislava, Limbová 12, 833 03 Bratislava
*sykoram@uniba.sk

Introduction

Tunability of the physical and chemical properties of metal NCs by their size and shape makes them appealing materials for exploitation in applications ranging from electronics to medicine [1-5]. Metal NCs comprising Au, Ag or Cu, in the size range below 50 nanometers have shown activity as antimicrobial agents. Several recent studies suggest that these NCs can inhibit growth of bacteria with antibiotic resistance [6]. This is significant, as antibiotic resistance of bacteria represents a world-wide health problem, causing over a million deaths per year [7]. Motivated by these early reports, the goal of our study was: (a) synthesis of Ag and Au NCs with range of sizes 3-50 nm and size dispersions less than 20 %; (b) testing of the stability of the NCs in biological growth media with respect to aggregation; (c) investigation of the effect of the synthesized NCs on the bacterial growth.

Experimental section

Au and Ag NCs were prepared by colloidal synthesis in aqueous solution via chemical reduction of corresponding salts, e.g., $HAuCl_4$ or $AgNO_3$ (precursors) using reducing agents, tannic acid (TA), sodium citrate (SC) [7,8]. The materials were obtained from: SC 99.5% Glentham; TA 99.5% and HCl 35% Centralchem; K_2CO_3 99% and $AuCl_3$ 99% Sigma Aldrich; $AgNO_3$ 99% VWR, and used without further purification. Transmission Electron Microscopy (TEM) images were obtained using Analytical transmission electron microscope JEM ARM 200cF. The absorption spectra of NCs were collected on diode-array spectrometer Agilent 8453. The biological growth media were obtained from several suppliers (TSB, BHI and ZB (Neogen, USA); MHB (Bio-Rad, France); LB Broth, Miller (BD, Difco Laboratories, France) and refrigerated until use. The changes in optical properties of NCs upon transfer to the biological growth media were analyzed by comparison of the turbidity (absorption spectra) of the NCs in water solution (control) and appropriate growth medium.

Results and discussion

Following the procedures reported previously in literature [8,9], we were able to prepare Au NCs in the range of 4 - 25 nm and Ag NCs in the range of 10 - 40 nm. The sizes of the prepared NCs were determined by TEM (see Fig. 1 a-c). The size dispersion of the prepared materials ranged from 10-20 % (Fig. 1 d-f). The example optical spectra of the Au NCs in water are shown in Fig. 2a. The spectra are characterized by a distinct plasmonic peak at 522 nm (2.37 eV). In aqueous media the absorption characteristics were stable for period of at least 1 year.

Upon transferring to biological growth media, the absorption characteristics of NCs show distinct changes (Fig. 2b, c.). These observed changes were analysed by fitting the experimental data in aqueous and biological media by methods described previously [10]. The differences in the fits were tentatively attributed to the aggregation of the NCs. Using this assumption, the analysis provides an indication of the relative stability of the NCs in various growth media. The results suggest that the stability of the Au and Ag NCs with respect to aggregation is best in TSB (Tryptic soy broth) growth medium and PBS (Phosphate buffer saline).

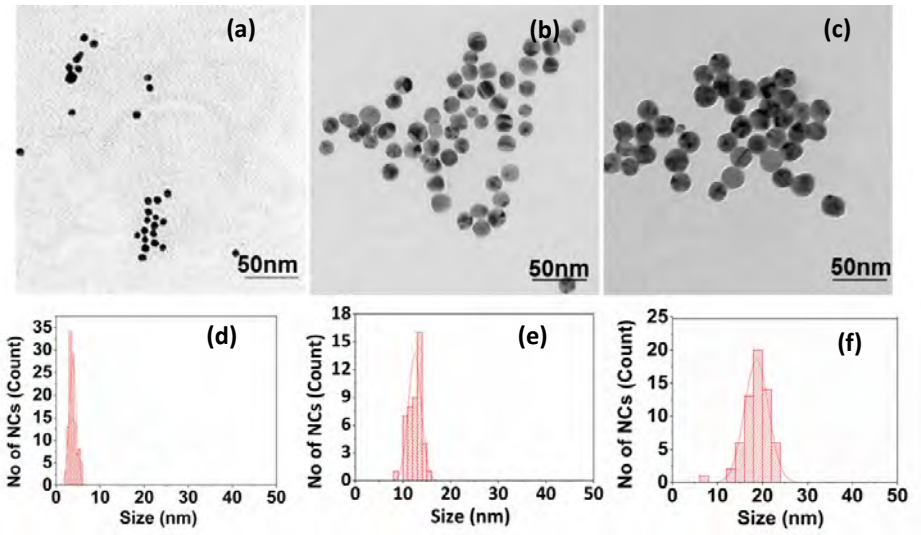

Figure 1: (a-c) Examples of TEM images and (d-f) size dispersion histograms for the synthesized Au NCs.

The investigation of the interactions between the NCs and bacteria was performed using an analysis of the optical changes in the microbiological plate containing NCs and bacteria in TSB. The experiments were performed using four types of bacteria: *Escherichia coli* CCM 3954, *Enterococcus faecalis* CCM 4224 and two *Klebsiella pneumoniae* (CCM 4224 and ZPM 135) with Ag and Au NCs with sizes ranging from 3-25 nm. The typical NC concentration range was 150 – 25 mg/L. After mixing bacteria with NCs, the mixtures were incubated for 24 hours at 37 °C. Bacterial growth appeared as increased turbidity in the well, which was quantified spectroscopically. The results indicated

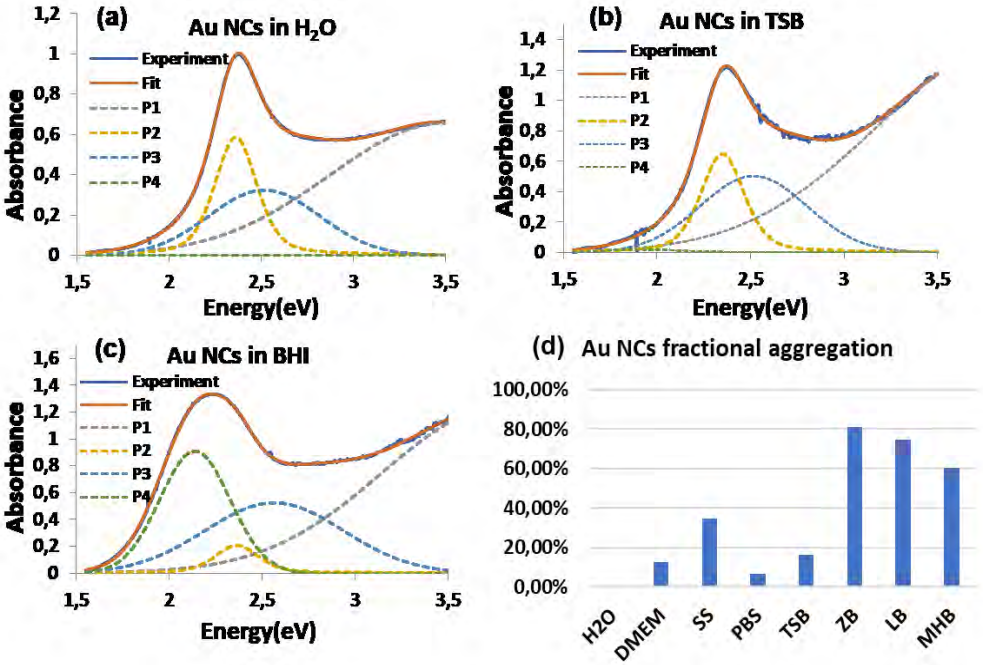

Figure 2: A comparison of the absorption spectra of Au NCs (a) in water; (b) in TSB; (c) in BHI. The dashed lines show the modelled composition peaks used to reconstruct the best fit (orange trace) to the experimental data (blue trace). Panel (d) shows the Au NCs fractional aggregation extracted from the spectral fit analysis of Au NCs in various growth media.

quantitatively the extent of the bacterial growth over the 24 hour period in the absence and presence of NCs. The example results for interaction between Ag NCs with size 22.6 nm and bacterium *E. coli* are shown in Fig 3. The results reveal that in this case the bacterial growth is fully inhibited at NC concentrations >100 mg/L. The bacterial growth was also analysed by colorimetric approach, where the extent of the growth was tested using indicator dye MTT (methylthiazolyldiphenyl tetrazolium). The results of both methods were consistent.

Conclusions

We prepared and characterized NCs of gold with sizes of 4-25 nm and silver with sizes of 10-40 nm. The materials are stable with respect to aggregation in aqueous solution and show characteristic plasmonic absorption peaks with the peak energy varying systematically with the NC size. The absorption characteristics of the plasmon bands are significantly distorted in the biological growth media. Using an assumption that the observed distortions are mainly due to the NC aggregation, we identified biological growth media most suitable for studies of the bacteria-NCs interactions. The initial studies of interactions of NCs with bacteria suggest that both Ag and Au NCs can inhibit the growth of specific bacteria at concentrations above 50-100 mg/L. More quantitative analysis of the inhibition concentration and the mechanism of NC bacteria interactions are currently in progress.

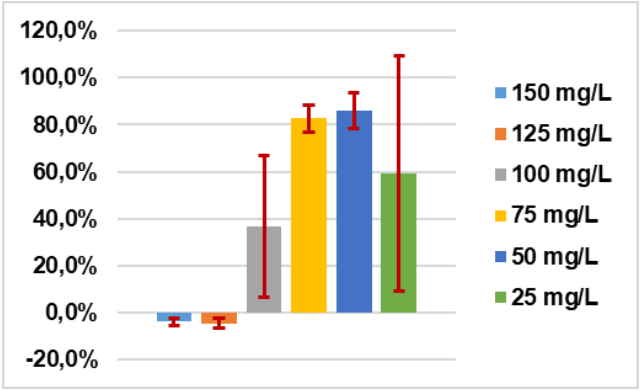

Figure 3: An example of growth inhibition for bacteria *E. coli* in the presence of Ag NCs with diameter 22.6 nm, as a function NC concentration.

Acknowledgements

This work was financially supported by the European Union's Horizon 2020 research and innovation programme under grant agreement No. 810701, Slovak Research and Development Agency under grant agreement No. APVV-19-410, Slovak Ministry of education under grant agreement No. 1/0892/21, Slovak Medical University in Bratislava Grant No 132021-SVG1 and by UK grant No. UK/425/2021.

References

[1] K. An, G.A. Samurai, ChemCatChem. **4** (2012) 1512-1524.
[2] J.N. Anker, W.P. Hall, O. Lysanders, N.C. Shah, J. Zhao, R.P. Van Duyne, Nat. Mater. **7** (2008) 442-453.
[3] N.L. Rosi, C.A. Mirin, Chem. Rev. **105** (2005) 1547-1562.
[4] C.J. Murphy, A.M. Goole, J.W. Stone, P.N. Sisco, A.M. Alcalay, E.C. Goldsmith, S.C. Baxter, Acc. Chem. Res. **41** (2008) 1721.
[5] P. Hervés, M. Pérez-Lorenzo, L.M. Liz-Marzán, J. Dzubiella, Y. Lu, M. Ballauff, Chem. Soc. Rev. **41** (2012) 5577-5587.
[6] M. A. Faramarzi, A. Sadighi, Advances in Colloid and Interface Science. **189–190** (2013) 1-20.
[7] D. Pires, M. E. A. de Kraker, E. Tartari, M. Abbas, D. Pittet, Clin. Inf. Diseases. **64** (2017) 1780–1783.
[8] J. Piella, N. G. Bastús, V. Puntes, Chem. Mater. **28** (2016) 1066-1075.
[9] N. G. Bastús, F. Merkoçi, J. Piella, Chem. Mater. **26** (2014) 2836-2846.

[10] T. Ida, M. Ando, H. Toraya, J. Appl. Cryst. **33** (2000) 1311-1316.

Role of Surface Energy on Adhesion of Cancer Circulating Cell

D. Burčík[a]*, J. Macko[a], N. Podrojková[a], A. Oriňak[a]

[a] Department of Physical Chemistry, Moyzesova 11, Košice 04001, Slovakia
*5170274@upjs.sk

In modern society a variety of diseases present serious dangers for human beings. One of the most lethal of them is cancer. Reason of its origin could be different, but it very often arises because of a change in genetic information of a cell. Cancer cells multiply in the human body and their masses form tumors. If this tumor does not have metastatic potential, it is less dangerous for humans. If a tumor starts to create circulating tumor cells (CTCs), the cancer can develop into distinct tissues and organs. CTCs travel through lymphatic or blood vessels. Then they fasten on epithelial cells, which form the surface of blood vessels. In the next stage they penetrate them and move deeper into the specific organ. Many science disciplines try to disable the process of creating CTCs or metastasis. Others suggest to block these CTCs with the immune system or a variety of chemicals. We know many types of cancer cells, because their origin is from the health line of cells from some organ or tissue. We do not know of a universal medicament for all cancers, so we could try to use a variety of preventive chemicals that have an antiadhesive effect on cancer cells. Cell adhesion presents an important part of cancer mechanism [1]. All cells – healthy or cancer – have on their surface many receptors or ligands. They are the main actors in the process of adhesion. Cells need to communicate with their surroundings – extracellular matrix or other cells. In most cases they use for that cell adhesion molecules (CAMs), which play the role of receptors and ligands. We know four large families of these CAMs: immunoglobulins, integrins, cadherins and selectins. They are located on the cell surface, but they can develop as an answer for situations in organism. CAMs on the surface of cancer cells could be different from health cells. So, medicaments can only block them and healthy cells could stay intact.

Worldwide scientists discovered and invented several chemicals that can block the adhesion function of cancer cells. We can mention S-nitrosocaptopril, chitosan, aspirin, or 3, 4-methylenedioxy-β-nitrostyrene. In this study we worked with ursolic acid, which derivatives are already used as medicaments with mentioned antiadhesion effect [2]. In our case we try to use surface energy of cells to find out if ursolic acid will adhere to fibroblasts and cancer cells. In this process we can observe changes in surface energy. Every molecule has specific parts, which interact with the cell surface. In the beginning of this experiment we have prepared models, which present intacted carbon layer or carbon layer with defect. These models are the simplest way how to show hydrophobic molecule of ursolic acid and possibilities how it interacts with this carbon layer. This is only a basic model, but it can be modified in next experiments to be more similar with cell membrane. Deactivation of cell-cell adhesion is a good way how to lower the chance of metastasis development. It also has a preventive function. Many mentioned chemicals can be delivered to specific locations without any other agents, but a lot of them are only carriers. They can only deliver them to cancer cells, but in some cases they can interact with cancer cells on their own. Adhesion can be deactivated by occupying surface receptors or from inside of cells through several biochemical mechanisms. So, we need to develop nanocarriers which will protect medication and deliver it to the right location. If we understand the process of adhesion, impact of surface energy in its mechanism and then use knowledge from nanotechnologies, we can find out how to prolong lives of oncogenic patients or save their lives.

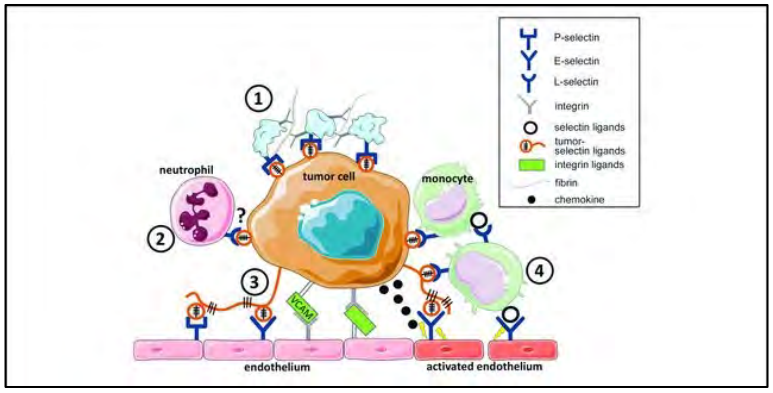

Figure 1: Interaction of cancer with surounding cells via its ligands and receptors [3].

Description: 1.) aggregation of platelet and cancer cell is mediated by P-selectin and integrins through fibrin and fibrinogen. 2.) interaction with neutrophils promote tumor cell proliferation. 3.) interaction with endothelium is mediated by P-and E-selectins. Tumor cell firm adhesion is facilitated by integrins. 4.) interaction with monocytes contributes to initiation of cancer extravasation [3].

Acknowledgements
Thanks for financial support of APVV-16-0029, APVV-20-0278 and VEGA 1/0095/21.

References

[1] P. Bongrand et al., *Physical Basis of Cell Adhesion, Vol. 2* (Bongrand P., ed.). Taylor & Francis Group, 6000 Broken Sound Parkway NW, Suite 300, Boca Raton, page 227.
[2] L. Xiang et al., Oncotarget **6** (2015) 9295-9312.
[3] https://www.researchgate.net/figure/Cell-adhesion-facilitates-tumor-cell-survival-in-the-circulation-and-tumor-cell_fig1_335670615

Synthesis and Characterization of the Ternary Chalcogenide Perovskites

R. Bystrický[a,b]*, S. K. Tiwari[a], P. Hutár[a,c], M. Sýkora[a]*

[a] Laboratory for Advanced Materials, Faculty of Natural Sciences, Comenius University, Ilkovičova 6, 842 15 Bratislava, Slovakia

[b] Institute of Inorganic Chemistry, Slovak Academy of Sciences, Dúbravská cesta 9, 845 36 Bratislava, Slovakia [c] Institute of Electrical Engineering, Slovak Academy of Sciences, Dúbravská cesta 9, 841 04 Bratislava, Slovakia

*roman.bystricky@uniba.sk, *sykoram@uniba.sk

Introduction

During last decade, there has been a dramatic increase of interest in a group of materials possessing perovskite crystal structure. This is mainly due to the subgroup of perovskite materials called Organo-Halide Perovskites (OHPs), which have remarkable combination of electric and optical properties [1-3], optimal for exploitation in photovoltaics and optoelectronics. In spite of their significant promise, the development of applications utilizing OHPs has been hindered by the requirement that they contain toxic lead and by their low thermal and chemical stability [4-6]. As aresult, one of the main current challenges in the research of the perovskite materials is the identification and development of the lead-free perovskites which are thermally and chemically stable under normal operating conditions. Series of recent theoretical studies [7-9] suggest that ternary chalcogenides could be a very promising alternative to OHPs. Several recent reports [9-12] showed that ternary chalcogenide compounds based on S (without lead), mainly with distorted PS should possess a combination of properties similar to those observed in OHPs, while having significantly higher thermal and chemical stabilities. Although, the first ternary chalcogenides were synthesized more than 50 years ago, up to now only 26 ternary chalcogenides with perovskite structure were prepared in the form of powder and only one, $BaZrS_3$, was prepared in the form of thin film. The preparation methods available in the literature are often yield impure materials and/or use toxic compounds such as CS_2 and H_2S. As a resuly, the systematic experimental studies of their electronic properties and stability are quite limited. The first information about the chemical stability of ternary chalcogenides which appeared in recent years [13, 14] confirmed that ternary chalkogenides are more stable than the OHPs. However, these studies have so far been limited to only three materials and only some of their characteristics. In this work, we have developed new synthetic method for preparation of chelcogenide PSs based on sulfurization of oxides and carbonates using boron sulfides. In order to realistically test the ternary chalcogenides in practical applications, we prepared a wider range of materials and systematically evaluated their thermal stability.

Experimental section

In a typical reaction, starting materials (ternary oxide, boron, sulfur) were ground in an agate mortar for 10-15 min. Well ground powder was transferred to a 15 mm i.d. quartz tube. The tube was connected to a Schlenk line and evacuated at <2 Pa for 30 min. After the flame sealing, the ampule with the reagents was transferred into a temperature calibrated furnace where it was heated at temperatures 800-1000 °C. The typical heating ramp rate was 5 °C/min with the holding time 5 hrs. at 300 °C and 600 °C and the cooling rate was 5 °C/min. After the cool down, the ampoules were opened at ambient conditions and characterized. The crystalline phases present in the powder samples were identified using X-ray diffraction (XRD) (Panalytical Empyrean, Netherlands, Cu Kα radiation). Reflectance spectra were measured on Jasco V-770 (Uv-Vis/NIR) spectrophotometer attached to a manual absolute reflectance measurement accessory ARSN-917. Thermal analysis (TG-DTA) was performed with Linseis STA1600, (Linseis Messgeraete GmbH, Germany) with heating rate of 8 °C/min up to 800 °C in air.

Results and discussion

XRD analysis

We prepared 6 ternary chalcogenides by mixing the ternary oxide with boron and sulphur, specifically $BaZrS_3$, α-$SrZrS_3$, β-$SrZrS_3$, $BaHfS_3$, $SrHfS_3$, α-$EuZrS_3$. In the Figure 1, the XRD patterns of the prepared materials are shown, together with the reference patterns from ICDD database. The peaks match with the reference patterns of the corresponding CPs from the ICDD database. No Bragg reflections of any other phases were detected. The results show that the compounds were prepared in the pure form.

Optical bandgap

The optical band gap of the prepared materials was determined from diffuse reflectance spectra by using Tauc analysis. The bandgap ofor α-$EuZrS_3$, α-$SrZrS_3$, $BaZrS_3$, $BaHfS_3$, β-$SrZrS_3$, $SrHfS_3$ were found to be 1.01, 1.49, 1.80, 1.97, 2.00, 2.25 eV, respectively. This is in a close agreement with previous experimental studies [11].

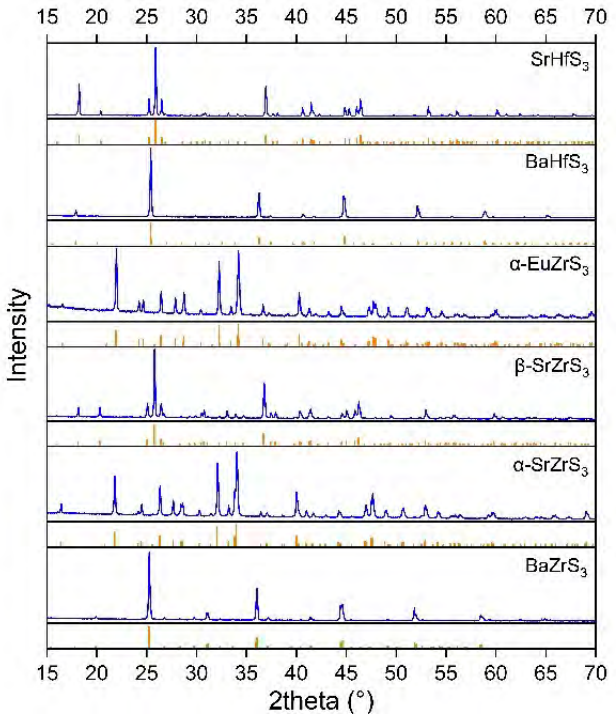

Figure 1: Powder X-ray diffraction patterns for prepared ternary chalcogenides. The blue traces show the patterns for the samples prepared in this work. The orange traces are reference literature patterns obtained ICDD.

Thermal stability

To evaluate thermal stability of prepared materials, we performed thermal analysis. The mass change and DTA curves reveal that the oxidation of the sulphides takes place between 450 °C and 800 °C. The weight loss can be understood as the substitution of Sulphur with lighter Oxygen atoms. The competing weight gain at higher temperatures is attributed to the formation of metal sulfates, which was confirmed by the XRD measurement of the powders after heating. The needle-like α-$EuZrS_3$ is the first compound which starts to oxidize at around 470 °C. On the other hand,

$BaZrS_3$ showed the highest stability with an oxidation onset a little above 650 °C. This is in agreement with published results [13].

Conclusions

We synthesized 6 ternary sulphides in pure form by a newly developed synthetic method based on heating of the mixture of ternary oxides, boron and sulphur in evacuated quartz ampoule at temperatures between 800-1000 °C for several hours. The optical bandgap of prepared materials varies from 1.01 to 2.25 eV. The thermal analysis showed that the materials are stable up to 450 °C in air.

Acknowledgements

This work was supported by the European Union's Horizon 2020 research and innovation programme under grant agreement no. 810701 and by the Slovak Research and Development Agency under grant agreement no. APVV-19-410. SKT acknowledges partial support from project USCCCORD (ŽoNFP: NFP313020BUZ3), co-financed by the European Regional Development Fund within the Operational Programme Integrated Infrastructure.

References

[1] A. Kojima, K. Teshima, Y. Shirai and T. Miyasaka, J. Am. Chem. Soc. **131** (2009) 6050–6051.
[2] H. J. Snaith J. Phys. Chem. Lett. **4**, 21, (2013) 3623–3630
[3] A. K. Jena, A. Kulkarni, T. Miyasaka, Chem. Rev. **119**, 5, (2019) 3036–3103
[4] D. Wang, M. Wright, N. K. Elumalai, A. Uddin. Solar, En. Mat. & Solar Cells **147** (2016) 255-275.
[5] G. Divitini, S. Cacovich, F. Matteocci, L. Cina, A. Di Carlo, C. Ducati, Nature Energy **1** (2016) 15012.
[6] G. P. Nagabhushanaa, R. Shivaramaiaha, A. Navrotsky, Proc. Natl. Acad. Sci. **113** (2016) 7717-7721.
[7] S Ahmad, P.K. Kanaujia, H.J. Beeson, G.V. Prakash, J.J. Baumberg, ACS Appl. Mater. Interfaces **7** (2015) 25227-25236.
[8] T. A. Berhe, W.-N. Su, Ch.-H. Chen, A. A. Dubale, B.-J. Hwang, Ener. Env. Sci. **9** (2016) 323-356.
[9] Y.-Y. Sun, M.L. Agiorgousis, P. Zhang, S. Zhang, Nano Lett. **15** (2015) 581-585.
[10] W. Meng, B. Saparov, F. Hong, J. Wang, D.B. Mitzi, Y. Yan, Chem. Mater. **28** (2016) 821-829.
[11] S. Niu, H. Huyan, Y. Liu, M. Yeung, K. Ye, L. Blankemeier, T. Orvis, D. Sarkar, D.J. Singh, R. Kapadia, J. Ravichandran, Adv. Mater. **29** (2017) 1604733.
[12] J. W Bennett, I. Grinberg, A. M. Rappe. Phys. Rev. B **79** (2009) 235115.
[13] S. Niu, J. Milam-Guerrero, Y. Zhou, K., Ye, B. Zhao, B.C. Melot, J. Ravichandran, J. Mater. Res. **33** (2018) 4135-4143.
[14] T. Gupta, D. Ghoshal, A. Yoshimura, S. Basu, A. Soni, S. Zhang, N. Koratkar, Adv. Funct. Mater. **30** (2020) 2001387.

Metal-Organic Framework Modified by Nickel Ions to Provide Enhanced Cycle Performance of Lithium-Sulfur Batteries

D. Capkova[a]*, T. Kazda[b], N. Kiraly[c], M. Almasi[c], O. Cech[b], A. Strakova Fedorkova[a]

[a] Department of Physical Chemistry, Faculty of Sciences, Pavol Jozef Safarik University in Kosice, Kosice, Slovak Republic
[b] Department of Electrical and Electronic Technology, Faculty of Electrical Engineering and Communication, Brno University of Technology, Brno, Czech Republic
[c] Department of Inorganic Chemistry, Faculty of Sciences, Pavol Jozef Safarik University in Kosice, Kosice, Slovak Republic
*dominika.capkova@upjs.sk

The increasing demand for energy storage with inexpensive and high energy density brings to the forefront next-generation batteries. Promising energy-storage solutions for energy are lithium-sulfur (Li-S) batteries due to their high theoretical capacity (1675 mAh g^{-1}) and energy density (3000 Wh kg^{-1}) [1]. Moreover, sulfur is an environmentally friendly and abundant element on the Earth's crust. However, volumetric expansion of sulfur and polysulfide shuttle during cycling negatively affects the specific capacity, increases the self-discharge rate, and decreases the Coulombic efficiency [2]. To avoid these issues, metal-organic frameworks (MOFs) may be applied in cathode material for Li-S batteries. MOFs are formed by the coordination of organic ligands to the metal sites and exhibit tuneable pore sizes and surface chemistry [3].

Herein, we report the example of porphyrinic MOF self-assembled from porphyrin H_2TCPP^{4-} ligands, which was post-synthetically doped by Ni^{2+} ions as the sulfur conductive additive for Li–S batteries. The composition of the cathode material was 60 % of sulfur, 15 % MOF, 15 % carbon Super P, and 10 % polyvinylidene fluoride (PVDF) as a binder. The initial discharge capacity of the electrode with unmodified GaTCPP reaches the value of 667 mAh g^{-1} at 0.2 C, and after fifty cycles, the capacity increases up to 699 mAh g^{-1}. The doping by Ni^{2+} ions increases the conductivity of the electrode material, which increases the capacity to 734 mAh g^{-1}, and the capacity after 50 cycles increases up to 778 mAh g^{-1}. The coulombic efficiency for the S/GaTCPP(AS) electrode was around 92.9 % and for the S/GaTCPP(Ni) electrode reached the value of 91.7 %. It can be concluded that the modification of MOF material with Ni^{2+} ions can increase the conductivity of the electrode material. However, the coulombic efficiency was higher for the S/GaTCPP(AS) than the S/GaTCPP(Ni) electrode indicating higher stability of the cathode material with unmodified MOF.

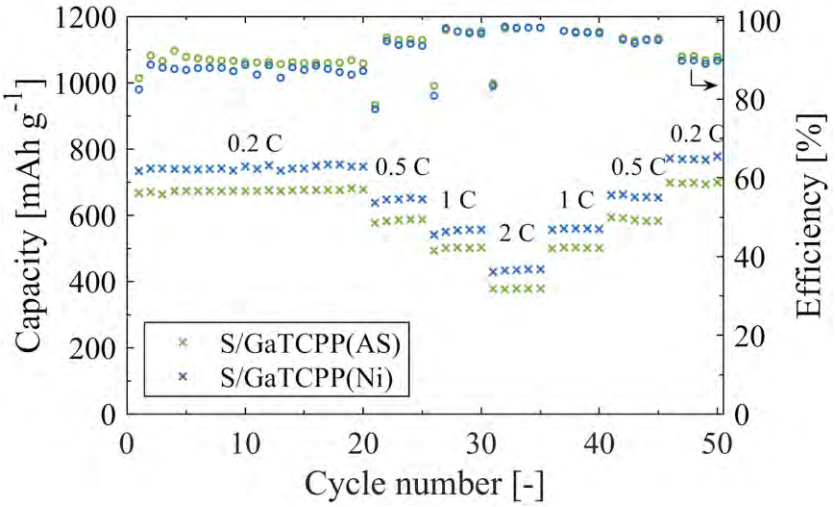

Figure 1: Galvanostatic cycling of the S/GaTCPP(AS) and S/GaTCPP(Ni) electrodes at various C-rates in the Li-S battery cell.

Acknowledgements

This research was sponsored by the following projects: APVV-20-0138, Development of Novel 3D Materials for Post Lithium Ion Batteries with High Energy Density; APVV-20-0111, Towards Lithium Based Batteries with Improved Lifetime; iCoTS No. 313011V334, Innovative Solutions for Propulsion, Power and Safety Components of Transport Vehicles; VEGA 1/0074/17, Nanomaterials and Nanostructured Layers with Specific Functionality, VEGA 1/0294/22, Porous Coordination Polymers for Environmental Applications, and specific graduate research of the Brno University of Technology No. FEKT-S-20-6206.

References

[1] T. Kazda, P. Čudek, J. Vondrák, et al., J. Solid State Electrochem. **22** (2018) 537–546.
[2] S. Qiu, J. Zhang, X. Liang, et al., Chemical Engineering Journal **450** (2022) 138287.
[3] N. Kiraly, D. Capkova, M. Almasi, et al., RSC Adv. **12** (2022) 23989-24002.

Two-Dimensional Transition Metal Dichalcogenide/Conducting Polymer Based-Electrocatalysts for Overall Water Splitting

S. Cogal[a,b]*, M. Omastová[a]

[a] Polymer institute, Slovak Academy of Sciences, Dubravska cesta 9, Bratislava 84541, Slovakia
[b] Burdur Mehmet Akif Ersoy University, Faculty of Arts and Science, Department of Chemistry, 15030, Burdur, Turkey
*sadik.cogal@savba.sk

Water splitting is a promising candidate for sustainable energy development. The overall water splitting consists of two half reactions, which are hydrogen evolution (HER) and oxygen evolution reactions (OER). The performance of these reactions highly depends on the catalytic activities and bifunctionality of the electrocatalysts. Generally, noble metal-based (Pt, Ir, Ru) materials are the most performing catalysts, which have been used in two half reactions [1]. However, these noble metals are rarely found in earth and are rather expensive, thus they are not suitable for large-scale applications. Therefore, it is of great importance to develop non-noble metal-based efficient electrocatalysts exhibiting high activities both in HER and HER.

Among different alternatives, transition metal dichalcogenides (TMDs) can be formed in different number of layers and exhibit diverse electronic properties and promising electrocatalytic active edge sites for electrochemical water splitting [2]. Various research approaches have been applied in order to obtain TMD materials with few layers structure. In the present work, conducting polymers (CPs) have been used as a conductive support to prepare hybrid/composite materials of TMDs [3-4]. CPs with their π-conjugated system exhibit unique electronic properties and used in various electrocatalyst production. Recently, the combination of CPs with TMDs has attracted much attention not only for understanding their fundamental properties but also for various applications [5].

Molybdenum diselenide ($MoSe_2$), as a typical TMD layered material, and its composites with conducting polymers such as polyaniline (PANI) and polypyrrole (PPy) were obtained via a facile hydrothermal method. The conducting polymers, PANI and PPy, were synthesized using oxidative chemical polymerization method. Different amounts of PANI or PPy were added into the solution of precursors of $MoSe_2$ to find the best content of the conducting polymer. The $MoSe_2$/CP composites were then applied in electrochemical water splitting. Electrochemical behaviours and electrocatalytic activities of the catalysts were investigated via cyclic voltammetry (CV) and linear sweep voltammetry (LSV) in alkaline solution and three-electrode configuration was used to determine the electrochemical parameters.

Acknowledgements
The Authors thank Programme SASPRO2 of the Slovak Academy of Sciences for financial support.

References

[1] C. Zhang, Y. Zhang, S. Zhou, C. Li, J. Alloys Comp. **818** (2020) 152833.
[2] S. Presolski, M. Pumera, Mater.Today **19(3)** (2016) 140-145.
[3] M. Omastová, M. Mičušík, Chem. Pap. **66(5)** (2012) 392-414.
[4] M. Omastová, M. Trchová, J. Kovářová, J. Stejskal, Synt. Met. **138(3)** (2003) 447-455.
[5] S. Cogal, S. Ramani, V.R. Bhethanabotla, J.N. Kuhn, ChemCatChem **13** (2021) 2017-2024.

Surface Properties of Zn-based Samples

V. Čákyová[a]*, R. Gorejová[a], R. Oriňaková[a]

[a] Department of Physical Chemistry, Faculty of Science, P. J. Šafarik University in Košice, Moyzesova 11, 041 54, Košice
*viktoria.cakyova@student.upjs.sk

The choice of biomaterials as implants and their overall functionality depends on factors such as biocompatibility, bulk properties (e.g., modulus of elasticity, hardness, toughness, strength) and surface properties (e.g., surface tension, surface roughness and surface energy). Successful acceptance of the implant and healing of the surrounding tissue depends on how fluids, proteins and cells interact with foreign material (implant). For this reason, the surface properties of the biomaterial, such as composition, charge, wettability, and roughness, must be optimized for the desired application and therefore studied [1]. Hydrophilicity and hydrophobicity are the first parameters that affect protein adsorption. Hydrophobic surfaces thermodynamically favor the adsorption of proteins from aqueous solutions, but also induce irreversible adsorption, which can lead to protein denaturation. On the other hand, hydrophilic surfaces can hinder protein adsorption. In addition, cell adsorption, which is crucial for proper osseointegration, takes place in the range of contact angle values of 60°-80° [2].

In this work, the contact angles of 3 types of uncoated Zn based biomaterials marked Zn, Zn-1Fe and Zn-2Fe were studied. Zn contains 100 wt% Zn. Zn-1Fe contains 99 wt% Zn and 1 wt% Fe. Zn-2Fe contains 98 wt% Zn and 2 wt% Fe. Contact angle measurements were performed by dropping water and diiodomethane onto the uncoated Zn, Zn-1Fe and Zn-2Fe. Volume of the droplet was 6μL. Measurement of contact angles of coated samples was not possible due to the high hydrophobicity of the PEG coated samples. For surface energy calculations were used equations (1), (2) and (3) [3].

$$\gamma_S = \gamma_S^D + \gamma_S^P \tag{1}$$

$$\gamma_S^D = \left(\frac{\gamma_{di}(\cos\theta_{di}+1) - \gamma_{wa}(\cos\theta_{wa}+1)\sqrt{\frac{\gamma_{di}^p \gamma_{wa}}{\gamma_{wa}^p}}}{2\left(\gamma_{di}^d - \sqrt{\frac{\gamma_{di}^p \gamma_{wa}^d}{\gamma_{wa}^p}}\right)} \right)^2 \tag{2}$$

$$\gamma_S^P = \left(\frac{\gamma_{wa}(\cos\theta_{wa}+1) - 2\sqrt{\gamma_S^D \gamma_{wa}^d}}{2\sqrt{\gamma_{wa}^p}} \right)^2 \tag{3}$$

Where γ is the total surface tension of the liquid, γ_L^D is the dispersion component of the surface tension of the liquid, γ_L^D is the polar component of the surface tension of the liquid. Together γ_L^D and γ_L^P gives γ. Table 1 shows the surface tension values for water and diiodomethane.

By using the contact angle measurement results to formulas (1), (2) and (3), we calculated the surface energy values of the uncoated samples. Table 2 shows these results. The highest surface energy value was observed for the sample of pure Zn, while for the samples of Zn-Fe materials the observed values were approximately half the value of pure Zn. Differences in the measured values can be attributed to the differences in the phase composition of the individual samples. From a contact angle value, we can say that the Zn sample is moderately hydrophilic, and Zn-1Fe and Zn-2Fe are slightly hydrophilic.

Table 1: Surface tensions of liquids used in the measurement of surface tenson components of prepared samples.

	γ (mN m^{-1})	γ_L^D (mN m^{-1})	γ_L^P (Nm m^{-1})
Water	72.8	21.8	51
Diiodomethane	51	48.6	2.4

Table 2: Values of contact angle and surface energy of uncoated samples.

Samples	Contact angle		Surface energy $\boldsymbol{\gamma_s}$ [mN/m]
	Water	Diiodomethane	
Zn	62.7 ± 7.21	30.45 ± 7.57	46.53
Zn-1Fe	91.55 ± 13.28	36.88 ± 5.17	22.16
Zn-2Fe	92.25 ± 9.53	42.77 ± 5.67	21.49

Acknowledgements
This work was supported by the project APVV-20-0278 of the Slovak Research and Development Agency.

References
[1] M. Saini, Y. Singh, P. Arora, V. Arora, K. Jain. World J. Clin. Cases. **3** (2015) 52-57.
[2] TT. Paterlini, LFB. Nogueira, CB. Tovani, MAE. Cruz, R. Derradi, AP. Ramos. Biophys. Rev. **9** (2017) 683-698.
[3] A. Rudawska, E. Jacniacka. Int. J. Adhes. Adhes. **29** (2009) 451–457.

Sodium Titanates as Anode for Sodium-ion Cells

O. Čech[a]*, L. Chladil[a], P. Čudek[a], T. Kazda[a]

[a]Department of Electrical and Electronic Technology, Faculty of Electrical Engineering and Communication, BUT, Technická 10, 616 00 Brno, Czech Republic
*cechondrej@vutbr.cz

Introduction

The Sodium-ion batteries are very promising complementary power sources to the lithium-ion batteries because they utilize the same principles and technology. At the cost of lower energy density, they can potentially offer solid energy storage system without the need of rarer elements – mostly lithium. Sodium is abundant element, it occupies 2.6 % of the Earth's crust and which is extremely easy to obtain.

The general sodium-ion battery working principle and it same as the well-known and described lithium-ion technology, which can significantly increase interest in their research use. Main drawbacks of sodium-ion technology lie in the fact, that no sufficient anode material, cheap, durable and with high energy density. Titanates, expecially the monoclinic $Na_2Ti_3O_7$ with layered structure, are promising candidates due to very low intercalation potential of Na+ ions.

This work is focused on the synthesis and electrochemical characterization of electroactive material for sodium ion battery anode based on sodium titanates with different crystallographic phases and Na/Ti/O

Experiment

Sodium titanate samples were prepared by microwave assisted hydrothermal reaction. Titanium isopropoxide (CAS 546-68-9), sodium hydroxide and hydrogen peroxide were used as the starting precursors. Hydrothermally treated precipitate was washed intensively by centrifugation and then calcined at temperatures 700 °C, 800 °C and 900 °C respectively. The purity and crystallographic composition of the samples were examined by XRD and the morphology was observed by SEM. Electrochemical behaviour was studied by cyclic voltammetry and galvanostatic cycling. All measurements were performed in three-electrode cells with metallic sodium as the counter and the reference electrodes. 1 mol/l $NaClO_4$ in the mixture of ED:DMC was used as an electrolyte.

Results and Discussion

Figure 1 shows the SEM images of pristine hydrothermally treated sample and samples prepared at 700°C, 800°C and 900°C respectively. The raw material shows foamy turbostatic structure unlike the calcined materials are crystalline consisting of nanorod-shaped crystals. The size of the crystals differs significantly with temperature applied in final calcination where higher temperature gains crystals with same length but higher diameter. All the samples were cooled down naturally at the end of the calcination and the difference in crystal size can be caused by different cooling time.

XRD data depicted at Figure 4 show that calcination below the temperature of 800 °C does not produce result with purely two desired phases but residual peaks from raw hydrothermally treated powder are still present. The phase composition of samples prepared at 800°C and 900°C does not change with temperature but on the other hand, the SEM images revealed that at temperatures higher than 800 °C the thickness of the crystallites grows rapidly. Under these conditions, sample prepared at 800 °C with crystallographic composition of 42% $Na_2Ti_3O_7$ to 58% $Na_2Ti_6O_{13}$ was selected for further electrochemical characterization by electrochemical impedance spectroscopy, cyclic voltammetry and galvanostatic cycling.

Cyclic voltammetry shows two peaks at both oxidation and reduction pasts. It was shown previously that each peak corresponds to the intercalation into a different crystallographic phase occurring in the sample. Voltammograms captured at scan rate 2mV/s depicted on Figure 2 exhibit very good stability, it is obvious that the material undergoes formation until it reaches stable state. It is also clearly shown that there is a significant change between the first and

the rest of the cycles pointing to irreversible capacity. Figure 2 shows cyclic voltammograms performed at 0.1 mV/s and there is some increase of peak currents also apparent between the first and the second cycle. The lower peak at 0.3V at anodic direction splits into two separate peaks at the lower scan rate showing possible surface activity and pseudocapacitive behaviour of the sample in this region.

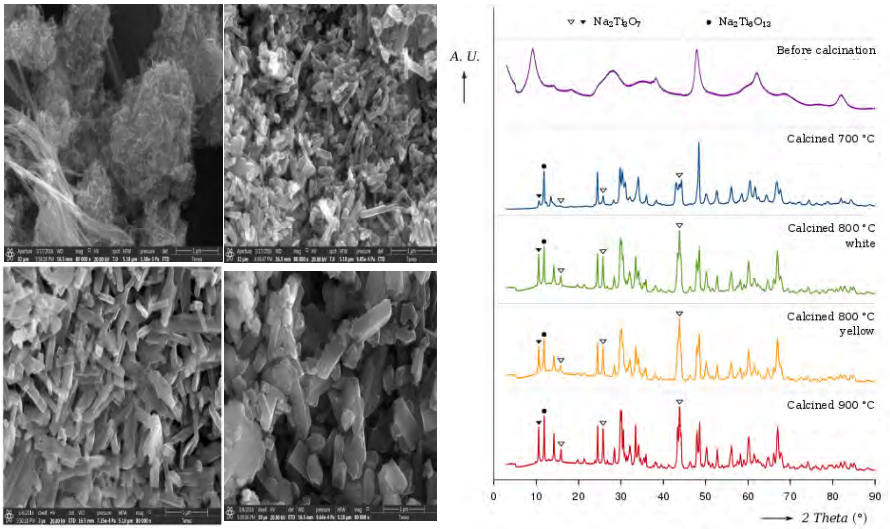

Figure 3: SEM images and XRD spectra of hydrothermally synthesized $Na_2Ti_3O_7/Na_2Ti_6O_{13}$ mixed titanate showing a) pristine material after hydrothermal treatment b) calcination at 700 °C c) calcination at 800 °C d) calcination at 900 °C.

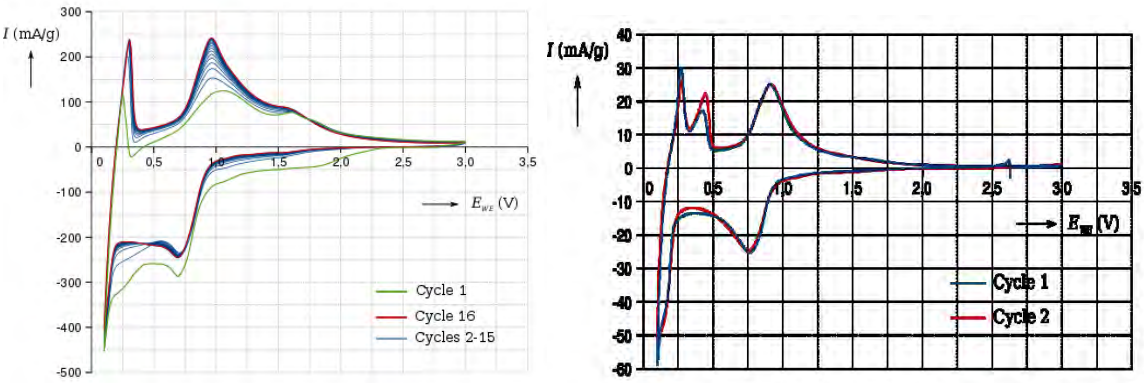

Figure 2: Cyclic voltamogram of $Na_2Ti_3O_7/Na_2Ti_6O_{13}$ mixed sample prepared at 800°C gathered at 2mV/s and 0.1mV/s.

Initial charge capacity of the sample at the rate of C/50 was 160 mAh/g with discharge capacity of 90 mAh/g. It indicates high irreversible capacity in the first cycle, as shown in Figure 7 but such result can be also given by extremely low current rate in the first cycle.

Figure 3 is a graph showing another 4 cycles obtained at the discharge rate of C/5 with stable discharge capacity of 65 mAh/g.

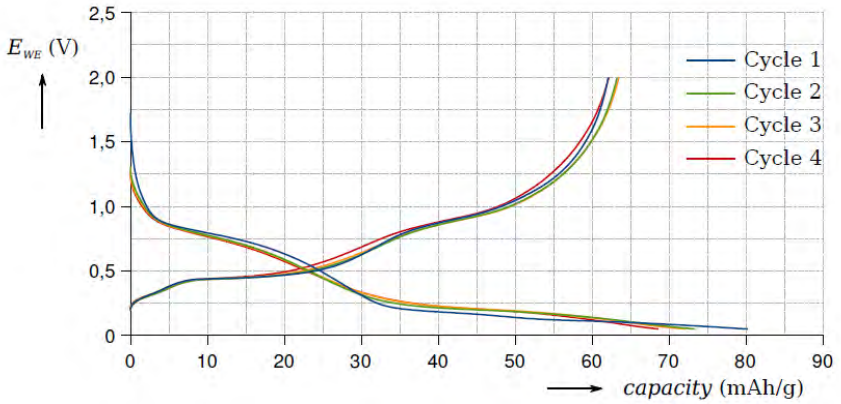

Figure 3: Four charge/discharge cycles of mixed titanate with current rate 0.2 C.

Conclusion

Nanostructured sodium titanate with mixed stoichiometry was successfully synthesized by calcination of hydrothermally treated pristine titanate. Structural characterization showed that the powder calcined at 800 °C consists of nanorods less than 1 μm long with diameter less than 100 nm. Phase composition was 42 % of $Na_2Ti_3O_7$ and 58 % of $Na_2Ti_6O_{13}$ as was examined by XRD.

Electrochemical activity with respect to reversible intercalation of sodium ions was also proven. The results of the cyclic voltammetry show stable material undergoing further formation during cycling. Initial discharge capacity at the first cycle was 90 mAh/g at C/50 and at further cycling applied C/5 the material exhibit capacity 65 mAh/g .

Acknowledgements

CzechNanoLab project LM2018110 funded by MEYS CR is gratefully acknowledged for the financial support of the measurements/sample fabrication at CEITEC Nano Research Infrastructure. This work was supported by the specific graduate research of the Brno University of Technology No. FEKT-S-20-6206. Authors also gratefully acknowledge the financial support from the Ministry of Education, Youth and Sports of the Czech Republic under project No. LTT19001 and Technology Agency of the Czech Republic project Ellytemat (No. TK04030083).

Electrical and Thermal Properties of Elastomer Nanocomposites with Hybrid Carbon Based-Nanofillers

T. Evgin [a,b]*, H. D. Koca [c], M. Mičušík [a], J. Preťo[d], A. Turgut [c], M. Omastova [a]

[a] Polymer Institute of the Slovak Academy of Sciences, Dúbravská cesta 9, 845 41 Bratislava, Slovakia
[b] Dokuz Eylul University, Engineering Faculty, Mechanical Engineering Department, Tinaztepe Campus, 35397, Buca, Izmir, Turkey
[c] Dokuz Eylul University, The Graduate School of Natural and Applied Sciences, Mechanical Engineering Department, Tinaztepe Campus, 35397, Buca, Izmir, Turkey
[d] Vipo, a.s., Generála Svobodu 1069/4, 958 01 Partizánske, Slovakia
*tuba.evgin@deu.edu.tr

One of the significant issues for electronic devices is thermal management for their manucfactuıres with long service life and high work stability [1]. However, electrical insulation and thermal dissipation are challenging issues for rubber nanocomposites. As compared to ceramic and metal filler materials, it is considered that carbon-based nanofillers are suitable candidates to obtain advanced nanocomposites because of their superior thermal, electrical, and mechanical properties [2]. Nevertheless, the dispersion of carbon-based nanofillers is a crucial problem in rubber nanocomposites. To overcome this problem, the use of different carbon-based nanofiller combinations is a good way to get balance cost and properties [3].

Present work deals with the electrical and thermal properties of ethylene propylene diene monomer (EPDM)-based nanocomposites containing hybrid nanofillers (graphene nanoplatelets (GnPs, 5 phr) and multiwall carbon nanotubes (MWCNTs, 1, 3 and 5 phr)). The nanocomposites were fabricated by melt mixing in Brabender Plasticorder PLE 331 internal mixer (Brabender GmbH, Germany) with a 30 ml mixing chamber at 100 °C for 7 min of total mixing time at 50 rpm of mixing speed. The samples for the measurements were vulcanized using compression molding by using a hot press (Fontijne 200, Fontijne, The Netherlands) at 160 °C without pressure for 30 sec and under pressure (5 MPa) for 10 min. Broadband dielectric spectroscopy (BDS) measurements were conducted using a Novocontrol Concept 40 instrument with an Alpha dielectric spectrometer supplied by Novocontrol Technologies GmbH (Germany). The thermal diffusivity of the samples was measured by the photothermal radiometry technique (PTR) which is a non-destructive characterization method based on the detection of an infrared (IR) signal, called the photothermal signal, emitted after a change of the sample's temperature [4].

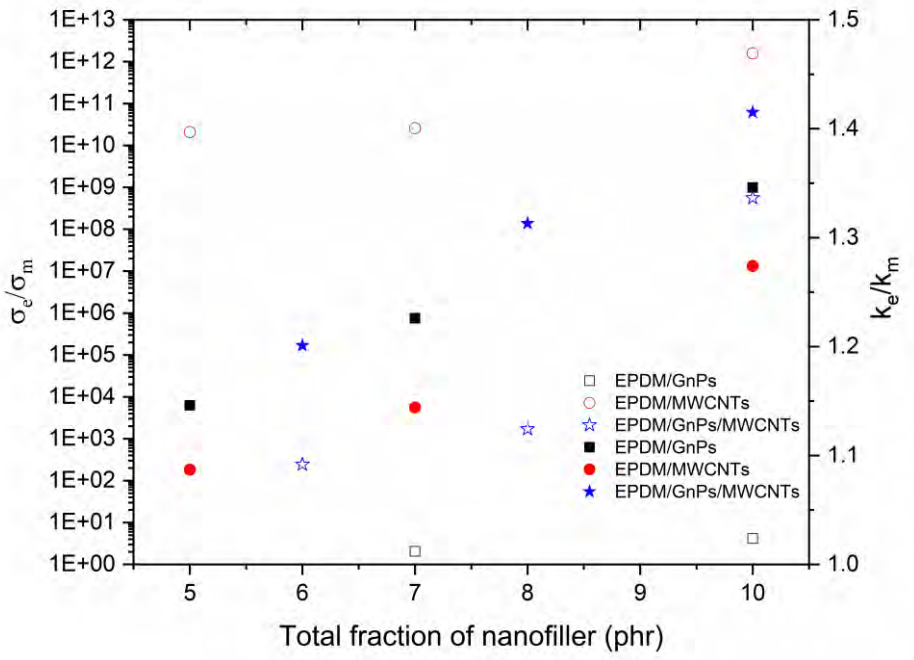

Figure 1: Relative electrical and thermal conductivities of EPDM-based nanocomposites (e: nanocomposites, m: matrix, open and filled symbols show relative electrical (σ) and thermal (k) conductivities, respectively).

The relative electrical and thermal conductivity of hybrid nanocomposites are given in Figure 1. The values of EPDM/GnPs and EPDM/MWCNTs are also included for a better comparison. As seen in Figure 1, electrical and thermal conductivities of samples increase with increasing total nanofiller loading. The electrical conductivity of the pure EPDM matrix is 8.67×10^{-16} S/cm. The values of nanocomposites are bounded between those of the EPDM/GnPs and EPDM/MWCNTs nanocomposites, i.e. only the additive effect of GnPs and MWCNTs is observed, not the synergic one. For example, for 10 phr of nanofiller loading, while the electrical conductivities of the EPDM/GnPs and EPDM/MWCNTs nanocomposites are 9.69×10^{-16} and 1.37×10^{-3} S/cm, respectively, this value is 4.85×10^{-7} S/cm for EPDM-based nanocomposites containing 5 phr of GnPs and 5 phr of MWCNTs.

MWCNTs and GnPs demonstrate a clear synergic effect in enhancing the thermal conductivity of hybrid nanocomposites. The hybrid nanocomposite with 5 phr of GnPs and 5 phr of MWCNTs exhibits an increase of 41.5 % over the pure EPDM matrix, while the EPDM/GnPs and EPDM/MWCNTs nanocomposites with 10 phr nanofiller loading show 34.6 % and 27.4 % enhancements, respectively. In EPDM-based hybrid nanocomposites, MWCNTs (1D) can create a bridge between the adjacent GnPs (2D) and ensure extra channels to the phonon bypassing the EPDM matrix. Thus, the phonons exhibit a longer mean free path, which improve the thermal conductivity. As comparing our results with the literature, Zhang et al. [5] found a 40.4 % k increment in the EPDM/MWCNTs nanocomposites at 40 phr nanofiller content, and Binzahi et al [6] found that the addition of 10 phr MWCNTs raised the k of the EPDM up to 44.3 %. Lu et al [7] demonstrated that k enhancement of EPDM/GnPs nanocomposites is 243.5 % at 8 wt. % (~12 phr) of GnPs. Araby et al. [8] found that ~5.7 vol. % (~17 phr) GnPs enhance the thermal conductivity of the elastomer by 38.9 %. When compared to the published results, the obtained results showed a slight improvement in the k values of EPDM-based nanocomposites with hybrid nanofillers.

Conclusions

The incorporation of GnPs and MWCNTs into the EPDM matrix showed a distinct synergic effect on the thermal conductivity, while an additive effect on the electrical conductivity was observed. The EPDM-hybrid nanocomposites exhibit low electrical conductivity up to 10 phr of total nanofiller content, but increased thermal conductivity, Potential applications of hybrid carbon based-nanofillers filled elastomer composites could be in the field of tyre components, sensing devices, or electrical shielding and electrical heating materials.

Acknowledgments

This work was supported by Research and Development Agency under contract no. APVV-20-0593, and by project VEGA 02/0006/22. Tuba Evgin's stay at Polymer Institute SAS in Bratislava was supported by the National Scholarship Programme of the Slovak Republic.

References

[1] A. Ma, X. Wang, Y. Chen, J. Yu, W. Zheng, Y. Zhao, Y. Compos. Commun. **13** (2019) 119-124.
[2] G. Spinelli, R. Guarini, R. Kotsilkova, E. Ivanov, V. Romano, Nanomaterials, **11(6)** (2021) 1511.
[3] L. Valentini, S. B. Bon, M. A. López-Manchado, R. Verdejo, L. Pappalardo, A. Bolognini, A. Alvino, S. Borsini, A. Berardo, N. M. Pugno, Compos. Sci. Technol. **128** (2016) 123-130.
[4] D.P. Almond, P.M. Patel, *Photothermal Science and Techniques,* Springer Netherlands; 1996.
[5] X.G. Zhang, Y.J. Ji, S.G. Wang, Q.L. Hou, Appl. Mech. Mater. **184** (2012) 1221-1225.
[6] H. Bizhani, A.A. Katbab, E. Lopez-Hernandez, J.M. Miranda, R. Verdejo, Polymers, **12** (2020) 858.
[7] S. Lu, Y. Bai, J. Wang, D. Chen, K. Ma, Q. Meng, X. Liu, Nano. **14 (2019)** 1950075.

Hemolysis and Thrombogenicity of Zn-2Fe Degradable Materials Coated with Fucoidan and Ciprofloxacin Doped Polymers

R. Gorejová[a]*, Kadir Özaltin[b], R. Oriňaková[a]

[a] Department of Physical Chemistry, Faculty of Science, P.J. Šafárik University in Košice, Moyzesova 11, 041 01, Košice, Slovak Republic
[b]Centre of Polymer Systems, University Institute, Tomas Bata University in Zlín, Třída Tomáše Bati 5678, 76001 Zlín, Czech Republic
*radka.gorejova@upjs.sk

Biodegradable metallic devices for orthopaedical applications are expected to corrode *in vivo* during the remodelation of a new bone tissue. Magnesium, iron, and zinc-based materials are commonly used as a metal substrate which is often refined either by the surface or bulk modifications [1]. The preparation of alloys and the functional surfaces is among the most frequent ways of modifying metallic absorbable scaffolds [2]. The application of coatings is known for its positive effect on corrosion acceleration as well as biological properties [3]. At the same time, the alloying of zinc alloys proved to be a suitable way of improving their otherwise insufficient mechanical properties. All these materials must possess favourable biological performance, be non-toxic and anti-allergic. Moreover, it is necessary to study the behaviour of the metallic implants in direct contact with human blood. The ideal material must not be thrombogenic and at the same time must not cause an inappropriate hemolysis (red blood cells disruption). Marine sourced polysaccharides are known for their positive effect on thrombogenicity [4] while the antibiotics are commonly used to improve antibacterial properties of the biomaterial coatings. Polymer coated materials with added bioactive components (fucoidan, ciprofloxacin) have been prepared and their hemocompatibility was studied and evaluated.

Zinc-based metallic substrate with the chemical composition of 99 wt% of zinc and 2 wt% of iron was prepared from the metallic powders via powder metallurgical route. The green compacts in the form of cylinders (Ø = 1.2 cm, *d* = 0.4 cm) were prepared by the cold pressing of powders mixture at 600 MPa. Compacts were heated from room temperature to 350 °C, held at the 350 °C for 60 min and cooled to room temperature spontaneously. The sintering took place under inert atmosphere. Radio frequency (RF) air plasma was applied for 60 seconds to activate metallic sample surface before the coating application. Polyethyleneimine (PEI, 10 wt/v% in ethanol) and poly(lactic acid) (PLA, 2.5 wt/v% in dichloromethane) coating solutions were prepared and applied by the sol-gel method. Ciprofloxacin (CPR) loaded fucoidan (FU) (0.1 wt% of CPR) second coatings were prepared from aqueous solutions with the intention to enhance the anticoagulant and antibacterial properties of the material (**Fig. 1a**). Hemolysis and thrombogenic properties (platelet adhesion observed by the scanning electron microscopy) were studied and evaluated.

Hemolysis ratio of the prepared uncoated and PEI-FU-CPR/PLA-FU-CPR coated samples was found to be 3.65%, 12.25% and 2.12% for the uncoated Zn-2Fe, PEI-FU-CPR coated and PLA-FU-CPR coated samples, respectively. While the hemolysis for the uncoated and PLA-FU-CPR coated samples fell below the 5% threshold and could be marked as only slightly hemolytic, PEI-FU-CPR coated samples showed inappropriate hemolysis (over 5%) which ranks them among non-hemocompatible materials. This effect could be induced by the PEI coating due to its polycationic nature. On the other side, PLA coating showed positive effect on the hemolysis when compared to the uncoated metallic material. Platelet adhesion test (**Fig. 1b-g**) showed only the solitary platelets on the surface of the pure Zn-2Fe material (**Fig. 1b, e**) while the areas with the increased numbers of platelets were found on both PEI-FU-CPR (**Fig. 1c, f**) and PLA-FU-CPR (**Fig. 1d, g**) coated samples. Rather spherical, non-activated platelets with no spread filopodia were mostly found on the surface of all the studied samples. These results highlight the need to select a suitable polymeric coating material. Based on them, PLA was found to be more suitable for future applications. The influence of fucoidan depending on its concentration and the antibacterial activity of the prepared materials will be further studied.

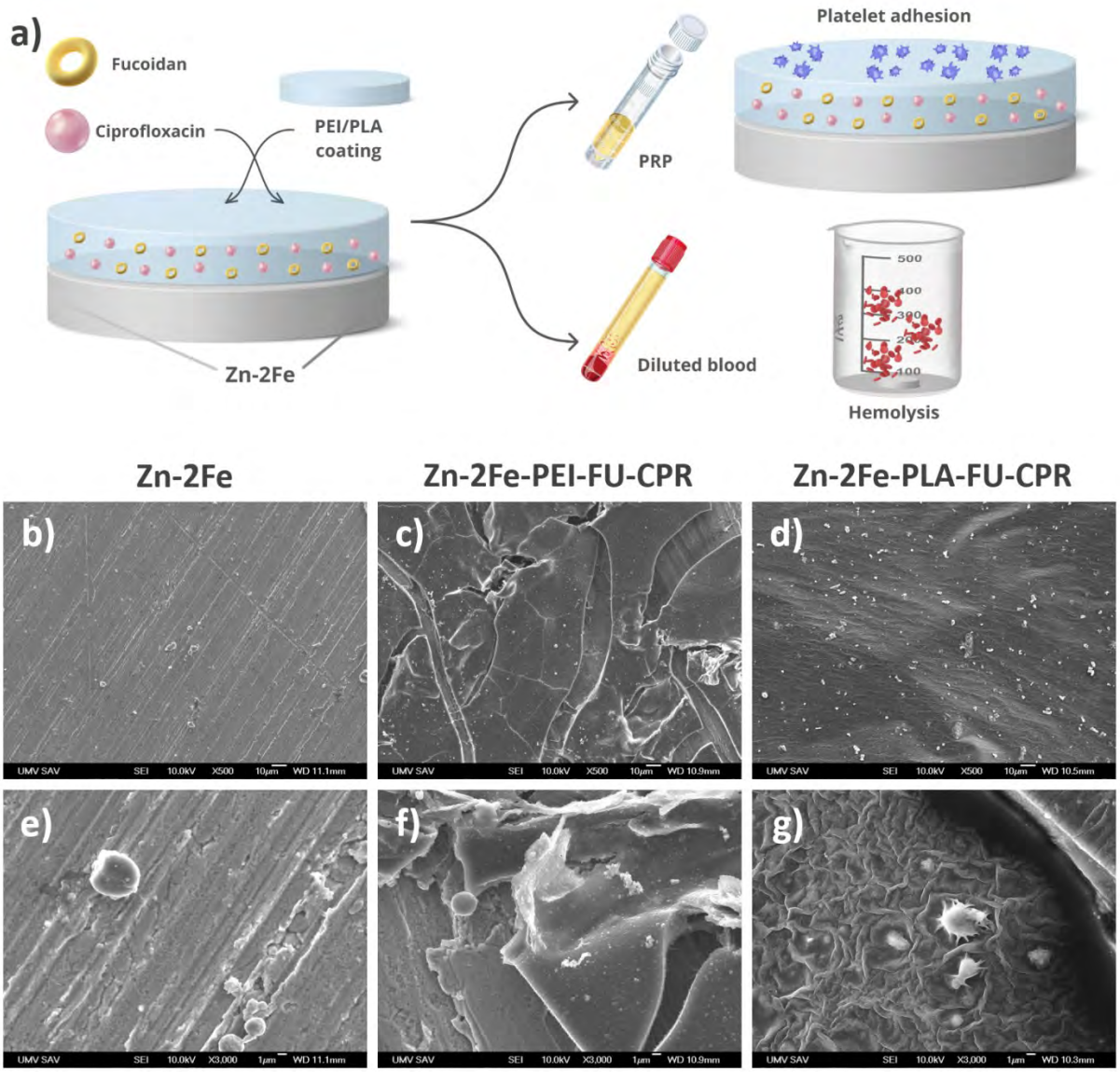

Figure 1: Schematic representation of the experimental design (a). Scanning electron microscopy (SEM) images of platelet distribution on the surface of Zn-2Fe (b,e), Zn-2Fe-PEI-FU-CPR (c,f) and Zn-2Fe-PLA-FU-CPR (d,g) degradable biomaterials.

Acknowledgements
This work was supported by the Slovak Research and Development Agency (project no. APVV-20-0278).

References

[1] H. Dong et al. Corr. Sci. **182** (2021) 109278.
[2] W. Yuan et al. Bioactiv. Mater. **7** (2022) 192-216.
[3] M. Hussain et al. Coatings. **11(7)** (2021) 791.
[4] K. Štepánková et al. Int. J. Mol. Sci. **23(13)** (2022) 7439.

Phosphated Metal Foams for Cost-Effective Catalysis of Hydrogen Evolution Reaction

A. Gubóová[a]*, R. Oriňaková[a], M. Strečková[b], M. Paračková[a]

[a] Department of Physical Chemistry, Faculty of Science, P.J. Šafarik University in Košice, Moyzesova 11, 041 54, Košice

[b] Institute of Materials Research, Slovak Academy of Sciences, Watsonova 47, 040 01 Košice

*alexandra.guboova@student.upjs.sk

Alkaline electrolysis in general can be described as the use of an electrical current passing through an electrolysis cell causing the decomposition of water to generate hydrogen gas. In an electrolysis cell two electrodes containing an electrocatalyst, separated by a physical barrier, a polymeric diaphragm which only allows the passing of ions from one electrode to another, are connected to a current source. Hydrogen gas is produced at the cathode while oxygen is produced at the anode. The electrodes are in contact with an electrolyte which provides OH^- ions, from a 20%–30% solution of KOH that completes the electrical circuit [1].

The biggest advantages of alkaline electrolysis systems are their robustness, long lifetime, and lower costs due to cheaper electrode materials [2]. The most common cathode material in alkaline electrolysers is nickel, usually with catalytic coating. Ni-based nanomaterials are excellent alternatives to widely used but expensive platinum due to similar chemical properties, same group number in periodic table, cut-price, and abundant quantity of Ni [3]. Besides, pure nickel maintains an extreme strength and durability at high temperatures, coupled with a good resistance level, even up to the point of downstream processing. At the same time, it has a comparatively high temperature coefficient of resistance (at 0.00600 1/°C) without losing its good conductivity. At room temperature, nickel endures environmental influences such as air, water, and hydrochloric acid [4].

Nickel, nickel-iron, and iron foams were prepared utilizing easy and cheap replication method from polyurethane matrix, which is coated with metal slurry and sintered to obtain porous sample. The phosphating of the prepared metal foams was a two-step process that proceeded according to reference [5]. Firstly, the surface of foams was cleaned by sonication in water, acetone, and hydrochloric acid. Then the cleaned foams were dried and loaded on a ceramic boat which contained $NaHPO_2.H_2O$ powder and placed under a stream of nitrogen atmosphere in an oven heated to 300°C with a heating rate of 1°C/min. The samples were kept at this temperature for 2 hours before being cooled back to room temperature, rinsed and dried.

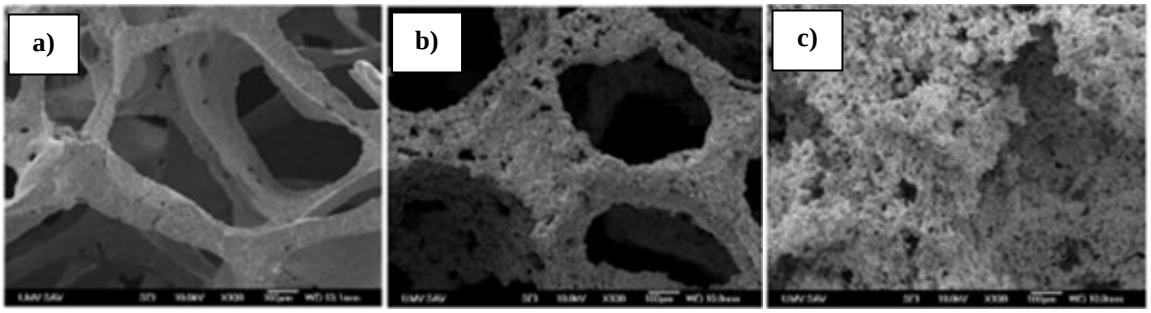

Figure 4: SEM images of basic and modified metal foams with 100x magnification a) FeP b) FeNiP c) NiP.

SEM images of phosphated foams together with EDX analysis confirmed the presence of phosphorus. As can be seen from Fig. 1, structure of foams obviously deteriorates with higher nickel percentage. Iron foams have clearly defined pores with pore size around 733±55 μm and wall thickness 72±6 μm while FeNiP foams have thicker walls ~156±29 μm and smaller pores ~438±61 μm. For NiP foams it is hard to precisely determine the size of macropores about 440±126 μm while thickness of walls ranges at 217±104 μm.

To evaluate catalytic activity of prepared samples towards hydrogen evolution reaction, polarization curves were recorded and recalculated toward reversible hydrogen electrode. Graph (Fig. 2) shows LSV curves for iron and nickel foams as well as their ratios 1:9, 1:1 and 9:1. As expected, pure nickel foam showed the best catalytic performance, followed closely by Fe10Ni90.

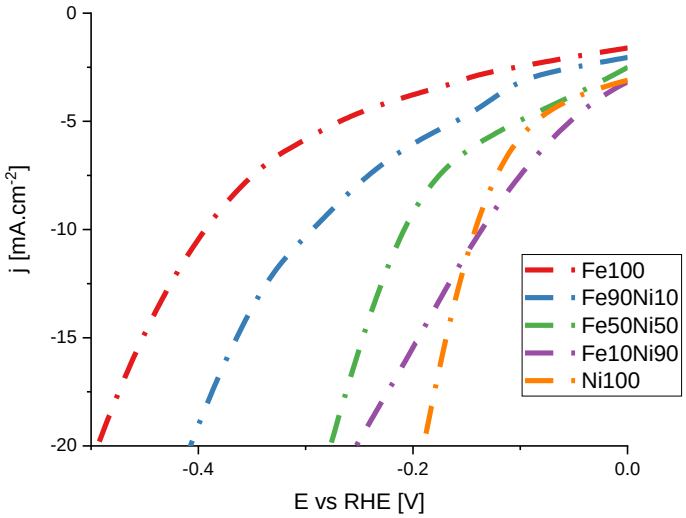

Figure 5: Polarization curves of metal foams in 1M KOH.

Graph 3 shows polarization curves for phosphate foams. NiP demonstrates the highest activity toward hydrogen evolution, with overpotential needed to achieve current density of -10 $mA.cm^{-2}$ only -161 mV. Overpotentials for FeP and FeNiP achieved values 378 mV and 343 mV, respectively.

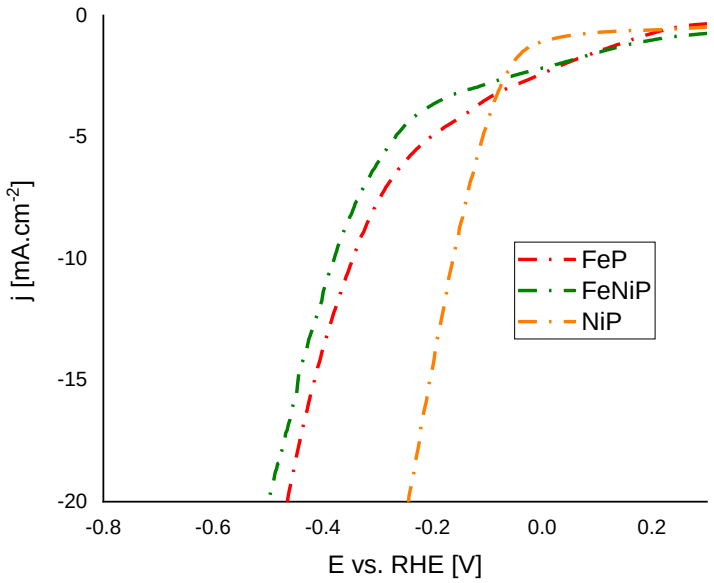

Figure 6: Polarization curves of phosphated metal foams in 1M KOH.

Acknowledgements

This work was supported by Slovak Research and Development Agency under the contracts no. APVV-20-0576 (Green ambitions for sustainable development (European Green Agreement in the context of international and national law), no. APVV-20-0299 (Electrocatalysts for efficient hydrogen production for future electrolysers and fuel cells) and Grant Agency of Slovak Academy of Sciences, project no. VEGA 1/0095/21(Application of innovative nano catalysts and DFT simulations for efficient hydrogen production).

References

[1] A. M. Fernnández, U. Cano, *Alkaline Electrolysis with skeletal Ni catalysts* in: *Electrolysis* (V. Linkov, J. Kleperis eds). IntechOpen, London UK
[2] M. Bodner et al., Wiley Interdisciplinary Reviews: Energy and Environment **4** (2014) 365–381.
[3] Sultan et al., Acs. Catalysis **7** (2017) 7196-7225.
[4] Deevi et al., Intermetallics **4** (1996) 357-375.
[5] J. Xing et al., Materials Research Society **33** (2017) 556-567.

Investigation of the Growth Mechanism and Optical Properties of Heterostructures of Binary and Ternary Chalcogenide Nanocrystals

A. Haque[a], F. Zechel[a], M. Sykora[a*]

[a]Laboratory for advanced materials, Faculty of Natural Sciences,
Comenius University, 842 15 Bratislava, Slovakia
*sykoram@uniba.sk

Over the past several decades, the colloidal synthesis has been established as an effective techique for rapid and economic preparation of nanocrystals (NCs) of metals, alloys, core-shell, and composites with narrow size distribution, reproducible control of particle size and shape and good crystallinity. In the hot injection method, the surfactants with appropriate functionalities (e.g., alcohols, acids, amines, and thiols) interact with the surface of the particles to stabilize the growth of particles and protect the particles from sedimentation, aggregation, and formation of surface defects. The growth of the NCs can be conveniently controlled by the choice of the appropriate ligand(s), solvent(s), reaction time and temperature. Thanks to the advantages of the hot-injection colloidal method the NCs found various applications in the solution-processable devices or thin film technologies. In our reserach we have been using hot injection colloidal synthesis methods for preparation of several new classes of nanomaterials with practical potential. In the first part of my presentation, I will discuss one example, where we used this approach to prepare novel ternary chalcogenide NCs. In the second part, I will discuss the preparation and characterization of core-shell heterostructures of binary chalcogenide nanorods (NRs)

Ternary chalcogenides are emerging as a promising material for applications in photovoltaics and photocatalysis. In 2017, Zunger et. al. predicted solar cell with the theoretical power conversion efficiency of 28% for a 300 nm thick absorber of $CuTaS_3$ [1]. For these applications, Cu-Ta-S ternary chalcogenide NCs would be particularly useful, as they are suitable for solution-processed device fabrication. However, a method for the preparation of Cu-Ta-S ternary chalcogenide NCs was not yet described in the literature. An understanding of the growth mechanism of such NCs systems is required for the rational synthesis of Cu-based ternary chalcogenides. In my talk, I will discuss a method we have recently developed for the preparation of copper tantalum sulfide NCs by hot injection colloidal synthesis [2]. Due to its soft Lewis acid nature, Cu^+ reacts with CS_2, a soft Lewis base, to form cubic $Cu_{2-x}S$. The Ta gets incorporated into the $Cu_{2-x}S$ NCs at the Cu vacancy site, followed by the diffusion through the lattice. DFT calculations suggest that Ta prefers to occupy the Cu vacancies in $Cu_{2-x}S$, followed by Ta diffusion into the lattice. The strength of the energy barrier for Ta diffusion is similar for {100}, {110} and {111} surfaces, which allows the nucleation growth of Cu_3TaS_4 uniformly through all facets as observed in high-resolution transmission electron microscopy images (see Fig. 1a). High energy barriers found along the Ta diffusion path compared to Cu atoms imply that the reaction is controlled by the sluggish Ta diffusion, which is the origin of the core-shell structure found in NCs.

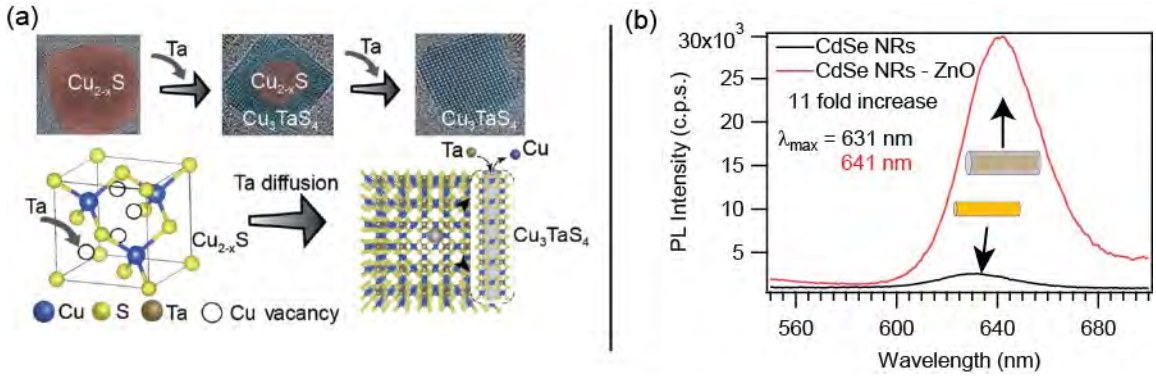

Figure 1: (a) Insights into the growth of Cu_3TaS_4 NCs. Initial $Cu_{2-x}S$ have Cu vacancies. Ta incorporation occurs in the $Cu_{2-x}S$ NCs at Cu vacancy sites, and form core-shell heterostructure and Finally they transform into Cu_3TaS_4 NCs followed by the diffusion of Ta by replacing Cu into the lattice. (b) PL spectra of core CdSe NRs and core-shell CdSe-ZnO heterostructures.

Cadmium selenide (CdSe) NCs such as quantum dots (QDs), rods (NRs), and platelets have been widely explored due to their size and shape-tuneable electronic properties, induced by the quantum confinement effects [3]. A particularly interesting category of these materials are nano-heterostructures, which combine two or more semiconductor materials. The combination of materials can give rise to novel optical and electronic properties, with practical utility in applications such as QD Lasers, displays, optical communication, light-emitting devices, biotechnologies, and others. In the case of spherical NCs, these nanostructures are known as core-shell quantum dots (csQDs). It has been experimentally observed that such csQDs exhibit improved photoluminescence (PL) efficiency over that of the bare QDs and the variation in the thickness of the shell can be used to tune the optical and electronic properties of these QDs [4]. In our work, we have investigated the variability in the electronic properties of CdSe/ZnO core-shell heterostructures with different dimensionalities, specifically csQDs and NRs. We prepared new structures and studied the size and investigated the influence of shell thickness on the optical properties. While CSQDs have been studied previously, core-shell CdSe/ZnO NRs have been prepared and investigated for the first time. Additionally, we evaluated the radiative lifetime of the core-shell for different sizes of core and thicknesses of the shell. A systematic increase in PL intensity has been observed in the core-shell NRs (see Fig. 1b). Also, the radiative lifetime increases after the shelling of the cores. We propose that the passivation of surface states, along with increased localization of the hole in the core CdSe layer, gives rise to an increase in the photoluminescence quantum yield.

Acknowledgements
This work was supported by the European Union's Horizon 2020 research and innovation programme under grant agreement No. 810701 and by the Slovak Research and Development Agency under grant agreement No. APVV-19-0410 and the Slovak Ministry of Education Grant. No. VEGA 1/0892/21.

References
[1] J. Heo, L. Yu, E. Altschul, B. E. Waters, J. F. Wager, A. Zunger and D. A. Keszler, Chem. Mater. **29** (2017) 2594–2598.
[2] A. Haque, S. Ershadrad, C T. Devaiah, D. Saha, B. Sanyal, P. K. Santra, J. Mater. Chem. A (2022) Advanced article. DOI: 10.1039/D2TA02714C.
[3] L. Li, J. Hu, W. Yang, A. P. Alivisatos, Nano Lett. **1** (2001) 349 – 351.
[4] V. V. Nikesh, S. Mahamuni, Semicond. Sci. Technol. **16** (2001) 687.

Catalyst Coated Membranes for Alkaline Water Electrolysis

J. Hnát[a]*, M. Plevová[a], J. Žitka[b], K. Bouzek[a]

[a] University of Chemistry and Technology in Prague, Technicka 5, 166 28 Prague 6, Czech Republic
[b] [1]IMC CAS, Heyrovského nám. 2, 16206 Prague, Czech Republic
*hnatj@vscht.cz

Introduction

Alkaline water electrolysis represents a technology with more than 100 years of history. It can thus be considered mature and well established. However, since the time of World War II, alkaline water electrolysis technology has been continuously replaced by alternative fossil sources-based technologies such as steam methane reforming (SMR) for hydrogen production. The reason lies in the price of the hydrogen produced. As a consequence of economic reasons, 50 % of the hydrogen produced worldwide is produced by SMR technology and only about 2–4 % by electrolysis. However, water electrolysis technologies have grown in interest due to the possibility of connection with renewable sources of energy (RSE), in recent decades. With the RSE as the source of electricity for water electrolysis technologies, new demands arise. These are: *i*) high flexibility for balancing the overproduction of RSE, *ii*) high efficiency and intensity of production, and *iii*) high purity of hydrogen to allow direct usage in fuel cells. These and even more parameters can, in the case of alkaline water electrolysis, be achieved by replacing the diaphragm type of the electrode separator by the anion-selective one. Meeting these demands will allow to maximize the utilization of the RSE.

Furthermore, by using anion-selective polymer membrane, it is possible to use the catalyst-coated membrane (CCM) approach for membrane electrode assembly (MEA) preparation. The CCM-MEA approach has been studied for energy conversion systems utilizing proton exchange membrane (PEM), *i.e.* for PEM fuel cells and electrolyzers. CCM-MEA offers several advantages over the more traditional approach of catalyst-coated electrode (CCE). These benefits include, for example, high ionic contact for the catalyst particles with the solid electrolyte, which can increase catalyst utilization, especially in an environment with low ionic conductivity (diluted solutions of KOH or water) [1]. Higher catalyst utilization results, in principle, in lower catalyst load and a thinner catalyst layer. However, it is necessary to use anion-selective polymer binder to prepare CCM-MEA. This represents the main limitation of the CCM-MEA preparation because of the lack of stable and highly ionic conductive polymer binders. The polymer binder has two important roles as it has to ensure sufficient mechanical stability of the catalyst layer and at the same time establish ionic contact between the catalyst particles. On the other hand, the polymer binder is not an electron conductor, so its higher loading decreases the electron contact between catalyst particles. Thus, the amount of polymer binder must be monitored and optimized [2].

Another aspect of CCM-MEA preparation is connected with the different swelling of different polymer materials. In the case of the important differences in swelling, the compatibility of the membrane and catalyst layer can be low, which will result in catalyst layer delamination.

In this work, we first compare the CCS and CCM approaches and study the possibility of reducing the catalyst loading. Then, with CCM-MEA we further optimize the composition of the catalyst layer, study the effect of method of preparation, and study the influence of the membrane chemical structure.

Experimental part

Materials

Chloromethylated block copolymer polystyrene-ethylene-butylene-styrene (PSEBS-CM) functionalized with 1,4-diazabicyclo[2.2.2]octane (DABCO) groups (thicknesses of the membrane 60 and 250 μm) and Fumapem® FAA-3-50 membrane (60 μm) were used as membranes for the preparation of CCM-MEA. The solution of PSEBS-CM is also used as a binder for the catalyst layer. This material showed good ionic conductivity, ion-exchange capacity, and

stability in KOH solution at elevated temperature. $NiCo_2O_4$ and $NiFe_2O_4$ are used as anode and cathode catalysts, respectively. Ni foams without pretreatment are used as electrodes.

Synthesis

Both catalysts used were prepared by coprecipitation of the nitrate metal salts by NaOH. More information on synthesis and properties can be found elsewhere [3, 4]. The precipitates were washed and calcinated at 325 and 475 °C for the $NiCo_2O_4$ and $NiFe_2O_4$ catalyst, respectively. Air-brush spraying or computer-controlled ultrasonic dispersion of catalyst ink is used to prepare CCM-MEA.

Experimental methods

The prepared CCS-MEA and CCM-MEA were characterized in a laboratory single cell alkaline water electrolyzer by means of the load curves in the cell voltage range 1.5–2.0 V using different concentrations of KOH (1–15 wt%) at temperature 50 ° C. To identify the influence of membrane thickness, we used a membrane with a thickness of 250 or 60 μm. To have a deeper understanding of the system, electrochemical impedance spectroscopy (EIS) is used under MAWE conditions at a voltage of 0, 1.5 and 1.8 V in the frequency range 100 kHz–0.1 Hz with an amplitude of 10 mV. Scanning electron microscopy (SEM) is used to observe the morphology of the layers. The chosen CCMs undergo the stability test measured at 50 °C in 10 wt.% KOH at current density of 250 mA cm^{-2} for 160 hours.

Results and discussion

The results obtained show a significant influence of the catalyst layer thickness on its properties. It was observed that decrease of the catalyst load from 10 to 2.5 mg of catalysts cm^{-2} did not result in a decrease in the water electrolysis performance. In addition, thinner layers showed improved stability of the CCM-MEA.

With respect to composition of the catalyst layer it was observed that catalyst to polymer binder ratio (CBR) has a significant impact on the performance of the membrane alkaline water electrolysis. This was addressed to the electron conductivity of the catalyst layer. Electron conductivity measured for CBRs 50/50 and 80/20 in the cross-section direction showed an improvement of two orders of magnitude when the content of the polymer binder decreased from 50 to 20 wt.%. However, the optimal CBR for the anode and cathode was determined to be 93/7. Such CBR shows even better electron conductivity and has the possibility of establishing mechanical properties of the catalyst layer.

In the next step, two different methods of CCM-MEA were used. Air brush hand spraying was compared to computer-controlled ultrasonic dispersion deposition (CNC). The results showed that using CNC method, it is possible to decrease the cell voltage by 0.06 V and even improved stability of CCM-MEA. This is due to the higher homogeneity of the deposited layers using the CNC method.

The last but not least step was the comparison of membranes with different chemical structures, particularly block copolymer (PSEBS-CM-DABCO) and linear polymer-based membranes (FAA-3-50). Using the PSEBS-CM-DABCO membrane, the influence of thickness was evaluated, too. The results obtained during the stability test showed that the PSEBS-CM-DABCO membrane of thickness 250 μm achieved a cell voltage comparable to the FAA-3-50 membrane (50 μm). Reducing the thickness of the PSEBS-CM-DABCO membrane to 60 μm cell voltage during the stability test decreased by 0.08 V.

Conclusions

The results obtained show the possibility of: *i*) replacing CCS with CCM, *ii*) reducing the catalyst load by 75%, *iii*) improving performance with optimized catalyst/binder ratio, and *iv*) improving performance with reduction of the membrane thickness.

Acknowledgements
This project has received funding from the Fuel Cells and Hydrogen 2 Joint Undertaking under grant agreement No 875118. This Joint Undertaking receives support from the European Union's Horizon 2020 research and innovation programme, Hydrogen Europe and Hydrogen Europe research.

References
[1] J. Hnát, M. Plevova, R.A. Tufa, J. Zitka, M. Paidar, K. Bouzek, Int. J. Hydrog. Energy. **44** (2019) 17493-17504.
[2] M. Plevová, J. Hnát, J. Žitka, L. Pavlovec, M. Otmar, K. Bouzek, J. Power Sources. **539** (2022) 231476.
[3] D. Chanda, J. Hnát, M. Paidar, J. Schauer, K. Bouzek, J. Power Sources. **285** (2015) 217-226.
[4] D. Chanda, J. Hnát, M. Paidar, K. Bouzek, Int. J. Hydrog. Energy. **39** (2014) 5713-5722.

Impact of Layered Double Hydroxides on Properties of EPDM-Based Rubber Composites

J. Hronkovič[a], P. Meluš[a], J. Oravec[a], J. Preťo[a], I. Chodák[b], M. Omastová[b], M. Mičušík*[b]

[a]VIPO a.s., Gen. Svobodu 1069/4, 95801 Partizanske, Slovak Republic
[b] Polymer Institute of the Slovak Academy of Sciences Dúbravská cesta 9, 845 41 Bratislava, Slovak Republic
*matej.micusik@savba.sk

Introduction

Polymer composites containing nanofillers attract interest due to their novel and improved properties, among others, reduced gas permeability in contrast to the native polymer or conventional organic-inorganic fillers. Among nanofillers used in polymer composites there is a group of layered nanofillers, comprising, beside others, layered double hydroxides (LDHs), known as anionic clays [1].

The use of LDHs has been already reported in elastomer composites of ethylene-propylene-diene rubber (EPDM), acrylonitrile-butadiene rubber (NBR), chloroprene rubber (CR), silicone rubber (SR), and solution styrene butadiene rubber (SSBR). It has demonstrated that incorporation of LDHs into a rubber matrix can enhance mechanical and thermal polymer properties as well as reduce gas permeability [2].

The presented work summarises the initial study of the influence of an LDHs filler on basic properties of ethylene – propylene – diene terpolymer (EPDM) rubber and it is part of a more extensive research aimed at the application potential of selected nanofillers to reduce the diffusion of gasses and other low molecular weight substances through the elastomeric continuum.

Experimental

For composite preparation with rubber compounds Hydrotalcite 652288 was chosen. This nanofiller is a layered Mg-Al double hydroxide, a laboratory prepared product used in different technical and medicinal areas produced by Sigma-Aldrich Corp. St. Louis, Missouri, USA.

The experimental rubber compounds were prepared on the basis of ethylene-propylene-diene rubber (EPDM). Altogether, 6 types of EPDM rubber composites were prepared, containing 0, 0.5, 1, 3, 5 and 10 % - parts per hundred rubber (phr) of Hydrotalcite 652288. The following characteristics of the rubber compounds were determined:

Physico-mechanical properties

- Tensile strength & elongation
- Modules 50, 100, 150, 200 and 300%
- Hardness
- Density

Vulcanizing characteristics

- Induction time – TS2
- 90% of curing time – TC90
- Minimum torque – S'min
- Maximum torque – S'max
- Difference maximum torque – minimum torque – S'(max-min)
- Maximum curing speed – Peak Rate

Rheological characteristics

- Elastic modulus – G'
- Loss modulus – G″
- Complex modulus – G*
- Elastic viscosity – η'
- Loss viscosity – η"
- Complex viscosity – η*
- Dissipation factor – Tan(δ)
- Torque elastic component – S'
- Torque viscous component S"
- Complex torque – S*

Results and Discussion

To evaluate the statistical significance of the influence of Hydrotalcite 652288 on the determined properties of rubber compounds regression models of dependencies of respective properties on the filler concentration were created and analysed. The most important findings are as follows:

- The elongation modules drop significantly at the concentration of 0.5 phr, the maximum is reached at the concentration of 1.0 phr, and with further increase of the concentration the modules drop with the exception on module 50 %
- A statistically significant dependence exists between the filler concentration and elongation
- Except for the concentration of 0.5 phr the filler does not influence the rubber hardness
- Except for the concentration of 0.5 phr the filler increases the values of the induction time TS2 and the 90 % of curing time TC90, the highest increase being observed at the concentration of 0.5 phr
- The minimum torque S'min increases with higher concentration of the filler
- The values of the maximum torque S'max, the difference maximum torque, minimum torque S'(max-min) and the maximum curing speed Peak Rate are generally lower the those observed at the pure matrix, the lowest values being observed at the concentration of 0.5 phr
- At the concentrations of 0.5 and 10 phr the vulcanizing curves show significantly slower rate of vulcanization and maximum torques than the pure matrix
- The values of the complex modulus G* are generally higher than at the pure EPDM without nanofiller, the highest values being observed at the concentration of 3 phr
- Within the concentration range 0.5 – 5 phr the values of the dissipation factor Tan(δ) are generally lower than at the EPDM matrix without nanofiller, however with extremes observed at the frequency of 2 Hz, while at the concentration of 10 phr the values of the dissipation factor Tan(δ) are significantly higher than at the EPDM without nanofiller.

Conclusion

The experiments with the synthetic nanofiller Hydrotalcite 652288 incorporated in the EPDM matrix and subsequent statistical analyses thereof demonstrated the significant influence of the nanofiller on the rubber properties, while the most distinctive effects were observed at the filler concentration of 0.5 phr.

Acknowledgement
This work was supported by Research and Development Agency under contract no. APVV-20-0593, „Nanocomposites based on elastomeric blends with improved resistance to diffusion of gases including hydrogen“.

References
[1] R. Salomão et al.: InterCeram: International Ceramic Review. **62 (**2013) 187-191.
[2] A. Laskowska, A. et al.: eXPRESS Polymer Letters. **8** (2014) 374–386.

CO_2 Separation Using Mixed Matrix Membranes Based on 6FDA-BisP

K. Iablochkin[a], M. Z. Ahmad[a,b], M. Bernauer[a], V. Fila[a*]

[a]Department of Inorganic Technology, University of Chemistry and Technology Prague, Technicka 5, 166 28 Prague 6, Czech Republic
[b]GENERON IGS, 992 Arcy Lane, Building 992, Pittsburg, 94565 California, USA
*Vlastimil.Fila@vscht.cz

Introduction

Membrane technologies offer an alternative to conventional methods for gas separation. CO_2 separation from gaseous mixtures is applied in processes such as biogas purification or raw natural gas treatment. The incorporation of fillers into the polymer matrix enhances the gas separation performance of polymer materials, which leads to an increase in overall process efficiency.

The aim of this study was the preparation and characterization of mixed matrix membranes (MMMs) based on the novel polyimide 6FDA-BisP and fillers such as UiO-66 and ZIF-8. The XRD, BET, FTIR, TGA, DSC, SEM, and EDS methods were used to characterize prepared MMMs and the nanoparticles. The effect of the mass content and type of fillers on the separation efficiency and morphology of prepared membranes were studied. Permeation measurements were performed under the different cross membrane pressures (2, 4, 6, and 8 bar) with a model gas mixture containing CO_2 and CH_4 at different ratios (1/1; 3/1; 1/3).

Experimental

To synthesize 6FDA-BisP polyimide a classic two-step polymerization method was used. In the first step, the diamine and the dianhydride were reacted in N-Methylpyrrolidone under nitrogen atmosphere to obtain the polyamic acid solution (PAA). The second step was the imidization of the PAA through thermal annealing at 250 °C.

Dense membranes were prepared from 1 wt.% solution using chloroform as a solvent. The obtained solution was stirred for 24 h on the magnetic stirrer. Then, the homogeneous solution was casted on a Petri dish and dried under laboratory conditions for 2 days. The membranes were finally dried at 110 °C for 24 hours (**Figure 1.**)

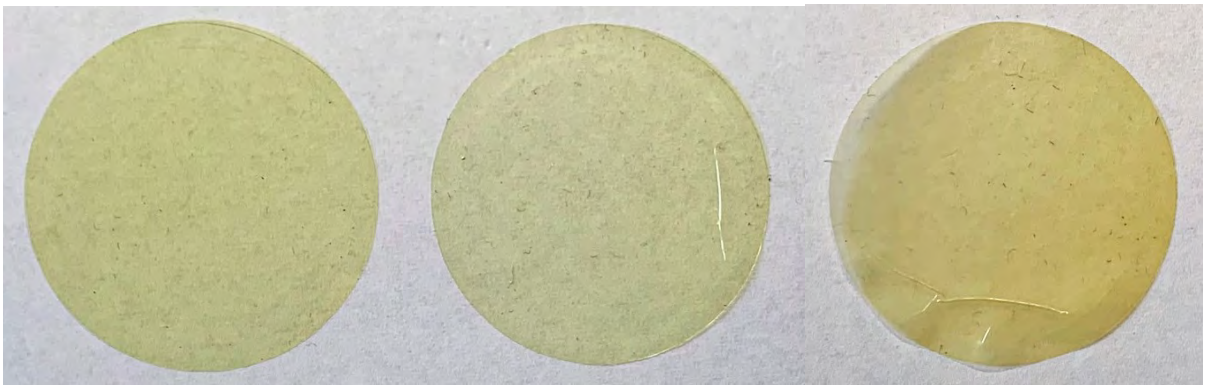

Figure 7: Prepared membranes a) 6Fda-BisP, b) 6Fda-BisP UiO-66 10%, c) 6Fda-BisP ZIF-8 10%.

CO_2 and CH_4 separation analyses were performed by the Wicke-Kallenbach method in a laboratory-scale module, using a pressure-rise permeation apparatus. The set-up scheme is presented elsewhere [1]. The analyses were carried out in steady-state conditions using a CO_2 and CH_4 mixture as feed and helium as a sweeping gas. The outlet mixture composition was analyzed using GC equipped with methanizer and FID detector.

Results and Discussion

The neat polymer 6FDA-BisP presented the permeability of 30 barrer and a selectivity of 41 (2 bar, CO_2/CH_4 1/1). The addition of the inorganic fillers had a positive effect on the membrane permeability in all prepared membranes. The best separation efficiency was measured for the MMM with 15 wt.% of ZIF-8 particles, where the CO_2 permeability of 135 barrer and selectivity of 42 were reached. In this case, the increase in permeability of CO_2 is around 335 % compared to the neat membrane. The MMMs based on UiO-66 presented relatively high values of permeabilities at similar selectivities. In the case of MMM with 15 wt.% of UiO-66, the increase in CO_2 permeability was around 155 % compared to the neat polymer with maintained selectivity. The results for the MMMs with 15wt. % of filler are summarized in **Figure 2.**

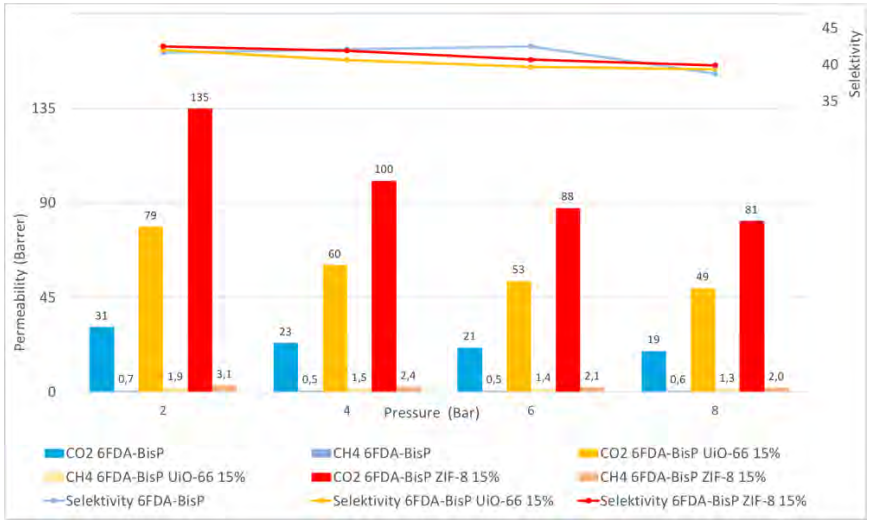

Figure 8: Gas permeability and selectivity of 6FDA-BisP and MMM, feed composition CO_2/CH_4 1:1.

Membranes based on ZIF-8 and UiO-66 fillers show a relatively good dispersion of particles in the entire volume of the polymer matrix. In the case of using the ZIF-8 particles, their distribution is slightly better than in the MMM with the UiO-66. The distribution is confirmed by EDS measurements. **Figure 3** presents the results from EDS analysis.Tthe occurrence of Zr ions of UiO-66 particles is marked by the blue color and Zn ions of ZIF-8 particles by the violet.

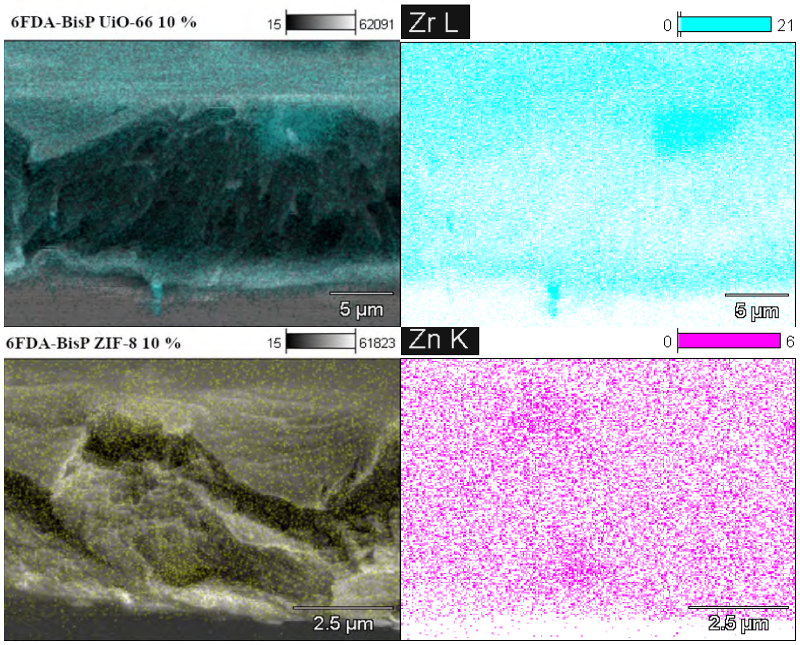

Figure 9: EDS photos of MMM with 15wt. %.

Conclusion

As part of this work, the synthesis procedure for the preparation of polymer based on 6FDA anhydride was optimized. The synthesized polymer was further used to prepare mixed matrix membranes. FTIR, TGA-DSC, EDS, SEM, and XRD methods were used to analyze the chemical structure, thermal stability, and morphology of the prepared particles and membranes. Furthermore, the influence of particles, the composition of the input mixture, and the pressure in the interval of 2 to 8 bar on the separation efficiency of the membranes were tested. The thickness of the prepared membranes ranged from 20 to 25 µm.

The addition of filler positively influences the permeability of 6FDA-BisP and preserves the original selectivity of neat polymer membranes. The best performance was obtained by the membrane with 15 wt. % ZIF-8 particles (permeability 135 barrer and selectivity 43).

Comparing the separation efficiency of prepared membranes the results are situated in the 2008 Robeson diagram [2,3] **Figure 4.** The performance of the prepared mixed matrix membrane overcomes the 1991 Robeson upper bound limit and almost reaches the 2008 one.

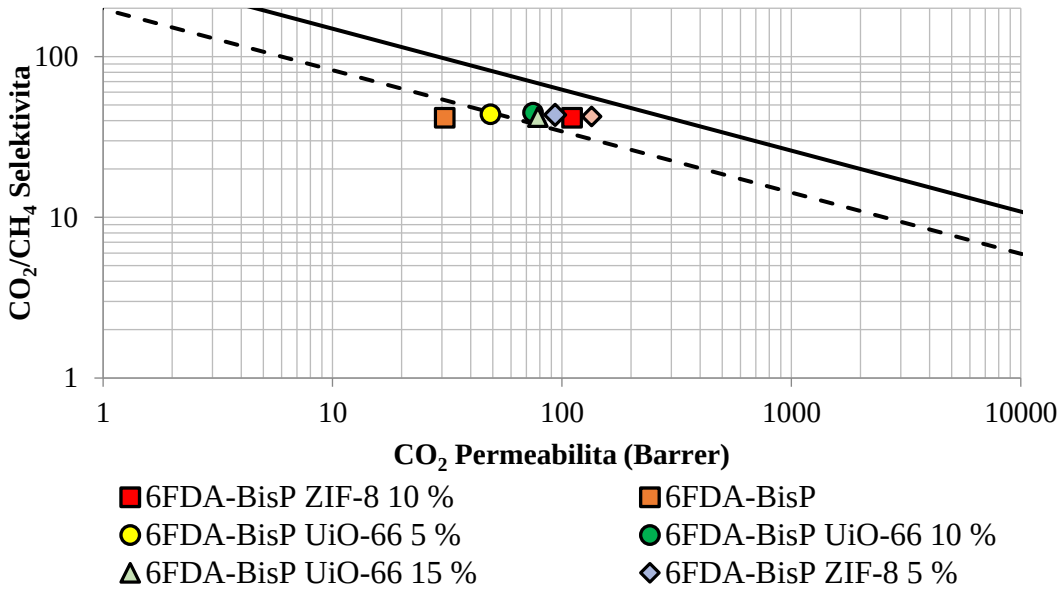

Figure 10: Comparison of obtained results with Robeson upper bound for CO_2/CH_4 separation. (dashed line - the 1991 upper bound [2], black full line - the revisited 2008 upper bound [3]). Presented results were measured at feed composition CO_2/CH_4 1:1 and pressure 2 bar.

References

[1] R. Castro-Muñoz, V. Fíla, V. Martin-Gil, C. Muller, Sep. Purif. Technol. **210** (2019) 553–562.
[2] L.M. Robeson, J. Membr. Sci.**62** (1991) 165–185.
[3]] L.M. Robeson, J. Membr. Sci. **320** (2008) 390–400.

Effect of C/S Ratio on the Electrochemical Properties of a Li-S Cell

K. Jaššo[a]*, T. Kazda[a], P. Benešová[a]

[a] Department of Electrical and Electronic Technology, Brno University of Technology, Technicka 10, 616 00 Brno, Czech Republic
*kamil.jasso@vut.cz

Abstract
Lithium-Sulfur (Li-S) rechargeable batteries have gained a lot of attention since they have the potential to deliver high energy at low cost. However, before they can be deployed in commercial production, several problems associated with the use of a combination of sulfur and lithium metal still need to be resolved. The most significant problems include low conductivity of sulfur and its reaction products, lithium dendrite growth, sulfur electrode volume changes, and the shuttle effect. The combination of weak electronic and ionic conductivity of sulfur and its charge/discharge products with its poor electrochemical reversibility cause a relatively low-rate capability of Li-S cell. To improve the weak electrical conductivity, conductive additives, most often carbon, are added to the positive electrode material, thus reducing the sulphur content in the positive electrode volume at the expense of the conductive element. In this work, the impact of the C/S ratios on the performance of a Li-S cell is investigated.

Introduction

One of the fundamental drawbacks of using sulfur as an active material is its low potential vs. Li/Li+ and poor electrical conductivity ($5x10^{-30}$ S cm^{-1} at 25°C) resulting from the fact that sulfur is an insulator **Chyba! Nenašiel sa ž iaden zdroj odkazov.**. Due to its poor electrical conductivity and low electroactivity, sulfur has not been considered a suitable cathode material for low-temperature batteries in the past. Sulfur and its polysulfides (especially Li_2S_2 and Li_2S) exhibit poor ionic and electrical conductivity, which increases the internal resistance of the battery and deteriorates the reaction kinetics. This results in increased polarization, which reduces the resulting energy efficiency. In addition, during cycling, an insoluble passivation layer forms on the electrode surface that prevents further reduction, leading to impaired utilization of the active material [1].

Due to the insulating nature of sulfur and its products, the electrical conductivity is being increased by adding a conductive material to the electrode. To overcome the low conductivity, a large amount of carbon (up to 50 wt%) is often used, which results in low energy density cell. One of the crucial factors that significantly influences the electrochemical performance of the Li-S cell is the carbon-to-sulfur (C/S) ratio. Increasing the amount of carbon has been shown to improve the electrochemical properties of the Li-S cell, but together with the binder it forms an inactive part of the cathode, resulting in a decrease in the energy density [2]. However, as with Li-ion batteries, the aim is to reduce the amount of carbon down to 5% to ensure a high energy density Li-S batteries. Reducing the carbon content can affect several electrode properties and be beneficial in a number of ways [3][2]:

Porosity – The density of carbon is very low and therefore its excessive use leads to highly porous electrodes. These electrodes often show good sulphur recovery, but a large amount of electrolyte is required to wet the entire electrode surface sufficiently, which increases the cell weight and reduces the energy density (increasing the electrolyte-to-sulfur [E/S] ratio).

Wettability – Hydrophobicity of carbon impairs wettability by polar electrolyte. The high carbon content of the cathode material therefore limits the wetting of the active material by the electrolyte, resulting in poor ion transport and a reduction in cell capacity.

Bonding – For efficient electron transfer it is important to create a good conductive path, which occurs when all electrode materials are sufficiently well bonded to each other. Non-polar carbon interacts poorly with polar

polysulfides, leading to weak bonding and impaired electron transfer. This can lead to incomplete conversion of polysulfides to Li_2S and their release into the electrolyte, which causes the shuttle effect.

Most publications regarding the C/S ratio focus on the ratios of 0.5 and above. These high ratios often show an improvement in the electrochemical properties of the Li-S cell but are inapplicable to commercial Li-S pouch cells.

Experimental

Materials

The following materials were used to produce the positive electrode: Sulfur powder (Sigma-Aldrich, St. Louis, USA), Super P Carbon black (Timcal, Bodio, Switzerland) and CMC binder (CP Kelco, Atlanta, USA) in form of highly purified sodium carboxymethylcellulose. The electrolyte was prepared from 0,25M LiNO3 and 0,7M LiTFSI lithium salts dissolved in a mix of DME/ DOL (2:1) solvents (all Sigma-Aldrich, St. Louis, USA).

Preparation of the cells

First, cathodes with different S-C-Binder ratios were prepared by modifying the carbon and sulfur amounts in the slurry. The electrodes were prepared at a specified thickness; consequently, the sulfur loading in the cathode for each C/S ratio was different. Disc electrodes (Ø18mm) prepared from the slurries were placed in the electrochemical measurement cell (El-Cell®). Lithium metal (Ø16mm) was used as a counter electrode. The amount of electrolyte remained constant for all cells, which in effect means that the E/S ratio decreased with increasing sulphur loading. Selected properties of assembled Li-S cells can be seen in the table below.

Table 1: Li-S cell properties.

S-C-Binder ratio [% wt.]	C/S ratio	Sulfur loading [mg cm^{-2}]	E/S ratio [µl mg^{-1}]
64-32-4	0,50	0,55	92
70-26-4	0,37	1,43	36
76-20-4	0,26	1,88	27
82-14-4	0,17	2,06	25
88-8-4	0,09	2,31	22

Electrochemical analysis

Assembled Li-S cells were subsequently subjected to electrochemical analyses. After initialization analyses, 50 cycles of galvanostatic cycling at variable loads (0.2C, 0.5C, 1C, 2C, 1C, 0.5C and again 0.2C) were performed (see Figure 1).

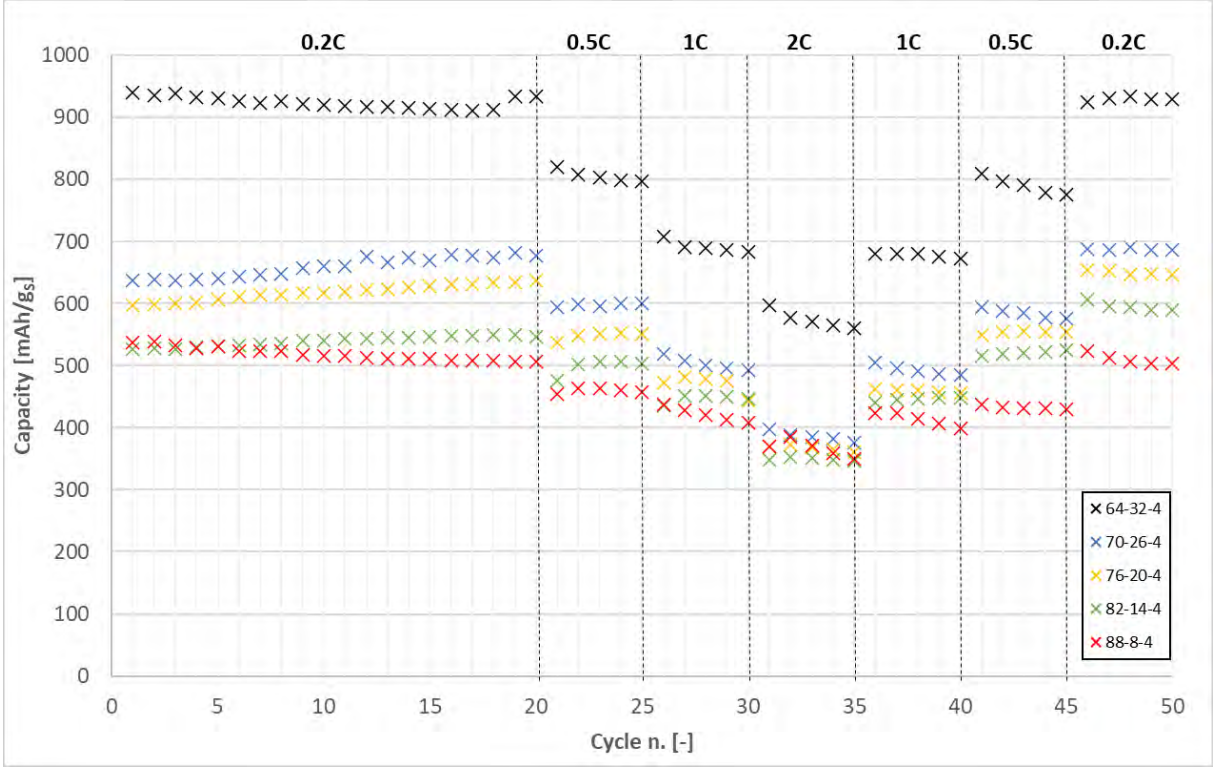

Figure 1: Specific discharge capacities of measured Li-S cells with different C/S ratio at different discharge rates.

From the measured values of the specific discharge capacities, it can be seen that the electrode with the highest carbon content (32 wt.%) exhibits the highest capacity throughout the GCPL measurement, indicating the best sulphur utilization. As the carbon content decreases, the specific discharge capacities decrease, but the difference between the following cells is not so significant. The decrease in capacities in the first step of GCPL in response to decreasing carbon content is as follows: 940, 637, 598, 527 and 537 mAh g^{-1}. Thus, with decreasing carbon content, the sulfur utilization dropped from 56% to only 32%. It can be seen that in the first cycles of GCPL, the capacities of the electrode with the lowest carbon content (8% wt.) are slightly higher than the capacities of the electrode with the higher carbon content (14% wt.). However, towards the end of the GCPL cycling, this balances out and the electrode with the lowest carbon content shows the poorest sulfur utilization. The initial higher values can thus be attributed to the initial cell annealing. In the last step of GCPL, the decrease in capacities according to the decreasing amount of carbon is as follows: 929, 687, 646, 590 and 504 mAh g^{-1}. It is possible to notice a slight increase in sulfur utilization for electrodes with a moderately reduced carbon content (26% and 20% wt.). This phenomenon is not uncommon when using a given CMC binder. Based on the measured results, the dependence of sulfur utilization (at 0.2C) on the C/S ratio has been plotted (see Figure 2).

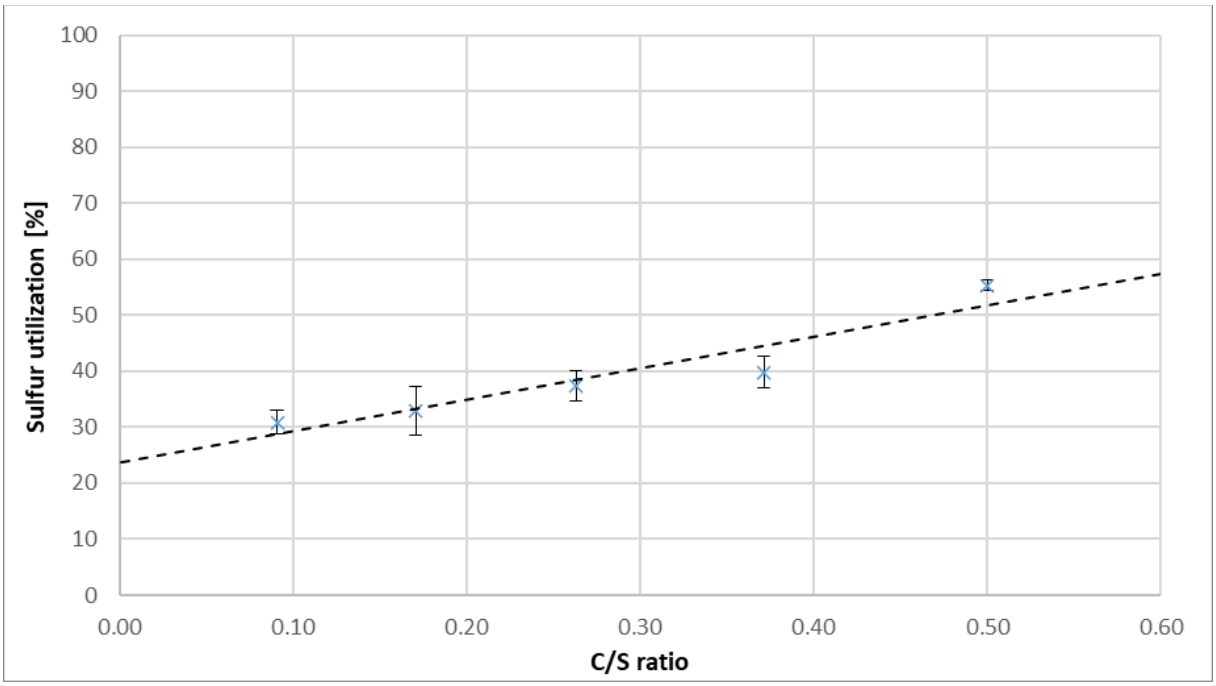

Figure 2: Dependence of sulfur utilization on C/S ratio (at 0.2C).

Figure 2 clearly shows the linear correlation of the sulfur utilization to the amount of carbon in the cathode material.

Conclusion

Five different C/S ratios were measured. The results show that the decreasing carbon content in the cathode has a significant negative effect on the sulfur utilization. However, this negative dependence can also be supported by the decreasing E/S ratio. To better understand this multi-parameter dependence, it is necessary to make multiple measurements where only one of these parameters will be altered.

Acknowledgements

Authors gratefully acknowledge the financial support from the Ministry of Education, Youth and Sports of the Czech Republic under project No. LTT19001, BUT specific research program (project No. FEKT-S-20-6206).

References

[1] B. Lee, T. Kang, H. Lee, J.S. Samdani, Y. Jung, C. Zhang, Z. Yu, G. Xu, L. Cheng, S. Byun, Y.M. Lee, K. Amine, J. Yu, Adv. Energy Mater. **10** (2020) 1903934.
[2] H.M. Bilal, D. Eroglu, ,Int. J. Energy Res. **46** (2022) 15926–15937.
[3] A. Bhargav, J. He, A. Gupta, Joule. **4** (2020) 285–291.

Understanding Structure-Bandgap Relationship in Chalcogenide Perovskites: Insights from Machine Learned MD-NPT Study

N. Jaykhedkar[a], R. Bystrický[a,b] , M. Sýkora[a*] , T. Bučko[b,c*]

[a]Laboratory for Advanced Materials, Faculty of Natural Sciences, Comenius University, Ilkovičova 6, 842 15 Bratislava, Slovakia
[b]Institute of Inorganic Chemistry, Slovak Academy of Sciences, Dúbravská Cesta 9, 845 36, Bratislava, Slovakia
[c]Department of Physical and Theoretical Chemistry, Faculty of Natural Sciences, Comenius University in Bratislava, Ilkovičova 6, 842 15 Bratislava, Slovakia,
*tomas.bucko@uniba.sk *sykoram@uniba.sk

Motivation

Halogenide-based perovskites have over the past 10-15 years emerged as promising materials for development of highly efficient solar cells and optoelectronic devices.[1] Development of practical applications has been, however, hampered by the fact that the most promising halide perovskites contain highly toxic lead and are thermally and chemically unstable.[2] Recent studies suggest that a family of chalcogenide perovskites could serve as an alternative to their halide prototypes with similar electronic structure and optical properties and better chemical and thermal stability.[3] From the perspective of practical applications in optoelectronics, it is important to understand how these materials are affected by various thermodynamic conditions. An understanding of the temperature dependent behaviour is also important for identifying appropriate experimental conditions for preparing of materials with desired electronic properties. While these effects have been extensively studied in halide and oxide perovskites, similar studies have been lacking in case of the chalcogenide perovskites. To address this deficiency, we performed theoretical investigations on finite temperature structural and electronic properties of a class of Zr-based chalcogenide perovskites ABX_3 (A = Ca, Sr, Ba; B = Zr, X = S, Se). Our results help to identify appropriate thermodynamic conditions for the synthesis of desired phase and offers atomic level insights regarding the origin of structural evolution of these phases. In addition, the predictions aid in selecting the most suitable candidates for experimental development.

Computational Methods

The computational studies were performed using periodic density functional theory (DFT) calculations as implemented in VASP software package.[4] We begin modelling our system first using static approach by solving Kohn-Sham equations variationally in a plane-wave basis set with the maximum kinetic energy of 400 eV using PBE [5] exchange-correlation functional in the generalized gradient approximation. We use a supercell comprising of 8 unit cells consisting of 160 atoms. Subsequently, we performed ab-initio molecular dynamics simulations in an NPT ensemble at zero pressure and temperatures of 300 K, 60 K, 900 K and 1200 K. These were further accelerated by machine learned force fields (MLFF) [6,7,8] that allowed for dramatic CPU time savings as compared to conventional MD.

Results

Our initial studies focused on the distorted perovskite phase of prototype material $SrZrS_3$ with orthorhombic crystal structure, and a three-dimensional network of corner sharing octahedra. This structure is related to the undistorted cubic phase and the transformation to DP is a result of symmetry lowering. The DP phase exhibits anisotropic thermal expansion upon heating, with two vectors (b and c) monotonously expanding while vector a contracting after initial expansion. Our results show that these thermally induced structural changes in the DP phase are a consequence of structural and energetic proximity to the cubic phase, into which it transforms quasi-continuously at around 1500 K (see Fig. 1.) This transformation has a large impact on its electronic band gap, which decreases with temperature by ~0.5 eV between the two temperature extremes. Following the same approach, we have investigated other compositions of chalcogenide perovskites. The results show that other chalcogenide perovskites exhibit similar behaviour, although to a different extent, where changes in temperature lead to dramatic distortions in physical structure and the band gap with increase in temperature. The specific results will be discussed.

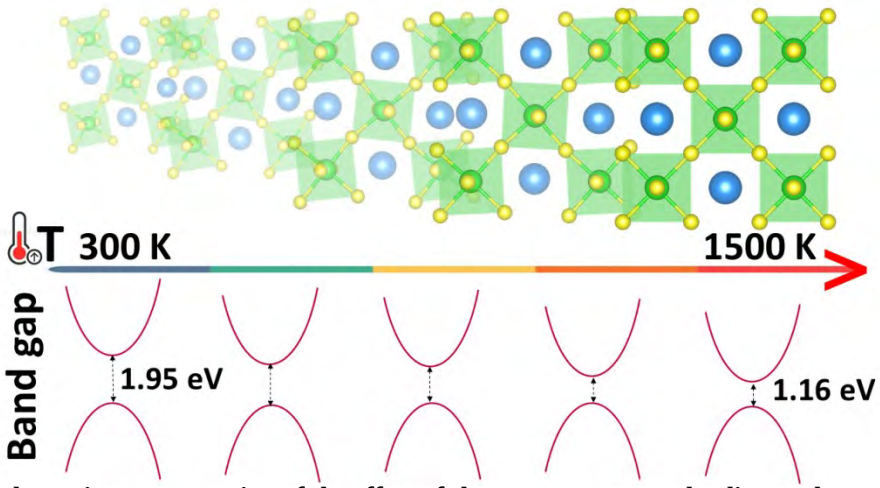

Figure 11: Schematic representation of the effect of the temperature on the distorted perovskite phase of chalcogenide perovskites. The upper half shows the transformation of the DP into undistorted cubic phase as a result of increase in temperature. As a consequence of the lowering atomic distortions due to proximity to the cubic phase, the electronic bandgap shows a significant decrease with temperature as shown in the bottom part of the scheme.

Conclusions

Our results show that temperature has a significant effect on the physical and electronic structure of Zr-based chalcogenide perovskites. Subjecting these compositions to high temperature results in gradual phase transitions which significantly the electronic bandgap. The temperature at which these transitions occur and the magnitude of bandgap variation is sensitive to the material chemical composition.

Acknowledgements

This work was supported by the European Union's Horizon 2020 research and innovation programme under grant agreement No. 810701 and by the Slovak Research and Development Agency under grant agreement No. APVV-19-0410. NJ and TB gratefully acknowledge the use of HPC facility by PRACE (Partnership for Advanced Computing in Europe) within the programme DECI-16 and of the supercomputing infrastructure of Computing Center of the Slovak Academy of Sciences acquired in projects ITMS 26230120002 and 26210120002 supported by the Research and Development Operational Program funded by the ERDF. The use of the high-performance computing facilities CLARA@UNIBA.SK at Comenius University in Bratislava, services and staff expertise of Centre for Information Technology is acknowledged.

References

[1] H. Snaith. J. Phys. Chem. Lett. 4 **21** (2013) 3623-3630.
[2] D. A. Egger, A. M. Rappe and L. Kronik, Acc. Chem. Res. **49** (2016) 573-581.
[3] K. V. Sopiha , C. Comparotto , J. A. Márquez and J. J. S. Scragg , Adv. Opt. Mater. **10** (2021) 2101704.
[4] Kresse, G. and Hafner, J. Phys. Rev. B **48** (1993) 13115-13118.
[5] J. P. Perdew, K. Burke, M. Ernzerhof, Phys. Rev. Lett. (E) **78** (1997) 1396.
[6] R. Jinnouchi, F. Karsai, and G. Kresse, Phys. Rev. B **100** (2019) 014105.
[7] R. Jinnouchi, J. Lahnsteiner, F. Karsai, G. Kresse, and M. Bokdam, Phys. Rev. Lett. **122** (2019**)** 225701.
[8] R. Jinnouchi, F. Karsai, C. Verdi, R. Asahi and G. Kresse, J. Chem. Phys. **152** (2020) 094107 1-8.

Influence of Catalyst Type and Loading on PEM Fuel Cell Operation

T. Jedlička[a], J. Mališ[a], M. Paidar[a]*, K. Bouzek[a]

[a]University of Chemistry and Technology, Prague Technicka 5,166 28 PRAHA 6, Czech Republic
*paidarm@vscht.cz

PEM fuel cell represent nowadays-mature technology suitable for stationary and mobile application. Its main advantage is capability to operate at room temperature and high efficiency of energy conversion. Hydrogen as carbon-free fuel for PEM fuel cell makes this technology important part in decarbonisation of society. In the field of transport, it represents a promising alternative to battery-powered cars. Despite it, PEM fuel cell still suffers with several drawbacks. One of them is the need of platinum metals as catalyst. The catalyst price plays a significant role in making this technology competitive on the market. Research community intensively study the possibilities for reduction of required platinum loading. One way how to reduce Pt loading is the use nanoparticles made from Pt alloys of base metals prepared by magnetron sputtering. Another way is to use catalyst prepared by conventional methods where part of Pt is replaced by less expensive metal like Co or Ni. The high catalytic activity over all lifetime period of fuel cell is crucial for successful reduction of Pt loading.

The aim of this work is to evaluate possibility for Pt loading reduction and its impact on PEM fuel cell performance.

Two types of catalysts were selected for this study. Magnetron sputtered Pt and Pt-CeO_2 catalyst were deposited directly onto testing electrode or membrane. Commercial catalyst Pt on carbon black with 10, 20 and 40% Pt content was used as state of the art. Alloy catalysts Pt-Co and Pt-Ni with metal content 27% Pt, 3% Co or Ni on carbon was used as newly introduced catalyst on the market.

Rotating disc electrode (RDE) represents powerful tool for electrochemical Pt active surface area (EASA) determination. By periodic cycling in 0.1 mol dm^{-3} H_2SO_4 the stability of EASA was tested. The decrease of EASA indicate electrochemical or chemical dissolution or particle agglomeration. Most durable catalyst exhibits minimal decrease of EASA. To confirm results obtained by screening on RDE the test in real environment of PEM fuel cell was done. Thus, catalysts were incorporated into membrane electrode assembly (MEA). The selected catalysts were deposited on membrane by magnetron sputtering in desired load. Laboratory PEM fuel cell of active area 2.5x2.5 cm was operated for 100 h to confirm catalyst behaviour determined by RDE. The tested catalyst was placed on anodic (fuel) side of fuel cell. The commercial 40% Pt on carbon black was used on cathodic (oxygen) side.

With higher content of Pt on carbon the determined EASA increased but the increase is slower than can be expected from Pt content increase. It is due to interaction of Pt nanoparticles in the case of higher Pt content in catalyst. Only limited decrease of EASA during potential cycling indicates high durability of all Pt on carbon black catalysts. Relative similar results were found also for commercial catalysts PtNi and PtCo but the determined EASA were slightly lower due to lower content of Pt. It is important to point that Pt active area is only indicative parameter for catalyst comparison and presence of other elements should enhance catalytic activity in real fuel cell. Magnetron sputtered pure Pt catalyst showed minimal catalytic activity at the beginning of cycling and subsequently gradually increased with operating time. Significant drop of EASA shortly after experiment start was observed for Pt-CeO_2 catalyst followed with slow increase of active area during next potential cycles. Despite it the determined value of EASA is well comparable to commercial Pt/C catalyst.

Insufficient results were measured for low Pt content catalyst prepared from magnetron sputtering in PEM fuel cell. Catalysts showed high activity for a very short period of operation, then lost close to 98% of their activity. As the main reason of observed behaviour, the very low thickness of catalyst layer was identified. Due to lack of supporting material and deposition directly onto membrane surface the catalyst layer is extremely sensitive to the flooding of catalytic layer and also drying. Also the loss of contact between catalyst nanoparticles and carbon cloth based gas diffusion layer is another reason for observed decrease of fuel cell performance in time.

The obtained results indicate, that Pt content decrease in fuel cell is not only issue of durable catalyst preparation but also their final incorporation into fuel cell together with operation conditions plays important role. On the other hand, the sufficient stability of newly prepared catalyst were confirmed during RDE test. The next research focusing on catalyst incorporation is necessary.

Acknowledgements
The work was supported from European Regional Development Fund-Project "Fuel Cells with Low Platinum Content" (No. CZ.02.1.01/0.0/0.0/16_025/0007414).

Thermogravimetric Analysis of Amino-modified Magnetic Manoparticles

A. Juríková[a]*, I. Antal[a], I. Khmara[a], M. Koneracká[a], M. Kubovčíková[a], R. Sobotová[a], V. Závišová[a]

[a] Institute of Experimental Physics Slovak Academy of Sciences, Watsonova 47, 040 01 Košice, Slovakia
*akasard@saske.sk

Introduction

Amino-modified magnetic nanoparticles seem to be a good candidate for conjugation of a drug effective against different diseases. That is why we focused on the preparation and characterization several systems of magnetic nanoparticles modified with different biocompatible amino acids. One of the methods for analysing such systems is thermogravimetric analysis (TGA). In the work, we pointed out how TGA can be useful to confirm bounding amino acids on magnetic nanoparticles and to estimate the amount of amino acid covering the magnetic nanoparticle's surface.

Experimental

The bare magnetite nanoparticles were synthesized by a co-precipitation method. An aqueous solution of magnetic nanoparticles stabilized with perchloric acid (MNPs) was prepared by the Massart method with slight modification [1]. The functionalization of MNPs with chosen biocompatible amino acids (AAs) - glycine (Gly), D,L-lysine (Lys), tryptophan (Trp) and proline (Pro) was carried out by mixing an aqueous solution of AA with stabilized MNPs in different AA/MNPs weight ratios x (w/w) ranging from 0 to 30. The procedure was followed by shaking for 72 h at 25 °C, then the samples were centrifuged at 35 000 rpm for 20 min to separate unbound AA. Individual prepared samples are referred to as AA_x-MNPs.

Thermogravimetric measurements were carried out using TGDTA Setaram SETSYS 16 analyzer for washed and lyophilized samples for all the AA_x-MNPs systems with different AA/MNPs (w/w) input ratios as well as the pure amino acids, pure magnetite nanoparticles and physical mixture of AA and MNPs. Weight losses were measured from the room temperature up to 700 °C under air with a heating rate of 10 °C/min.

Results

Representative thermograms of AA_x-MNPs systems can be seen in Fig. 1 a). There are the TG curves for pure glycine and pure MNPs and for the samples of MNPs modified with different input ratio of glycine. The initial weight loss observed due to water evolving (below 100 °C) can be seen for the uncoated MNPs and AA-coated MNPs. TG curves of pure AAs show no weight loss up to about 200 °C. Subsequently, a continuous weight loss of pure AAs up to 500-600 °C, related to two- or three-step thermal decomposition, depending on the AA used, is observed. The mass loss in the sample of uncoated MNPs over the temperature range up to approximately 300 °C was detected due to the loss of residual water and the decomposition of the stabilized component in the sample. Then no significant mass loss was observed.

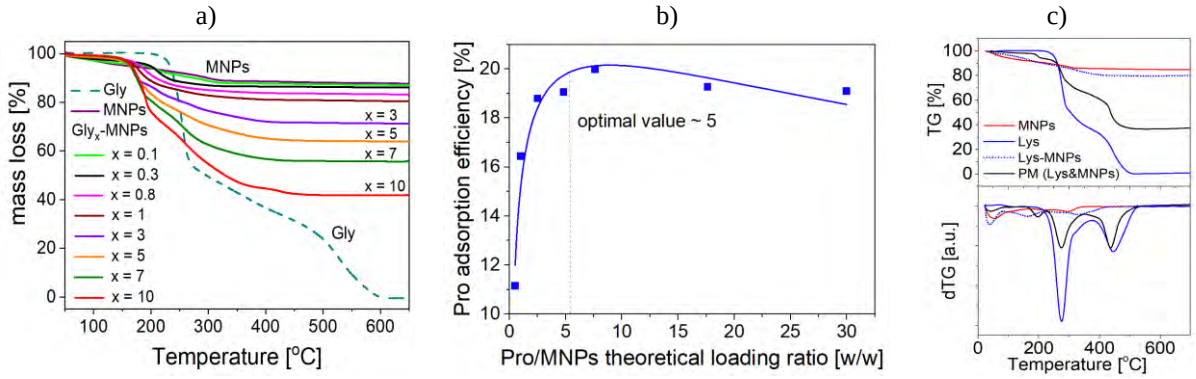

Figure 1: TG curves for MNPs, pure glycine and Gly_x-MNPs for different Gly/MNPs input ratios x (a). Dependence of Pro adsorption efficiency on the input ratio of Pro/MNPs (w/w) (b). TG and dTG curves for pure Lys, uncoated MNPs, lysine coated Lys-MNPs, and physical mixture Lys+MNPs (c).

The quantitative calculation of the amount of AA coating MNPs surface is based on assumption that AAs are completely decomposed in air above 600 °C and MNPs are thermally stable. The amount of AA adsorbed on the MNPs surface, given as mg of AA per mg of magnetite, for individual input ratios was calculated from the residual weight of the AA-coated MNPs and uncoated MNPs at 650 °C.

To find out the optimal input ratio for individual AA-MNPs systems, we calculate the adsorption efficiency as a ratio of the actual adsorbed amount of AA to theoretical loading of AA amount expressed in %. Having evaluated TG curves of the samples with different theoretical input weight ratios of AA/MNPs, the amount of AA adsorbed on MNPs was determined, and consequently, the adsorption efficiency was also calculated. Figure 1 b) displays typical adsorption efficiency for proline with regard to the theoretical proline loading. Having fitted the experimental data, the optimal Pro/MNPs weight ratio was found to be about 5 w/w indicating that maximally ~20 % of theoretical Pro loading amount can be adsorbed onto MNPs. These results are relatively in good coincidence with outcomes from the UV/Vis spectrophotometry. Thus, the sample Pro-MNPs with optimal input weight ratio Pro/MNPs ~5 and the adsorption efficiency of ~20 % was selected as the optimized formulation for the next drug conjugation. In Table 1 there are summarized optimal input ratios and respective adsorbed amount of AA determined for all studied AA-MNPs systems. It can be concluded that the amount of AA adsorbed on surface of MNPs has tendency to decrease with increasing molecular weight of AA. However, the adsorbed AA amount is influenced not only by the AA molecular weight, but also by their chemical structure (numbers of functional groups, presence of aromatic ring or heterocycle).

For the confirmation of AA bounding on MNPs, the samples of the physical mixtures (PM) were also prepared by simple mixing of lyophilized AA and MNPs with the same input ratios for comparison with AA-modified samples. The typical TG curves for the studied system of Lys-MNPs with the input weight ratio 2 are shown in Fig. 1c). For better distinguishing the decomposition processes, derivative dTG curves were added. It can be seen thermograms for the samples with the bound lysine to MNPs, for the physical mixture of D,L-Lysine and MNPs, pure lysine and the pure stabilized MNPs. As seen, in the physical mixture, most of the AA is free and unbound on the MNPs, and the stage decomposition temperatures correspond to that of the pure AA, however, in the system with AA bound to MNPs, the decomposition stages of AA occur at lower temperatures. The fact indicates that AAs are indeed bound to the MNPs in the prepared AA-MNPs systems. The temperature shifts of the thermal decomposition towards lower values for some other substances coating NPs have already been reported and suggests the catalytic effect of magnetite [2, 3].

Table 1: Summarization of the results for different AA-modified magnetic nanoparticles.

AA	Gly	Pro	Lys	Trp
molecular weight (g/mol)	75	115	146	204
chemical formula and structure	$C_2H_5NO_2$ 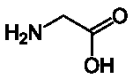	$C_5H_9NO_2$ 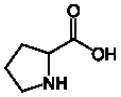	$C_6H_{14}N_2O_2$ 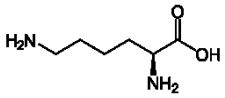	$C_{11}H_{12}N_2O_2$ 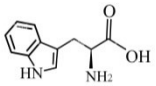
optimal input ratio AA/MNPs (mg/mg)	3.8	5.3	6.1	7.8
adsorbed AA/MNPs (mol/mol)	1.02	0.84	0.74	0.28

Conclusion

Thermogravimetric analysis is a powerful tool in characterization of amino-modified magnetic nanoparticles. It can quantify surface coating and determine optimal input ratio of AA coating of the magnetic nanoparticles. Such modified nanoparticles seem to be a promising candidate for *in vitro* and *in vivo* experiment and for the conjugation of commercially available corticosteroids (e.g. dexamethasone, hydrocortisone) and viral spike protein (S-protein), so that they can be used as one of the interventions in the development of a biomodel for monitoring complications associated with COVID-19.

Acknowledgements

This work is the result of the project implementation ITMS2014+ 313011AVG3 supported by the Operational Programme Integrated Infrastructure (OPII) funded by the ERDF.

References

[1] A. Antosova, Z. Bednarikova, M. Koneracka, I. Antal, J. Marek, M. Kubovcikova, V. Zavisova, A. Jurikova, Z. Gazova, Chem. Eur. J. **25** (2019) 7501–7514.

[2] O. Carp, L. Patron, D. C. Culita, P. Budrugeac, M. Feder, L. Diamandescu, J. Therm. Anal. Calorim. **101** (2010) 181–187.

[3] A. Jurikova, K. Csach, J. Miskuf, M. Koneracka, V. Zavisova, M. Kubovcikova, P. Kopcansky, Acta Phys. Pol. A **121** (2012) 1296-1298.

Structural Dependence of Hydrogen Evolution Reaction on Transition Metal Catalysts Sputtered at Different Temperatures in Alkaline Media

M. Kozejova[a]*, R. Bodnarova[a], V. Latyshev[a], M. Lisnichuk[a,b], V. Girman[a], H. You[c], V. Komanicky[a]

[a]Institute of Physics, Faculty of Science, P. J. Safarik University, Park Angelinum 9, Kosice, 040 01, Slovakia
[b]Institute of Materials Research, Slovak Academy of Sciences, Watsonova 47, Kosice, 040 01, Slovakia
[c]Argonne National Laboratory, 9700 S. Cass Avenue, Lemont, IL, 60439, USA
*miroslava.kozejova@upjs.sk

Nowadays, energy requirements are constantly increasing and therefore attention is focused on renewable and clean energy sources [1] to reduce CO_2 emission. Hydrogen has potential as an ideal energy carrier towards a sustainable energy economy due to its high energy density, ecological production, and earth-abundance [2,3]. Good electrode materials for acid such as alkaline electrolyzes should exhibit high electrical conductivity, high corrosion resistance, and minimum overvoltage [1,4]. One of the most important goals of modern electrocatalysis is to replace platinum metal groups catalysts (PGM) with cheaper but catalytically highly active materials [6]. Non PGM such as Fe, Ni, Cu, Mo or Co [7,8] are substantially cheaper but are subject to corrosion and passivation. The properties of non-PGM catalysts can be improved by preparing these metals or their alloys using various synthetic routes [5].

In the present work, we studied the catalytic activity of magnetron sputtered Mo, V, Ni, and Co thin films for hydrogen evolution reaction (HER) in the alkaline electrolyte. All samples (Mo, Ni, Co, V) were prepared at 25 °C and 800 °C and examined by TEM diffraction measurements since they either show the most significant change of HER overpotential with temperature (Mo, V) or minimal shift of HER overpotential (Ni, Co).

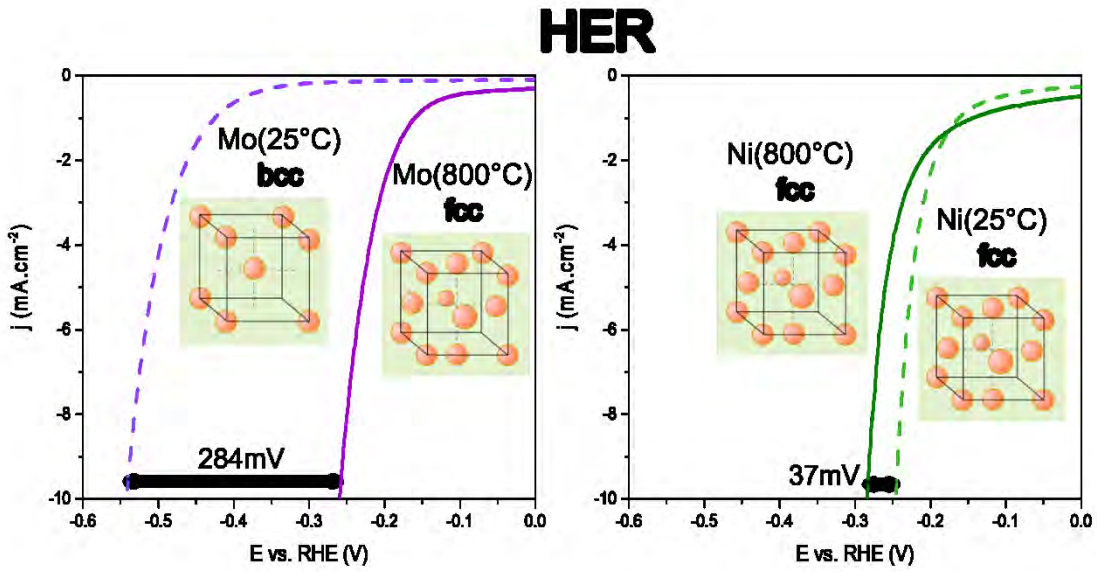

Figure 12: Polarization curves of thin metal films prepared at 25 °C and 800 °C. Mo represents metals with a large temperature effect, Ni represents metals with a small temperature effect.

We find that the HER potentials (η_{10}) of the Mo and V thin film catalysts sputtered at 800 °C shift positive with respect to those of the film catalysts sputtered at 25°C. For Mo metal the observed shift of η_{10} was 280 mV and for V metal observed shift of η_{10} was 390 mV. On the other hand, minimal effect of sputtering temperature on both Ni ($\eta_{10} = 37$mV) and Co ($\eta_{10} = 65$mV) thin film catalyst activity for HER was observed.

Structural analysis reveals that Mo and V prepared at 800 °C have uncommon face centered cubic (fcc, 0.74 packing density) structure as opposed to room-temperature sputtered Mo and V thin films which have common body centered cubic (bcc, 0.68 packing density) structure, resulting in significant increases of the packing densities when they are prepared at 800 °C. On the other hand, the high-temperature prepared thin films of Ni and Co retained fcc structures, resulting in no density changes compared to the room-temperature prepared fcc Ni and hexagonal close packed (hcp, 0.74 packing density) Co. Our study points out that structure phases of catalysts can be a key factor governing the activities of transition metals for HER in alkaline media.

Acknowledgements
This work has been supported by grant 313011V334, Innovative Solutions for Propulsion, Power and Safety Components of Transport Vehicles, and grants of the Slovak Research and Development Agency under contract APVV-20-0324 and APVV-20-0528.

References
[1] V. M. Nikolic, S. Lj. Maslovara, et al. App. Catal. B **179** (2015) 88-94.
[2] J. Wang, F. Xu, et al. Adv. Mater, **29.14** (2017) 1605838.
[3] Z. Chen, X. Duan, et al. J. Mater. Chem. A **7.25** (2019) 14971-15005.
[4] W. Kreuter, H. Hofmann, Int. J. Hydrog. Energy **23.8** (1998) 661–666.
[5] R. K. Shervedani, A. H. Alinoori, A. R. Madram, J. New Mater. Electrochem. Syst., **11.4** (2008) 259-265.
[6] F. Safizadeh, E. Ghali, G. Houlachi, Int. J. Hydrog .Energy **40.1** (2015) 256-274.
[7] N. Pentland, J. O'M. Bockris and E. Sheldon, J. Electrochem. Soc. **104.3** (1957) 182-194.
[8] A. Lasia, A. Rami, J. Electroanal. Chem. Interfacial Electrochem. **294.1–2** (1990) 123-141.

Electron tunneling in metal-insulator-semiconductor structures simulating the all-solid-state battery cells.

M. Kupka[a], M. Kupková[b]*

[a] Institute of Experimental Physics of SAS, Watsonova 47, 040 01 Košice, Slovakia
[b] Institute of Materials Research of SAS, Watsonova 47, 040 01 Košice, Slovakia
*mkupkova@saske.sk

Rechargeable all-solid-state batteries are considered as promising solutions for next-generation energy storage devices. The all-solid-state battery cells consist of solid electrodes and a solid electrolyte. As regards the solid electrolyte, it should have high ionic conductivity and ideally zero electronic conductivity. Any increase in electronic conductivity short-circuits the cell and degrades battery performance.

To gain knowledge on electronic transport in all-solid-state batteries, the study of electron tunneling in metal-insulator-semiconductor structures simulating all-solid-state battery cells has begun.

First preliminary results were obtained for a simplified model of a cell with metallic lithium anode, crystalline lithium iodide electrolyte, and semiconductor cathode. In the used model metal-insulator-semiconductor structure, the Fermi energy and Fermi wavevector of metal were those of metallic lithium, the energy band gap and lattice constant of insulator were those of crystalline lithium iodide [1,2], and interfaces were represented by repulsive delta-function potentials. Quantum tunneling probabilities were calculated [3]. Obtained tunneling probabilities varied with the open-circuit voltage of model cell, with the height of interface barriers, with the thickness of an insulator layer. The tunneling probabilities were non-negligible for some combination of parameters.

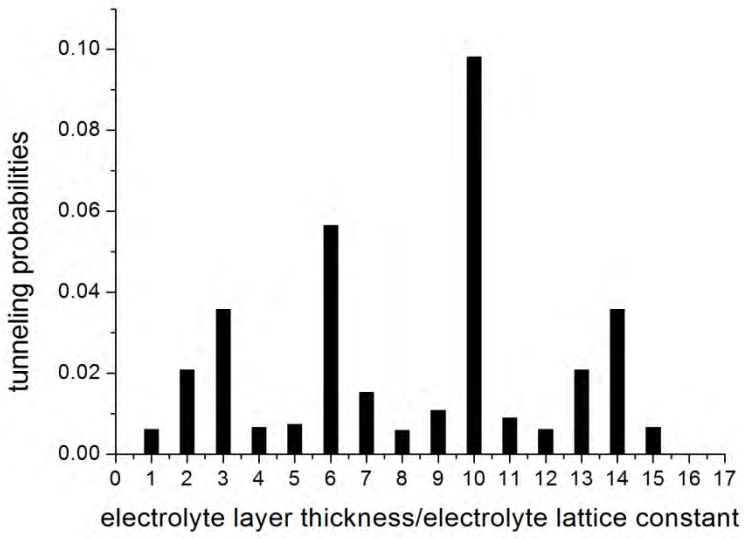

Figure 1: Calculated probability that an electron with the Fermi energy will "tunnel" through a layer of insulator with different thickness in metal-insulator-semiconductor model structure. The data presented are for a model cell with the open-circuit-voltage of 2.5V and repulsive potential at interfaces of –2V.

Acknowledgements
The authors thank for financial support of the research by the VEGA grant 2/0066/21.

References

[1] K. Hikima, K. Shimizu, H. Kiuchi, Y. Hinuma, K. Suzuki, M. Hirayama, E. Matsubara, R. Kanno, Commun Chem **5** (2022) 1-9.
[2] C.R. Gopikrishnan, D. Jose, A. Datta, AIP Advances **2** (2012) 012131.
[3] L.D. Landau, E.M. Lifshits, *in: Quantum mechanics. Non-relastivic Theory Course of Theoretical Physics*, Vol. 3. 3 rd edition. (Pergamon Press, Oxford, 1997).

Effect of Sintering Temperature on Dimensional Changes, Microstructure and Hardness of Biomaterials Prepared from Fe-Cu Powder

M. Kupková[a]*, K. Kovaľ[a], M. Kupka[b], A. Straková Fedorková[c], R. Oriňaková[c]

[a] Institute of Materials Research of SAS, Watsonova 47, 040 01 Košice, Slovakia
[b] Institute of Experimental Physics of SAS, Watsonova 47, 040 01 Košice, Slovakia
[c] Department of Physical Chemistry, Faculty of Sciences, Pavol Jozef Šafárik University in Košice, Moyzesova 11, 041 54, Košice, Slovakia
*mkupkova@saske.sk

Copper-containing iron-based materials have been recently recognized as potential biomaterials possessing antimicrobial ability. Since that time, iron-copper systems have been prepared by different methods and investigated [1]. This contribution is focused on PM materials made from composite powders.

Water-atomized iron powder ASC 100.29 from Höganäs AB, Sweden, fraction 63-200 μm, was used as a starting material. Surfaces of iron particles were electrolytically coated with a layer of copper. Composite powder was thus prepared with the content of 6.2wt.%Cu. Powders obtained were pressed at 400 MPa into cylindrical samples and then sintered at temperatures of 875 °C and 1120 °C in hydrogen atmosphere for 60 minutes.

The temperature of 875 °C is below the melting point of copper and the limit of solubility of copper in iron is about 2.6wt.% at this temperature. The temperature of 1120 °C is above the melting point of copper and the limit of solubility of copper in iron is about 7.2wt.% at this temperature. These facts essentially affected processes during sintering as well the properties of sintered materials.

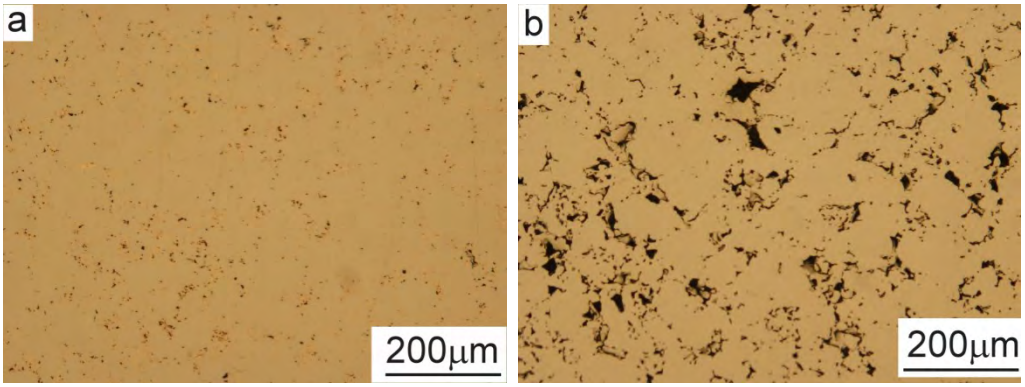

Figure 1: Pores in sintered materials: (a) Fe-6.2 wt.% Cu, 875 °C, and (b) Fe-6.2 wt.% Cu, 1120 °C, LM.

Upon sintering at 875 °C, the compacts contracted in all directions and their densities increased. Typical dimensional changes are presented in Table 1. At this temperature, the sintering was a usual solid-phase one, during which free internal surfaces were reduced and thus the specimens were densified (Fig. 1). The axial sliding during die compaction led to the wear of surfaces of adjacent particles and removed part of the copper coating from the contacts between particles to inter-particle voids nearby. Since the solution limit of copper in iron is low at 875 °C, only a small part of Cu content can dissolve into iron at this temperature and so the free copper is observed at the particle boundary in samples sintered at 875 °C (Fig. 2a,b).

Upon sintering at 1120 ºC, samples shrank in height (in the direction parallel to the compaction direction) and swelled in diameter (Table 1). The reason for such a behaviour was that the copper-based melt was (at least temporarily) present during sintering at this temperature.

Due to the large surface tension of solid iron, a moderate surface tension of molten copper, and a low interfacial tension between solid iron and molten copper, the molten copper efficiently wets the surface of solid iron. Hence, when the temperature of sintered specimen exceeded the melting point of copper, copper melt and began rapidly flowing along surfaces of iron particles and into boundaries of iron grains within these polycrystalline particles. This rapid spreading of molten copper over iron grains caused the expansion of iron particles and left pores at the sites vacated by the copper, which affected the porosity characteristic of the specimen (Figure 1).

The limit of solubility of copper in iron is about 7.2 wt.% at the temperature of 1120 °C. Thus, it was expected that in specimens with 6.2wt.% Cu copper should completely dissolve into iron particles. Indeed, Figs. 2c, d show a microgradient structure of sintered samples without any free copper.

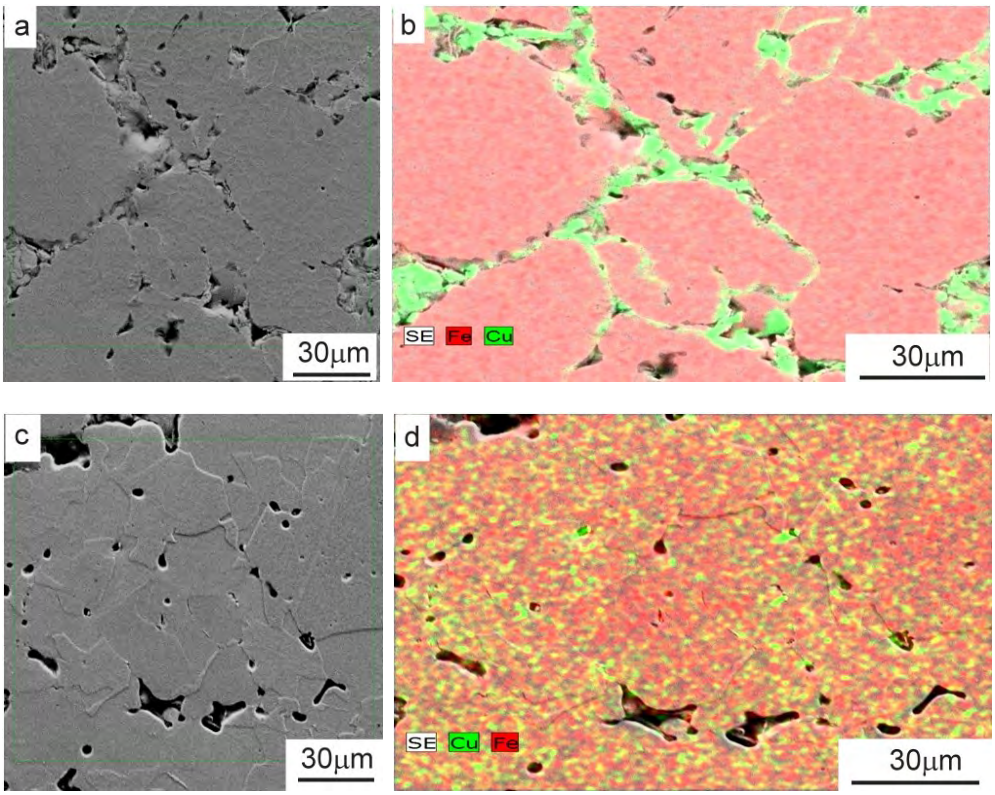

Figure 2: Microstructure of Fe-6.2 wt. % Cu materials: (a) sintered at 875oC and (b) elemental map, (c) sintered at 1120oC (d) elemental map, SEM.

In a specimen held for 60 min at 1120 °C, theoretically, the front of molten copper should travel from hundreds to thousands of microns along iron grain boundaries while the front of solid-solution formation should move a few microns from the surface of the iron grain towards its center. Thus, during an hour at the peak temperature, the copper should dissolve within the several microns thick peripheral regions of iron grains, forming a substitutional solid

solution of copper in iron. Thus, a specimen with a gradient microstructure of larger iron grains should be created with copper-free cores surrounded by copper-containing peripheries.

As the specimens were cooled down from 1120 °C to room temperature, the solubility of copper in iron dropped sharply to practically zero. Thus, the solid solution in peripheral regions of grains became supersaturated, that is thermodynamically unstable. As the copper and iron are not soluble in each other at room temperature, the copper tended to precipitate from the supersaturated solid solution.

Due to the production process based on the atomization of molten metal by jets of high-pressure water, individual particles of water-atomized iron powder contain many microscopically small pores, though the total porosity of particles is very low. During the sintering and subsequent cooling of sintered specimens, these pores could be clogged first by copper dissolving in iron and then by copper precipitating from a supersaturated solid solution. The submicron copper spots (bright spots) visible in Fig. 3 are most likely the copper precipitates in these pores. It should be noted that iron particles with evenly distributed microscopically small "relict" pores filled with copper represent a promising macroscopically homogeneous self-disinfecting bulk biomaterials.

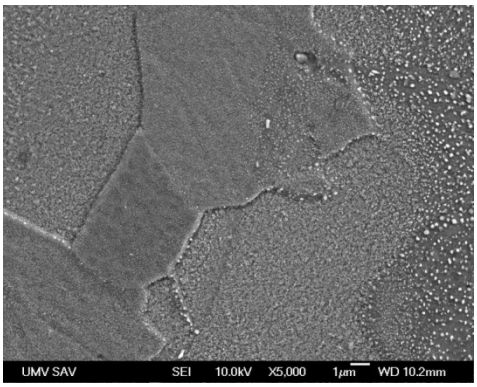

Figure 3: The areas occupied by copper (bright spots) on the grain section. The specimen with 6.2 wt.% Cu sintered at 1120 ºC is presented, SEM.

Besides the precipitates filling the “relict” intragrain voids, it is expected that there are also conventional bulk copper precipitates nucleated and growing within the iron lattice, since the copper does so to a certain extent naturally when the specimen is passing the cooling zone of the sintering furnace at usual rates.

The bulk precipitates are commonly very tiny, thus the individual conventional precipitates are beyond the resolving power of microscopes used.

The macroscopic hardness of investigated Fe-Cu specimens should decrease due to increasing specimen porosity and it should increase due to increasing hardness of skeletal material. Measured macroscopic hardness increased with increasing sintering temperature (Table 1). This indicates that the hardening of skeletal material induced by precipitates prevailed over the softening of the whole material induced by pores.

Table 1: Density, dimensional changes and hardness of compacts from tested materials.

Material	Green density [g.cm^{-3}]	Sintering temperature [^{o}C]	Change of density $\Delta\rho/\rho$ [%]	Change of height $\Delta h/h$ [%]	Change of diameter $\Delta\Phi/\Phi$ [%]	Vickers hardness HV10
Fe-6.2wt.%Cu	6.59	875	+0.92	–0.74	–0.20	86.8
		1120	–0.91	–0.41	+0.62	111.8

Acknowledgements

This research was funded by the Slovak Research and Development Agency, grant number APVV-16-0029 and APVV-20-0278.

References

[1] M. Kupková, M. Kupka, A. Morovská Turoňová, R. Oriňaková, R. Materials, **15** (2022) 1913.

Age-Related Changes of Ionizing Radiation on Cognitive Functions and Emotional Status of Mice

M. Lalkovičova[a*], I. A. Kolesnikova[a,b], Yu. S. Severyukhin[a,b], E. V. Pronskikh[a,b], D. M. Utina[a,b], S. Despotović[c]

[a]Joint Institute for Nuclear Research, Laboratory of Radiation Biology, Dubna, Russia
[b]State budgetary educational institution of higher education of the Moscow region University Dubna, Dubna, Russia
[c]Institute of Histology and embryology, University of Belgrade, Belgrade, Serbia
*lalkovicova@jinr.ru

Introduction

The use of ionizing radiation is nowadays common in biomedicine and oncology, however not without risks. The investigations of chemical, physiological and metabolic processes in the body are therefore a necessary part of the introduction of new diagnostic and therapeutic methods. When researching the effect of ionizing radiation on the central nervous system it is necessary to study not only different physical characteristics of the radiation, but also different age categories of experimental animals. The purpose of this study was to study the behavior of experimental animals 30 days after total exposure to 60Co gamma rays at a dose of 2 Gy.

Material and Methods

The study was carried out on male ICR mice at the age of seven months, the average weight of rodents was 45.7 grams, divided into two groups of 10 individuals: irradiated and intact controls. First group received total irradiation with Co^{60} gamma rays at a dose of 2 Gy, a dose rate of 0.505 Gy / min, an isodose of 90%, RIP = 75 cm on the Rokus-M installation of the JINR medical and technical complex. The behavior of both groups of animals was observed and recorded in the Open field test (OF), 30 days after irradiation, using the Noldus EthoVision XT 13.0 software. The testing time was divided into two periods (1-3 min, 4-6 min) in order to observe the animal's primary reaction to the new environment. The first period is considered stressful, since the animal gets from its usual environment to a new one, and aversion of a dangerous place could be observed. The second period is the attraction of a safe place. The following discrete acts were recorded: general locomotion, movement in place, upright standing positions, standing at the wall, grooming, hole dipping, freezing, crossing the center of the field, urination/defecation. The indicators were calculated: emotional status (ES) and an orientational exploratory reaction (OER), in the first three and second three minutes, respectively. Data processing was carried out in computer programs Past and Origin 2019 [1]. Statistical analysis was performed using the non-parametric Mann-Whitney U-test for abnormal distributions of samples in groups, as well as one-way Analysis of Variance (ANOVA) 2019 [2].

Results and Conclusions

In irradiated animals, the number of stand-up positions from the 4th to 6th minutes averaged 19 ± 6.5, which is statistically significantly less ($p = 0.01$) in relation to the control group, where 8.9 ± 4.7 numbers of behavior were recorded. Also, in this group, an increase in the nose hole reflex of 6.1 ± 2.2 was recorded in comparison with the control animals 4.1 ± 2.0 ($p = 0.05$). Urination and defecation were also counted during the Open field test, and averaged in values: 1.7 ± 1.3 of control group and 1.7 ± 1.7 of irradiated group. There was no significance measured. The irradiated animals generally preferred to be in the periphery and stayed in a state of freezing longer. The behavior of the irradiated animals deteriorated in comparison with control. Statistically significant differences were revealed with respect to the control group: 1) the grooming rate decreased from the 4th to the 6th minute ($p = 0.046$), 2) the ES index was reduced from 4-6th minute ($p = 0.042$). The heat map shows that the irradiated animals stayed in different parts of the arena for longer, freezing or moving in place, which is consistent with the results of statistical analysis of ES. When evaluating the results of behavioral tests in the open field setup, we took into account the age factor, gender, and genotypic, and irradiation method.

Our data show that total irradiation of Co^{60} in the post-radiation period had multiple detrimental effects. The presented data can expand the understanding of radiation damage, and its long-term effects. Also, to add up into the research of accelerated aging, regulation of permissible radiation doses, as well as the significance of exposure in doses used for the experiments. And finally, to point out more precisely the possible radiation effects on the body not in standard conditions, but in the older animals to be more understood also in humans.

References

[1] Ø. Hammer, Harper, DAT, Ryan, Palaeontologia Electronica. **4** (2001)
[2] D. Howell, Pacific Grove: Duxbury Statistical Methods for Psychology. – 2002.

The Characterization of Nanomaterials Using Adsorption Technique.

M. Lhotka[a]*, L. Mastný[b]

[a]Department of Inorganic Technology, Faculty of Chemical Technology, University of Chemistry and Technology, Prague, Technická 5, 166 28, Prague 6, Czech Republic
[b]Department of Inorganic Chemistry, Faculty of Chemical Technology, University of Chemistry and Technology, Prague, Technická 5, 166 28, Prague 6, Czech Republic
*miloslav.lhotka@vscht.cz

A nanomaterial means a natural, incidental or manufactured material containing particles as aggregates, agglomerates or particles in unbound state, where50% or more of them range in the number of size distribution and one or more external dimensions are in the size range of 1 nm-100 nm. (One of the possible definitions of the nanomaterials). Where technically feasible and requested in specific legislation, the compliance with the definition may be determined on the basis of the specific surface area by volume (VVSA). A material can be considered falling with the definition, when the volume specific surface area of material is greater than 60 m^2/cm^3. However, the material, which according to its size distribution value belongs to nanomaterials, can be considered complying with the definition even if its specific surface area is lower than 60 m^2/cm^3 [1].

The volume-specific surface area of a particulate material is one of two apparently very different metrics recommended by the European Commission for the definition of nanomaterial. The volume-specific surface area metric can classify nanomaterials and non-nanomaterials differently than the median size in number metrics, depending on the chemical composition, polydispersity, shape, size, porosity, and aggregation of the powdered particles. The volume-specific surface area is property of materials, which is obtained by dividing the samples external surface (S) by its solid volume (V) or by multiplying the specific surface area (SSA) by the materials skeletal density (ρ). It is conventionally stated in units of m^2/cm^3 and its value depends on the particle size and size distribution: small particles have a large volume-specific surface area and vice versa. The threshold value of 60 m2/cm3 has a direct relation to the primary (size-based) nanomaterial-defining criterion, and this value represents the theoretical volume-specific surface area of the material consisting of perfectly monodispersed spherical particles with the diameter of 100 nm [2]. The perfectly monodispersed cubic particles with the edge length of 100 nm have the same volume-specific surface area of 60 m^2/cm^3.

For dry powders, the volume-specific surface area can be determined via the gas-adsorption measurement of the specific surface area by nitrogen (with adsorption isotherms of type II, III or IV according to the IUPAC classification), and multiplying it by skeletal density from the He-pycnometry measurement. Prior to the gas-adsorption measurement of the specific surface area, the physically adsorbed materials have to be removed from the sample surface by degassing, to avoid irreversible surface changes. The gas desorption can be achieved by flushing with an inert gas at elevated temperatures or under the vacuum conditions.

To determine the specific surface of the nanomaterial, it is necessary to know the amount of adsorbate needed to cover the surface with the gas molecules monolayer, and to determine the area needed to adsorb one adsorbate molecule. The knowledge of these quantities will then allow to determine the specific surface area of a solid sample of known weight. There are the number of such theories, but currently the BET (Brunauer-Emmett-Teller) isotherm [3] is used to calculate the specific surface area. It is necessary to emphasize that each of these (isotherms) theories has its limitations and validity, e.g. the BET isotherm does not assume the presence of micropores and capillary condensation. Therefore, it is only possible to use it in the range of relative pressures of 0.05-0.35 and to observe the shape of the relevant adsorption isotherm. The measurement of very small specific surface area (mostly specific surface area around 1 m^2/g) is also very popular and the BET isotherm can be used here as well. However, due to operational reasons, it is difficult to measure the adsorption isotherms using nitrogen and argon on adsorbents with a very small surface area. To overcome this problem, krypton is used as the adsorption gas for measurement of small specific surface area.

This procedure interesting in comparison to the size-based criterion and is that BET is a well-known, low-cost, standardized method, which can be applied on dry powders without further sample preparation except degassing, is agglomeration-tolerant, and leads to reliable results. When applying the volume-specific surface area method for the positive identification of nanomaterials only on non-porous materials, the classification can be considered as very reliable. When the particles are porous, the volume-specific surface area will be larger than expected from their outer dimensions (due to the additional surface of the pores, which conventional BET cannot distinguish from the external surface) and consequently, such materials should be excluded from the analysis, and the classification should not be done based on volume-specific surface area measurements. However, from the pore surface can be separated from the outer particle surface by a detailed analysis of the full adsorption isotherm, e.g., using an appropriate t-plot method [4].

In this study was evaluated the potential of the volume-specific surface area method as a classification tool, both for the identification of nanomaterials and of non-nanomaterials. For nonporous materials: When deriving the average size of the smallest particle dimension from volume-specific surface area, taking into account the approximate particle shape (sphere, fiber, platelet) is a good agreement with the electron microscopy results. Achieving such a good agreement is also possible for porous particles using the t-plot method (not BET method), which is capable of separating the pore surface from the particles external surface. Platelet materials are a special case, where the volume-specific surface area approach yields a more reliable classification than conventional electron microscopy, because electron microscopy cannot always address the relevant smallest dimension of the particles.

References

[1] W. Liu, S. Song, M. Ye, Y. Zhu, Y. Zhao and Y. Lu, Nanomaterials **12** (2022) 1845.
[2] W. Kreyling, M. Semmler-Behnke and Q. Chaudhry, Nano Today **5** (2010) 165.
[3] S. Brunauer, P. H. Emmet a E. Teller, J. Am. Chem. Soc. **60** (1938) 309.
[4] B.C.Lippens, B.G. Linsen and J.H. de Boer, J.Catal. **3** (1964) 32.

Nanostructures for Negative Electrodes in Lithium Ion Accumulators

J. Maca[a]*, J. Libich[a], P. Cudek[a], K. Jasso[a], T. Kazda[a]

[a] Brno University of Technology, Department of Electrical and Electronic Technology, Technická 10, 616 00 Brno, Czech Republic
*macaj@vut.cz

Introduction

This paper deals with electrodeposited layers of lead. Deposited layers are used as electrodes in lithium ion batteries. Finding alternative batteries electrode materials is a very hot topic in last few years. Therefor the focus is set to increasing the capacity and safety of these battery materials. One way to do that is a modification of electrodes. Tested electrodeposited layers are designed, to be used as a negative electrode and substitute the flammable carbon electrode. Different electrodeposited processes were used for the thin layer creation. The morphology of the layers was observed and the charge discharge capacity was determined.

It is known, that the physical properties and morphology electrodeposited layers strongly depends on different parameters like: composition of deposition solution, pH, temperature, stirring, voltage or current density. The first phase of deposition is most important for the final deposited layer. Generally can be said, that for homogeneous layer it is needed creation only few same size initial centres with will expand evenly on the underlying material[1,2]. In addition to reactive metals like lithium or sodium, it is necessary to continue in research on less reactive metals such as lead or zinc. Lead belong to most used material in electrochemistry thanks to the lead acid batteries used in car industry. Recently lot of research on sodium ion batteries were made. It seems as a promising substitution for lithium ion batteries in some low-end applications thanks higher among of sodium in Earth crust and lower price. The disadvantage of sodium compares to lithium is it size with is 55% larger. The size makes it difficult to found material in with it can easy intercalate and deintercalated. One of possibilities are lead and lead compounds like nitrates. These materials can be use as negative electrode materials[3-6].

Experimental

The lead layer was deposited in solution of 0.2M $Pb(NO_3)_2$ and 0.3M HNO_3. For the correct pH setting was ammonium hydroxide NH_4OH used. The pH at deposition was 7. The electrodeposition was carried out at current density 10 $mA \cdot cm^2$ till the total charge of 40 C flowed through. Different deposition processes were tested. The reference continuity deposition process and deposition processes by help of rectangular pulses. In the pulse waveform, the duty cycle of the signal was changed for 50:1, 5:1 and 1:5 as is shown in figure 1. On selected deposition sample the charge discharge capacity was measured. The measurement was carried out against metal lithium. Used electrolytes was 1M $LiPF_6$ in EC:DMC solvent solution (1:1 weight). The voltage boundary was 0.1V – 2.5V with charge discharge current of 0.2C. Ten cycles was carried out.

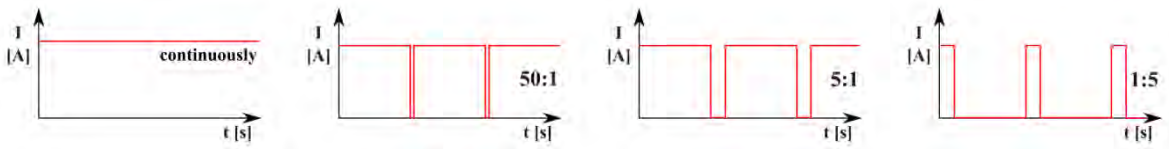

Figure 1: Used Electrodeposition signals for lead layers.

Conclusion

At the deposition with constant signal it is visible high proportion of needle shape dendrites on the deposited surface as is shown on figure 2 A. At signal duty 50:1 the proportion of needles is decreasing and the number of leaf shape

dendrites increase. This trend is obvious till the duty 1:5 where the needles are almost not present (figure 2 D). On the sample deposited by 1:5 duty ten charging/discharging cycles were made. The discharge capacity in first cycle was 36.6 $mAh \cdot g^{-1}$. Capacity in last cycle was 13.2 $mAh \cdot g^{-1}$. Coulombic efficiency at tent cycle was 92%.

Reached capacities cannot be compared with standard negative electrodes for lithium ion batteries based on carbon. However, it is a prerequisite for achieving higher capacities with use of sodium ions and potential use in sodium-ion batteries.

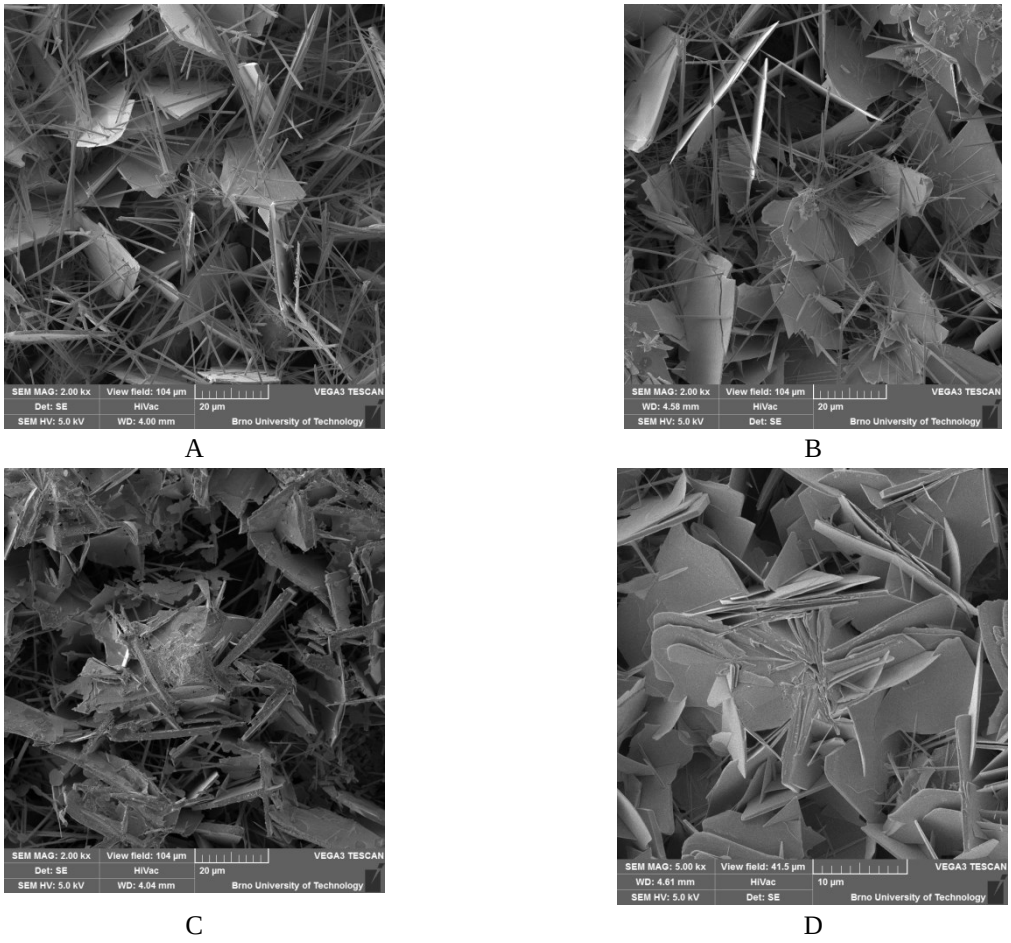

Figure 2: Surfaces layer of different depositions processes A) continuously, B) 50:1 duty, C) 5:1 duty, D) 1:5 duty.

Acknowledgements
Authors gratefully acknowledge the financial support from the Ministry of Education, Youth and Sports of the Czech Republic under project No. LTT19001 and BUT specific research programme (project No. FEKT-S-20-6206).

References

[1] A. C. Frank, P. T. A. Sumodjo, J. Electacta. **132**, (2014).
[2] M. G. Insinga, R. L. Oliveri, C. Sunseri, R. Inguanta, J. Jpowsour. **413**, (2019).
[3] T. J. Simons, A. K. Pearson, S. J. Pas, D. R. Macfarlane, J. Electacta. **174**, (2015).
[4] X. Lin, P. Li, L. Shao, X. Zheng, M. Shui, N. Long, D. Wang, J. Shu, J. Electacta. **169**, (2015).
[5] J. Bao, J. N. Lin, H. Lin, J. Guo, H. Gao, W. Gao, J. Jechem. **55**, (2021).
[6] A. F. Abdulrahman, R. Y. Mohammed, S. M. Ahmed, S. M. Hamad, J. Matpr. **44**, (2021).

Empirical Modelling of Li-S Batteries

M. Mačák[a]*, T. Kazda[a], P. Vyroubal[a]

[a] Department of Electrical and Electronic Technology, Brno University of Technology, Brno 616 00, Czech Republic
*martin.macak@vut.cz

Introduction

Li-S are one of the most promising next generation technologies for energy storage systems. Their advantage lies in their environmental friendliness and promising properties such as high specific capacity and energy density. In order to implement this technology, it is still necessary to overcome its shortcomings such as shuttle effect, self-discharge, volume expansion or low stability [1]. Currently, the experimental research is largely prevalent and primarily studies optimal material compositions to inhibit negative properties of this technology [2].

Unlike Li-Ion batteries, Li-S technology is governed by electrochemical and disproportionation reactions, which requires new descriptions of reaction mechanisms to build appropriate numerical models. For a discharge, the process starts with a dissolution of S_8, which is then subsequently reduced into lower polysulphides up until the final product Li_2S. During the charge, lower polysulphides are oxidized back to higher polysulphides up to S_8 [3]. However, this process is not symmetrical. Additionally, the exact mechanism depends on applied materials, which might change the equilibrium between intermediates. These processes were often studied with inert planar electrodes and not with actual battery electrodes, which would further influence the process. As a result, it is very difficult to describe the exact observed reaction mechanism, which could be used for physics-based numerical models [4]. Development of precise numerical models is necessary for the design and practical implementation of this technology.

Nevertheless, the research in numerical simulations of Li-S batteries is generally quite limited. Currently there are two main approaches for simulations of processes in Li-S batteries. The first approach uses a simplified cascaded mechanism consisting of five two-electron reactions accompanied by dissolution and precipitation of Li_2S_2 and Li_2S [5]. While this model is able to qualitatively capture some of the characteristics of a Li-S battery, it still exhibits important differences compared with experimentally observed Li-S behaviour [6]. Also, this model requires a large number of estimated parameters, which cannot be easily measured.

The other approach uses equivalent circuit models, which is a common method applicable for many battery technologies [7]. In this method, the battery is considered as a black-box and its behaviour is described through an electrical circuit. The circuit parameters are usually obtained from electrochemical impedance spectroscopy or pulse measurements. These models are usually very simple and accurate as they directly use experimentally obtained data. However, their accuracy depends on the applied electrical circuit and the quality of measured data. The disadvantage of this method is that the black-box description only allows for indirect investigation of the process [8].

This paper presents empirical models, which combine the advantages of experimentally obtained data and physics-based models. The model is based on fitting of cycling characteristics into governing equations. This approach results in a detailed model based on the most common measurements, which is able to capture external characteristics as well as the internal processes.

Numerical Model

The presented model is based on curve fitting of discharge/charge characteristics of a battery [9, 10]. The first approach is similar to equivalent circuit modelling. The governing equation of the model in this case is described through a battery voltage dependency on an open circuit voltage, electrical conductivity and a current. The model parameters (conductivity and open circuit voltage) are obtained through polarization curves at different depths of discharge. The second step involves including current dependency of Li-S battery capacity, to properly describe the capacity decrease. This dependency is obtained from cycles at different C-rates. Based on these two equations, the model is able to

accurately predict the battery behaviour at any C-rate. Figure 1. Shows the results from the presented model, which was based on a discharge at 0.05 C, 0.2 C and 1 C.

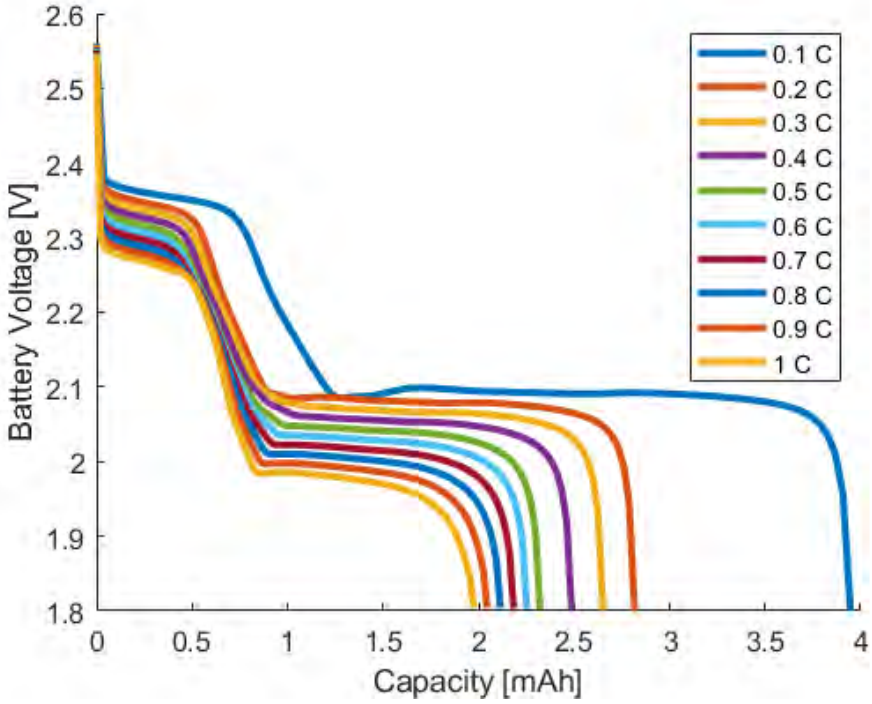

Figure 13: Simulations of Li-S discharge at different C-rates.

The second approach used curve fitting of cycling voltammetry data. In this case, the governing equations consisted of a set of equations defining multiple observed reaction steps. Following parameters were fitted: exchange current density, concentration dependence of the reaction and the reduction potential. As the presented equations did not impose as many restrictions as original physics-based models, it was possible to closely fit the voltammetry data, which could be also later used for the simulation of diffusion influence. Similarly, this model has been used for detailed cycling simulations, which could study the evolution of defined polysulphides during all stages of the process.

Acknowledgements
This work was supported by the BUT specific research program (project No. FEKT-S-20-6206).

References

[1] X. Qiu, Q. Hua, L. Zheng, Z. Dai, RSC Advances **10**(9) (2020) 5283-5293.
[2] T. Kazda, D. Capková, K. Jaššo, A. Fedorková Straková, E. Shembel, A. Markevich, M. Sedlaříková, Materials **14**(19) (2021) 5578.
[3] M. Cuisinier, C. Hart, M. Balasubramanian, A. Garsuch, L. F. Nazar, Adv. Energy Mater. **5**(16) (2015) 1401801.
[4] M. Wild, L. O'Neill, T. Zhang, R. Purkayastha, G. Minton, M. Marinescu, G. J. Offer, Energy Environ. Sci. **8**(12) (2015) 3477-3494.
[5] K. Kumaresan, Y. Mikhaylik, R. E. White, J. Electrochem. Soc. **155**(8) (2015) A576-A582.
[6] M. Mačák, P. Vyroubal, T. Kazda, K. Jaššo, J. Energy Storage **27** (2020) 101158.
[7] A. Fotouhi, D. J. Auger, K. Propp, S. Longo, IET Power Electronics **10**(11) (2017) 1289-1297.
[8] M. Mačák, T. Kazda, K. Jasso, P. Vyroubal, ECS Trans. **105** (2021) 609-616.

[9] K. H. Kwon, C. B. Shin, T. H. Kang, C. S. Kim, J. Power Sources **163**(1) (2006) 151-157.
[10] H. Gu, J. Electrochem. Soc. **130** (1983) 1459.

Stable cycle performance enhancement by addition of pyrite in sulfur cathode

J. Macko[a,*], D. Capková[a], T. Kazda[b], O. Petruš[c], A. Straková Fedorková[a], A. Oriňak[a], R. Oriňaková[a]

[a]Department of Physical Chemistry, Faculty of Sciences, Pavol Jozef Šafárik University in Košice, Moyzesova 11, 041 54, Košice, Slovak Republic
[b]Department of Electrical and Electronic Technology, Faculty of Electrical Engineering and Communication, Brno University of Technology, Technická 10, 616 00, Brno, Czech Republic
[c]Institute of Materials Research, Slovak Academy of Sciences, Watsonova 47, 040 01 Košice, Slovak Republic
*jan.macko@upjs.sk

Lithium-sulfur batteries provides high theoretical capacity of 1675 mAh g^{-1}, in addition. sulfur is naturally abundant in environment and low-cost [1]. To suppress large volume variation and polysulfide shuttle in lithium-sulfur batteries during cycling, an efficient host needs to be found. Addition of various transition sulfide in cathode material can improve stability and suppress the polysulfide diffusion. Polysulfide shuttle leads to irreversible loss of active material and in corrosion of lithium anode [2]. The electrode composite material was prepared of sulfur, carbon Super P and pyrite powder. Components were mixed on two selected ratios with pyrite content of 5% and 10%. Morphologically, The S/C/10%FeS_2 electrode is more porous than S/C/5%FeS_2 electrode. In the study, 10% pyrite addition to the cathode material improved discharge capacity of 788 mAh g^{-1} after 60 cycles at 0.2 C.

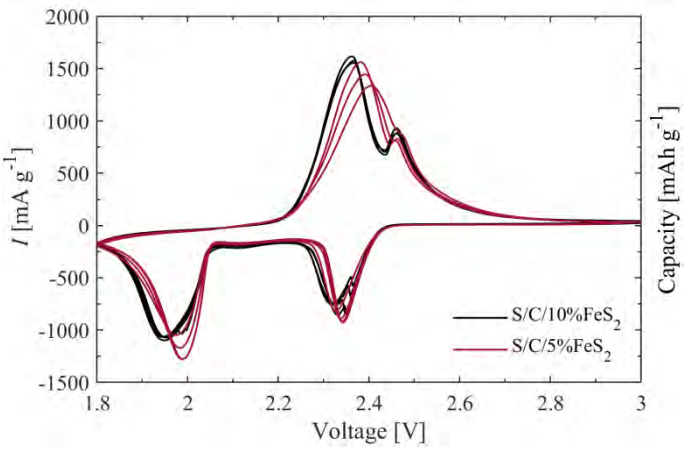

Figure 1: CV curves of the S/C/10%FeS_2 and S/C/5%FeS_2 electrodes at scan rate of 0.1 mV s^{-1}.

To investigate the electrochemical properties of the prepared electrode materials, the cyclic voltammetry (CV). Fig. 1 shows CV of both electrodes, it is clearly seen that cycling stability of the S/C/10%FeS_2 electrode is higher, the intensity of the peaks remains stable with the number of cycle and the current density of the S/C/5%FeS_2 electrode decreases with each cycle. Electrode surfaces of both electrodes were coated uniformly. There were not observed any disorders in the material. The porous electrode structure allows higher level of electrolyte penetration. It attenuates shuttle effect by capturing lithium polysulfides.

Acknowledgements

This research was supported by the project APVV-20-0138 of the Slovak Research and Development Agency: Development of Novel 3D Materials for Post Lithium Ion Batteries with High Energy Density.

References

[1] D. Capková, M. Almáši, T. Kazda, O. Čech, N. Király, P. Čudek, A. Straková Fedorková, V. Hornebecq, Electrochim. Acta **354** (2020) 136640.
[2] Z. Chang, Y. Qiao, J. Wang, H. Deng, P. He, H. Zhou, Energy Stor. Mater. **25** (2020) 164-171.

Electrochemical Characterization of Biomaterials Prepared by Space Holder Method

R. Macko[a]*, R. Gorejová[a], R. Oriňaková[a]

[a] Department of Physical Chemistry, Faculty of Sciences, Pavol Jozef Šafarik University of Košice, Šrobárova 2, 041 54 Košice
*rastislav.macko@student.upjs.sk

One of the most common health problems are fractures and bone defects. Since bones are found inside organisms, emphasis had to be placed on how to treat internal injuries. Biomaterial is a specifically manufactured material aimed to be used in medicine, therapy, diagnostics or other way of non-destructive use in organism [1]. This is one of the reasons why biomaterials have been used extensively. In terms of biomaterials, there is a field of biodegradable materials that is currently being vastly studied as a feasible replacement of bioinert materials, including the currently most used titanium or cobalt-chromium alloys. Iron, zinc or magnesium are already in human bodies and are able to be metabolized, therefore these are the most suitable for further examination.

In this work, samples were prepared by sintering tablets consisting of iron powder (Fe) as a base material and urea (Ur) acting as a space holder in ratios of 100:0, 95:5, 90:10, 85:15 and 80:20 weight percentages. Samples were marked as A#, where "#" is substituted by the weight percentage of space holder used. All of them were tested electrochemically and studied in the terms of corrosion properties. The tests to determine porosity and mass loss were performed. These were used to confirm the relation between increase of porosity and decrease of mass. Further morphological examination of the surface porosity was performed by the Scanning Electron Microscopy (Fig. 1). These images show, that pores are increasing in size and amount with increasing Ur content, that means the Ur was succesfully removed from the samples.

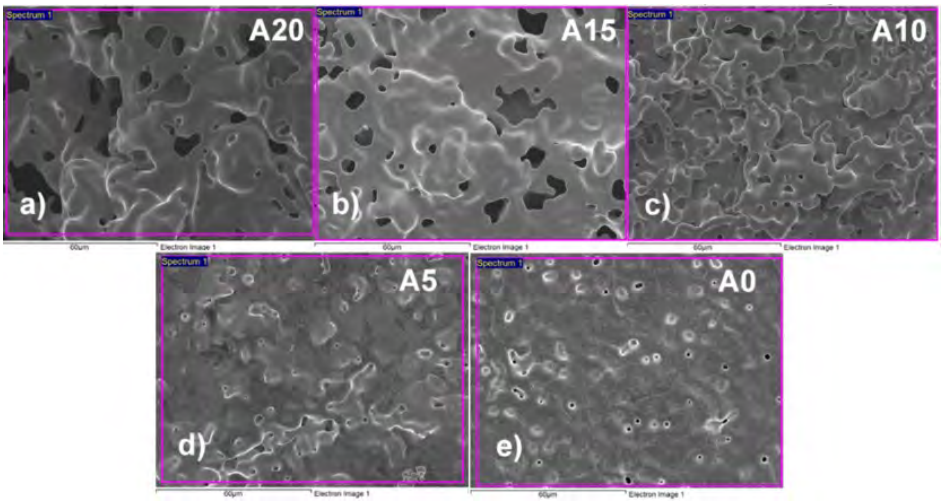

Figure 14: SEM images of manufactured samples: a) A20; b) A15; c) A10; d) A5; e) A0.

The main aim of the work was to characterize biodegradation properties by using electrochemical method of linear polarisation in Hanks' solution at 37±2°C and pH 7.5±0.2. Figure 2 shows the results of the electrochemical test.

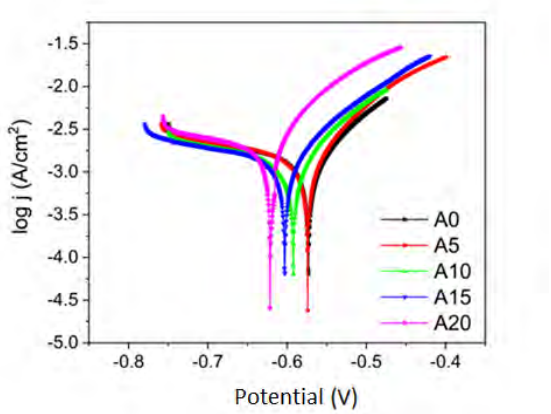

Figure 15: Tafel plots of prepared samples as a result of the electrochemical test.

As shown on Figure 2, the increasing amount of porosity caused the shift of corresponding corrosion potential to the more negative values. This is because the higher amount of pores means the larger surface area that can succumb to the corrosion process. Similar results can be seen in Sharma [3]. The highest corrosion rate of A20 is 0.746 mm/year, whereas it is 0.555 mm/year for A0 with the smallest surface area. This means that this method can be used to modify corrosion properties of samples in required way. The space holder method has shown its potential and it's suitable for further testing.

Acknowledgements
This work was supported by the projects APVV-20-0278 of the Slovak Research and Development agency.

References

[1] G. Schmalz, *Determination of Biocompatibility*; in: *Biocompatibility of dental materials, Vol 1* (Schmalz G., ed.). Springer-Verlag Berlin Heidelberg, Berlin, page 13-43.
[2] M. Tilton, A. Borjali, A. Isaacson, K. M. Varadarajan, G. P. Manogharan, Mater. Des. **201** (2021) 2.
[3] P. Sharma, K. G. Jain, P. M. Pandey, S. Mohanty, Mater. Sci. Eng. C. **106** (2020) 9-10.

An In-depth Study of the Wettability of MXene Films

P. Machata[a]*, M. Hofbauerová[b], Y. Soyka[a], A. Stepura[a], D. Truchan[b], Y. Halahovets[b], M. Mičušík[a], P. Šiffalovič[b], M. Omastová[a]

[a] Polymer Institute, SAS, Dúbravská cesta, 9, 845 41 Bratislava, Slovakia
[b] Institute of Physics SAS, Dúbravská cesta 9, 845 11 Bratislava, Slovakia
*peter.machata@savba.sk

Two-dimensional transition metal carbides and nitrides (MXenes) have accumulated tremendous interest recently due to their high conductivity and excellent figures of merit in electromagnetic interference shielding and other applications [1,2]. The most studied nanomaterial from the MXene family is titanium carbide $Ti_3C_2T_x$. One of the most highlighted properties of $Ti_3C_2T_x$ and other MXenes compared to the other nanomaterials is their hydrophilicity, which is exhibited by MXenes due to the presence of polar surface functional groups Tx. The most common method to determine the hydrophobicity or hydrophilicity of the material is a contact angle measurement. However, the measurement of the static contact angles (CAs) using a sessile drop method has been criticized in numerous articles due to a huge random effect and the reproduction of these experimental static contact angles becomes a challenge for the other laboratories [3]. As a result, for MXenes, static CAs have been reported in the literature and their values lie in a broad range from 18 to 91 degrees [4].

In this work, we investigated $Ti_3C_2T_x$–water interactions for 1, 2 and 3 layers of MXene on substrates of different chemical composition and different wettability using advancing and receding contact angle measurement [4]. As substrates, UV-ozone treated silicon wafer (OH-Si) and silicon wafer functionalized by (3-aminopropyl)triethoxysilane (APTES-Si), were used. The use of advancing (highest possible) and receding (lowest possible) contact angle measurement rather than static contact angle measurement provides not only reproducible contact angle data, but also offers a comprehensive understanding of the wettability of MXene films and can help to elucidate the experimental values of the static contact angles in the literature. The imperfections (edges, cracks and grain boundaries) of the MXene layers were investigated by microscopic techniques – atomic force microscopy (AFM) and imaging ellipsometry [4].

The values of the advancing contact angle on $Ti_3C_2T_x$ on both substrates were proved to be independent of the number of $Ti_3C_2T_x$ layers, demonstrating a negligible effect of the background substrate wettability (Fig. 1). In addition, a giant contact angle hysteresis (44-52°) was observed (Fig. 1) on very smooth surface, most likely as a result of chemical heterogeneity arising from the diversity of surface terminal groups (F, O, and OH) [4].

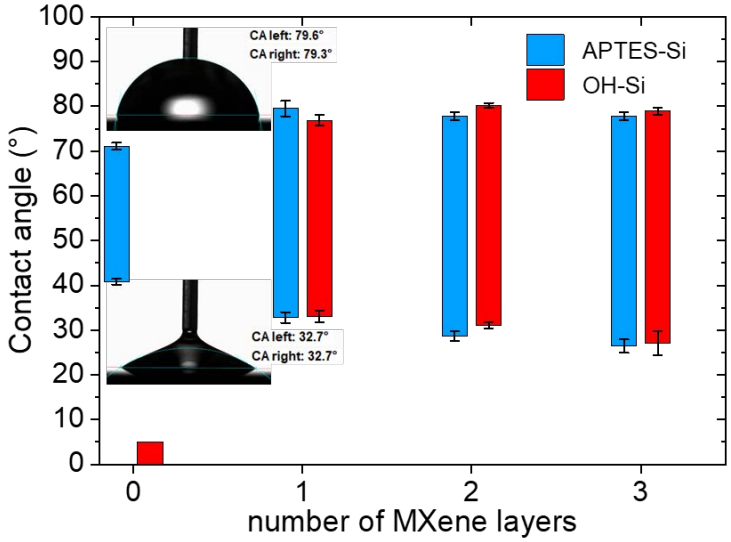

Figure 1: Experimental values of the CA hysteresis of water, including advancing and receding CAs, obtained by continuously increasing and decreasing the droplet volume by a needle for bare substrates and those with mono-, bi, and trilayered $Ti_3C_2T_x$. Inset: corresponding pictures of the advancing (top) and receding (bottom) CAs of water on $Ti_3C_2T_x$ monolayer.

The findings reported in this study provide a comprehensive understanding of the wettability of MXene and help to elucidate the experimental values of the static contact angles in the literature. Additionally, fundamental understanding of MXene–water interactions is an important step towards developing MXene-assisted surface coatings for microfluidics-based devices.

Acknowledgements
This work was supported by the Slovak Research and Development Agency under the contract No. APVV-19-0465 and by project VEGA 02/0006/22.

References
[1] M. Naguib, M. Kurtoglu, V. Presser, J. Lu, J. Niu, M. Heon,; L. Hultman, Y. Gogotsi, M. W. Barsoum, Adv. Mater. **37** (2011) 4207–4207.
[2] V. Gajdošová, L. Lorencová M. Procházka, M. Mičušík, M. Omastová, S. Procházková, F. Kvetoň, M. Jerigová, D. Velič, P. Kasák, J. Tkáč, Microchim. Acta, **187** (2020) 1-8.
[3] J. W. Drelich, Adv. Colloid Interface Sci. **267** (2019) 1–14.
[4] P. Machata, M. Hofbauerová, Y. Soyka, A. Stepura, D. Truchan, Y. Halahovets, M. Mičušík, P. Šiffalovič, E. Majková, M. Omastová, J. Colloid Interface Sci. **622** (2022) 759–768.

Aging of 2D MXene Nanoparticles in Air: an XPS and TEM Study

M. Mičušík[a]*, M. Šlouf[b], M. Procházka[a], A. Stepura[a], Y. Soyka[a], P. Fitl[c], M. Omastová[a]

[a]Polymer Institute SAS, Dúbravská cesta 9, 84541 Bratislava, Slovakia
[b]Institute of Macromolecular Chemistry, Czech Academy of Sciences, Heyrovského nám. 2, 162 06 Prague 6, Czech Republic
[c]University of Chemistry and Technology Prague, Department of Physics and Measurements, Technická 5, 16628 Prague, Czech Republic
*matej.micusik@savba.sk

Abstract

MXene is one of the many alternatives of 2D structures materials. The general formula for MXenes is $M_{n+1}X_nT_x$ (n = 1–3), where M represents transition metals (Sc, Ti, Zr, Hf, V, Nb, Ta, Cr, Mo, and others), X is carbon and/or nitrogen, and T_x refer to various functional groups on the surface (e.g. OH, O, F, etc.). The combination of 2D particles such as MXene and 1D fillers such as carbon nanotubes and consequent implementation into the polymeric matrix enables to prepare polymer composites with a high electroconductivity and electromagnetic interference (EMI) shielding capacity.

At first, we prepared and characterized MXene 2D nanoparticles, which were used as active filler in the polymer composites. For the final application it is always important to know the detailed structure of MAX phase used for MXene preparation[1].

One of the main drawbacks of MXene application is their relatively low stability on air. In our study we used XPS and TEM in multiple modes (bright field imaging, energy-dispersive analysis of X-rays, and selected-area electron diffraction) in order to study the chemical and morphological changes in 2D MXene type $Ti_3C_2T_x$ exposed to air for several months. Different batches of $Ti_3C_2O_xF_x$ MXene were prepared, and their stability in air and argon was studied. X-ray photoelectron spectroscopy (XPS) and transmission electron microscopy (TEM) in multiple modes (bright field imaging, energy-dispersive X-ray analysis, and selected-area electron diffraction) were employed to study the chemical and morphological changes in two-dimensional (2D) MXene exposed to air. We detected the progressive development of the Ti^{4+} state accompanied by TiO_2 formation, which lead to a slow disintegration of the 2D MXene nanosheets, although their overall morphology and crystalline structure can persist for several months. The presence of water is found to play an important role in the hydrolysis and degradation reactions during MXene aging. Our XPS and TEM studies showed how the surface chemistry changes during aging in air and which surface termination groups are indicative of stable $Ti_3C_2O_xF_x$ MXene and which storage conditions can stabilize MXene for more than a year.

Prepared MXene wil be used in engineering of Black metals (BM) sensors. BM decorated with surface receptors are high-potentiality materials for gas sensing. The goal will be to contribute to the surface/interface engineering of BM sensors by incorporation of 2D nanomaterials and to prepare new nanostructures with tailored surface chemistry with the aim to improve the sensitivity of prepared sensors.

Acknowledgements

This work was supported by the V4-Japan 2021 Joint Call on Advanced Materials under registration number V4-Japan/JRP/2021/96/BLACKSENS and by Slovak Research and Development Agency under the project APVV-19-0465 and APVV-19-0461 and by agency VEGA 2/0006/22 (Slovakia).

References

[1] M. Ivanovskaya, E. Ovodok, D. Kotsikau, I. Azarko, M. Mičušík, M. Omastová, V. Golovanov, RSC Adv. **10** (2020) 25602-25608.

Effect of Charging on the Electronic Structure and Plasmonic Properties of Derivatized Anthracenes

G. R. Mini Rajendran[a], P. Tisovský[a,b], L. F. Pašteka[c], M. Sýkora[a]*

[a] Laboratory for Advanced Materials, Faculty of Natural Sciences, Comenius University
[b]Department of Organic Chemistry, Faculty of Natural Sciences, Comenius University
[c]Department of Physical and Theoretical Chemistry, Faculty of Natural Sciences, Comenius University,Ilkovičova 6, 841 04 Bratislava, Slovakia
*sykoram@uniba.sk

Small Polycyclic Aromatic Hydrocarbons (PAHs), such as anthracene exhibit intense absorption in the visible region when charged. Recently it has been proposed that these absorption features can be explained in terms of molecular plasmon resonances [1]. Such resonances are possible in PAHs thanks to the delocalized nature of electrons in the π–π∗ orbitals, which allow for collective electron density displacements. It was also shown that the extent of the plasmon character of the optical transitions can be quantified theoretically using the time-dependent density functional theory (TD-DFT) [2,3]. Although the basic principles of the plasmon effects in PAHs are known, little is known about the effects of specific substitutions on the plasmonic properties of small PAHs. In the present work we synthesized series of anthracenes derivatized on the periphery with the carboxylic acid esters and bromine atom and investigated their optical properties in the neutral and charged state using electronic absorption spectroscopy and spectro-electrochemistry. We observed systematic changes in the absorption features of the charged compounds with the peripheral functionalization. The observed absorption features were analyzed with the aid of the TD-DFT modelling to quantify the plasmonic nature of the observed absorption features. Our results show that the energy and the plasmonic nature of the optical transitions in the anthracene are highly sensitive to the nature of the peripheral substituent. The extent of this effect is quantified.

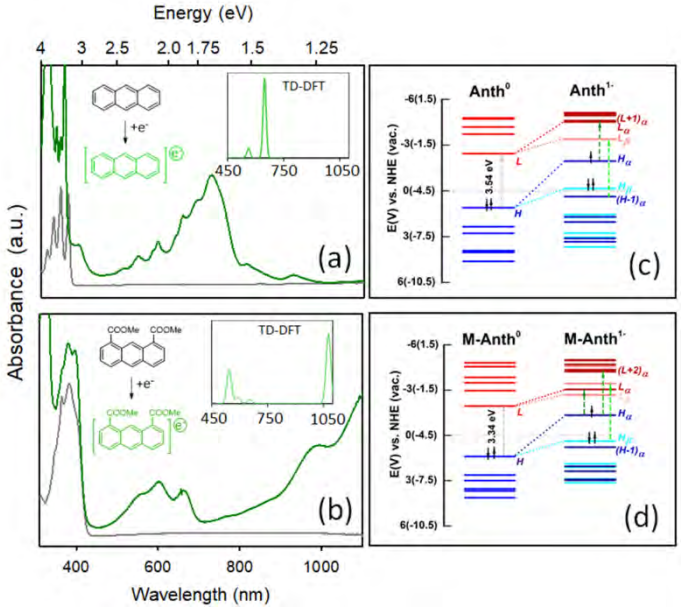

Figure 1: Effect of charging on the absorption spectra and the electronic structure of derivatized anthracenes. Experimental absorption spectra of the neutral (gray) and charged state (green) of anthracene (a) and methoxy anthracene (b). The inset shows the TD-DFT calculated spectra of the charged compounds. The panels (c) and (d) show the calculated molecular orbital diagrams of the neutral and charged compounds shown in (a) and (b).

Acknowledgements
This work was supported by the European Union's Horizon 2020 research and innovation programme under grant agreement No. 810701 and by the Slovak Research and Development Agency under grant agreement No. APVV-19-0410 and the Slovak Ministry of Education Grant. No. VEGA 1/0892/21 and Comenius University grants for doctoral students and young scientists No. UK/432/2022.

References
[1] A. Lauchner, A.E. Schlather, A. Manjavacas, Y. Cui, M.J. McClain, G.J. Stec, F.J. García de Abajo, P. Nordlander, N.J. Halas, Nano letters. **9** (2015) 6208-6214.
[2] R. Zhang, L. Bursi, J.D. Cox, Y. Cui, C.M. Krauter, A. Alabastri, A. Manjavacas, A. Calzolari, S. Corni, E. Molinari, E.A. Carter, ACS nano. **7** (2017) 7321-7335.
[3] J. Langford, X. Xu, Y. Yang, J. Phys. Chem. Lett. **12** (2021) 9391-9397.

Polypyrrole Encapsulated Sulfur for Li-S Battery

V. Niščáková[a]*, A. Straková Fedorková[a]

[a] Pavol Jozef Safarik University of Kosice, Department of Physical chemistry, Srobarova 2, 040 01, Kosice
*veronika.niscakova@student.upjs.sk

Lithium sulfur batteries (Li-S) are considered to be batteries of the next-generation, which are composed of a sulfur cathode and a high-energy lithium anode. However, even these new generation batteries suffer from certain shortcomings that need to be overcome, such as insulating nature of sulfur, production of lithium polysulfide during cycling, the large volumetric expansion of sulfur after lithiation (≈80%) etc. These obstacles result in low coulombic efficiency, insufficient sulfur utilization, and unstable cycling performance [1]. These drawbacks need to be resolved before fulfilling the promise of the market potential. It is the first priority to design the cathode that ensures the maximum usage of the starting materials, which sets the upper limit of the capacity performance. Second, the muti-step reduction process releases highly soluble lithium polysulfides

intermediates into the organic electrolyte [2]. Most efforts have been directed to prevent soluble polysulfides from shuttling, by encapsulation of sulfur with conducting membranes or porous structures. Among conductive polymers, polypyrrole has been widely investigated owing to its high electronic conductivity, low cost of precursors, and ease of synthesis [3].

In this work, a cathode containing polypyrrole was prepared for a Li-S battery with composition of 90% S/C/ppy composite and 10% PVDF (polyvinylidene fluoride as a binder). The prepared electrode was tested by cyclic voltammetry, and galvanostatic cycling. The cycling took place in the range of potentials from 1,8 V - 2,8 V. The initial discharge capacity of the prepared electrode at 0.1 C was around 753 mAh.g^{-1}

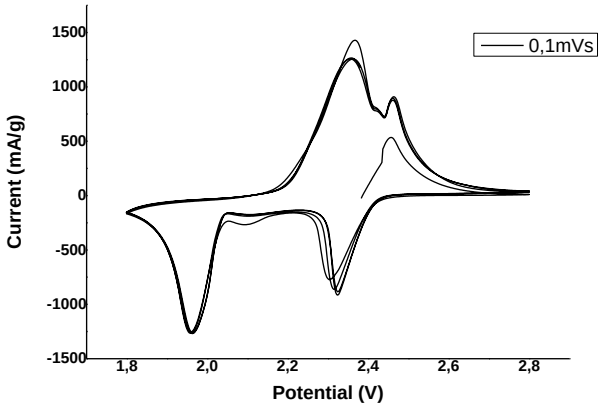

Figure 16: Cyclic voltammogram of S/C/ppy composite at scane rate 0,1 mV/s.

Acknowledgements
This publication was supported by the Operational program Integrated Infrastructure within the project: Innovative Solutions for Propulsion, Power and Safety Components of Transport Vehicles, 313011V334, cofinanced by the European Regional Development Fund and of the Slovak Research and Development Agency APVV-20-0138 and APVV-20-0111 and by the VVGS UPJS project No. 2022–2193.

References

[1] S. Huang, Z. Wang, Y. Von Lim, Y. Wang, Y. Li, D. Zhang, H.Y. Yang, Adv. Energy Mater. **11** (2021) 1–27.
[2] Y. Hu, W. Chen, T. Lei, Y. Jiao, J. Huang, A. Hu, C. Gong, C. Yan, X. Wang, J. Xiong, Adv. Energy Mater. **10** (2020) 1–19.
[3] Y. Ansari, S. Zhang, B. Wen, F. Fan, Y.M. Chiang, Adv. Energy Mater. **9** (2019) 1–7.

Polymeric Nanocomposites with Hybrid Two- and One-Dimensional Fillers

M. Omastová[a*], M. Mičušik[a], A. Stepura[a], M. Lavorgna[b], G. Gentile[b], M. Avella[b], E. Matysová[c], V. Špaček[c]

[a]Polymer Institute, Slovak Academy of Sciences, Dúbravská cesta 9, 845 41 Bratislava, Slovakia
[b]Institute of Polymers, Composites and Biomaterials, National Research Council of Italy, Napoli, Italy
[c] SYNPO akciova spolecnost, Pardubice, Czech Republic
* maria.omastova@savba.sk

Introduction

Polymers are great class of materials, which have been developing widely through decades. The huge variety of polymers and respectively big diversity of their properties provides application in numerous fields of human life. Preparation of polymeric composites often is a complex procedure, and results depend on many points and factors of preparation ways. There are only limited kinds of polymers, which are water soluble, but amongst such few polymeric matrices, recently HAVOH – highly amorphous polyvinyl alcohol – was patented and commercialized under the name G-polymer [1]. HAVOH is a polyvinyl alcohol modified with diol monomers. Its prominent properties include being environmentally friendly, with excellent water solubility and dispersibility, ease of melt processing and for coating, low oxygen permeability, etc. Thus, HAVOH is mainly used for food and medical packaging.

Regarding nanofillers for composites, classification and variety of materials, is slightly smaller, but still wide. Over the last two decades, the most studied, mostly utilized are graphene, graphene oxide, Ag, MoS_2, ZnO, cellulose nanofibers, carbon quantum dots and carbon nanotubes, and the "youngest", recently discovered, MXenes. MXenes are two-dimensional (2D) inorganic nanoparticles, which are layered structures of transitional metal carbides, nitrides or carbonitrides. Its general formula is $M_{n+1}X_nT_x$, where M stands for transitional metal, X is for carbon or/and nitrogen, and T_x represents surface termination groups, that are mostly =O, -F, -OH, -Cl. MXenes possess numerous outstanding properties, such as electrical, mechanical, optical etc., e.g. high electrical conductivity, big energy capacitance, absorption of microwaves etc. [2, 3]. However, the field of their application as fillers in composites remains poorly studied comparing to other areas. On the contrary, one-dimensional (1D) single-walled carbon nanotubes (SWCNTs), one of possible forms of carbon nanotubes, are often applied as fillers in polymeric nanocomposites. Comparing to MWCNTs (multi-walled carbon nanotubes), electronic behaviour of SWCNTs, whether it will be as in semiconductor or as in metal, is defined by ordering of carbons [4]. SWCNTs are stiff, elastic, with small intrinsic diameter, high surface area and strong Wan-der-Waals bonds. Besides as fillers, single-walled carbon nanotubes can be also used in supercapacitors, sensors, drug delivery, nanoelectrodes etc.

Materials and Methods

In this work, we report preparation of three series of composite samples with two types of nanofillers – 1D single-walled carbon nanotubes (HAVOH/SWCNTs), with 2D MXenes nanoparticles (HAVOH/MXenes) and hybrid ternary composites with both SWCNTs and MXenes fillers (HAVOH/SWCNTs/MXenes). The range of fillers concentrations varied from 1.0 to 5.0 wt.%. All samples were prepared by solvent casting method. SWCNTs were sonicated for 1 hour in water with ultrasonic probe, and afterwards the glass was transferred onto magnetic stirrer. Then calculated amount of HAVOH powder was slowly added straight into that mixture for its dissolving, by stirring 30 min at 50 °C and then 30 min at 90 °C. In case of ternary HAVOH/SWCNTs/MXenes composites, calculated amount of water-based MXene solution was also added to the HAVOH powder. After stirring, this solution was transferred for further mixing with mechanical (overhead) stirrer at 1200 rpm for 3 hours, and this mixture was poured out into Teflon Petri dish, left on an open air for few hours, and then put into vacuum drier for total water evaporation. Dried films were compression moulded between two hot plates at 220 °C.

Results

Electrical conductivity of all composites including neat matrix were measured with broadband dielectric spectroscopy (BDS) using Novocontrol Concept 40 (Germany). As it is common for polymers, neat HAVOH matrix had conductivity 10^{-14} S/cm, what indicates that it was not conductive. When only 1.0 wt. % of SWCNTs was added, conductivity reached 10^{-6} S/cm. In case of HAVOH/MXenes composites with slightly higher concentration of 5.0 wt. % of the filler, specimens conductivity showed values 10^{-7} S/cm, what lies in the semiconductor zone. Even three orders higher values, e.g. 10^{-4} S/cm, were received for ternary HAVOH composites, when both 3.0 wt. % of 1D single-walled carbon nanotubes and 1.0 wt. % of 2D MXenes were added simultaneously. In this case, it can be explained with synergetic effect of the fillers, when long and flexible carbon nanotubes create longer conductive paths by formation of connections between single sheets of MXenes. This was also confirmed with scanning electron microscopy (SEM) study of composite samples, by examination of a cryo-fractured surface in liquid nitrogen after coating with a thin layer of gold. The results of the analysis showed homogeneous structures, without significant agglomerations of carbon nanotubes and big clusters of MXenes.

Conclusions

HAVOH (highly amorphous polyvinyl alcohol) is a recently synthesized polyvinyl alcohol modified with diol monomers. Its main advantage in our work is its water solubility. HAVOH/SWCNTs, HAVOH/MXenes, HAVOH/SWCNTs/MXenes composites were firstly prepared using solvent casting method. The range of fillers load varied from 1.0 wt. % up to 5.0 wt. %. Using BDS method specimens were tested for electrical conductivity properties. Highest value – 7.9×10^{-5} S/cm – was obtained for HAVOH/3.0 wt. % SWCNTs/2.0 wt. % MXenes composite sample. Besides that, SEM study of the prepared specimens was performed. It showed homogeneous structure of fillers dispersed in all composites, but in HAVOH/MXenes samples lamellar structure was observed, whereas in HAVOH/SWCNTs or in hybrid composites more fibrous structure was detected. Possible future applications of this type of composites can be as conductive materials in the EMI-shielding and as coatings.

Acknowledgements

This work has received funding from the CRN-SAV-20-04 mobility project, from project VEGA 02/0006/22 (Slovakia), project MEraNet EPIC and COST project CA19118 EsSENce.

References

[1] Santillo C., Godoy A. P., Donato R. K., Andrade R. J. E., Buonocore G. G., Xia H., Lavorgna M., Sorrentino A. Compos. Sci. Technol. **207 (**2021) 108742.

[2] Anasori B., Gogotsi Yu., *2D Metal Carbides and Nitrides (MXenes).* Springer Nature Switzerland 2019, 534 p.

[3] Machata P., Hofbauerová M., Soyka Ya., Stepura A., Truchan D., Halahovets Yu., Mičušík M., Šiffalovič P., Majková E., Omastová M. J. Colloid Interface Sci. **622** (2022) 759-768.

[4] Eatemadi A.; Daraee H.; Karimkhanloo H., Kouhi M., Zarghami N., Akbarzadeh A., Abasi M., Hanifehpour Y., Joo Woo S.. Nanoscale Res. Lett. **9** (2014) 393.

Electrocatalytic Hydrogen Evolution Reaction

R. Oriňaková[a]*, A. Gubóová[a], M. Strečková[b]

[a]Institute of Chemistry, Faculty of Science, P.J. Safarik University, Moyzesova 11, 040 01 Kosice, Slovakia
[b]Institute of Materials Research, Slovak Academy of Sciences, Watsonova 47, 040 01 Kosice, Slovakia
* renata.orinakova@upjs.sk

With the expansion of the human population, the demand for energy in society is increasing and conventional fossil fuels (such as coal, oil, natural gas, etc.) cannot satisfy the needs of social development. The rising concerns about CO_2 emissions have led to a growing realization that it is not possible to sustain the world's current development based on fossil fuels without a substitution of clean and renewable energy [1]. Due to its high gravimetric energy density (up to 140 MJ kg^{-1}) and environmental friendliness, hydrogen is regarded as one of the ideal green energy sources [2]. Hydrogen is produced through a variety of methods, including thermal chemical technology, electrochemical technology, biotechnology, and photoelectrochemical means. However, recent industrial hydrogen production methods are mostly based on fossil fuels, which conflicts with the sustainable development of modern society [3]. The hydrogen evolution reaction (HER) of electrocatalytic water splitting is one of the most effective and eco-friendly approach to produce hydrogen gas based on the electricity generated from renewable energy sources [4]. This simple, efficient, and clean method for large-scale hydrogen production is now more important and promotes the rapid development of the hydrogen economy [5].

Electrocatalysts play a key role in these energy conversion technologies and can greatly accelerate reaction kinetics and efficiency by reducing the activation energy and thus the overpotential. HER in an acidic environment generally requires lower overpotentials than those in a basic environment.

A robust and efficient non-precious metal catalyst for hydrogen evolution reaction is one of the crucial components for carbon dioxide-free hydrogen production. Platinum, along with its alloys, is the benchmark electrocatalyst that requires very small overpotentials to drive the reaction, whereas the scarcity and high cost of Pt hinder its large-scale use for H_2 production. As a result, enormous research efforts have been devoted to finding and engineering low-cost alternative catalysts.

Until now, numerous nonprecious transition metal based catalysts have been explored to replace Pt in acidic media for HER, such as transition metal carbides, sulfides, nitrides, phosphides, and selenides [6]. Due to their large surface area and high stability in both acidic and basic environments, mesoporous carbon is an excellent type of catalyst support. The synergetic interaction between the active electrocatalytic material and the support material enhances the activity of catalyst. Our previous papers revealed that single and bimetallic phosphide nanoparticles incorporated into the carbon fibres are highly efficient electrocatalysts for both HER and oxygen evolution reaction (OER). Moreover, our recent study identified the nickel and nickel-iron foams as high-performance electrocatalytic materials for HER. An excellent stability allows the practical application of mentioned materials for electrocatalytic splitting of water to produce hydrogen.

Acknowledgements
This work was supported by Slovak Research and Development Agency under the contract no. APVV-20-0229 and Grant Agency of Slovak Academy of Sciences, project No. VEGA 1/0095/21.

References
[1] E.A. Quadrelli, G. Centi, J.L. Duplan, S. Perathoner, Chemsuschem. **4** (2011) 1194–1215.
[2] C.G. Morales-Guio, L.A. Stern, X.L. Hu, Chem. Soc. Rev. **43** (2014) 6555- 6569.
[3] R. Subbaraman, D. Tripkovic, K.C. Chang, D. Strmcnik, A.P. Paulikas, P. Hirunsit, M. Chan, J. Greeley, V. Stamenkovic, N. M. Markovic, Nat. Mater. **11** (2012) 550-557.

[4] R. Kumar, S. Sahoo, E. Joanni, R.K. Singh, R.M. Yadav, R.K. Verma, D.P. Singh, W.K. Tan, A. Pérez del Pino, S.A. Moshkalev, et al., Nano Res. **12** (2019) 2655–2694.
[5] T. Kosmala, A. Baby, M. Lunardon, D. Perilli, H. Liu, C. Durante, C. Di Valentin, S. Agnoli, G. Granozzi, Nat. Catal. **4** (2021) 850–859.
[6] S. Lu, W. Wang, S. Yang, W. Chen, Z. Zhuang, W. Tang, C. He, J. Qian, D. Ma, Y. Yang, S. Huang, Nano Res. **12** (2019) 3116–3122.

Morphology and Degradation Properties of Biodegradable Iron-Based Materials with Polymeric and Bioactive Coating

M. Petráková[a]*, R. Oriňaková[a], R. Gorejová[a], J. Macko[a]

[a] Department of Physical Chemistry, Institute of Chemistry, Faculty of Science, P. J. Šafarik University in Košice, Moyzesova 11, 040 01 Košice
*martina.petrakova@student.upjs.sk

In recent decades, many types of orthopaedic implants have been developed to repair defects, but implant-mediated inflammation and bacterial infections are still one of the critical problems that determine implant success. For this reason, interest in surface modifications of biomedical materials using organic, inorganic, or composite coatings containing drug micro-, or nanoparticles increased in recent years. In general, biomaterials are classified into three classes based on their interaction with living tissues. These are bioinert, bioactive and bioresorbable materials [1]. Bioinert materials do not form a chemical or biological bond at the interface between the implant and the host tissue. Due to their gradual degradation, bioresorbable materials are decomposed in the human body and replaced by living tissue [2]. By combining bioresorbable metals such as iron and polymer coatings containing drugs, it would be possible to prevent infections after the material is implanted. However, the slow degradation of iron is a limiting factor. The solution can be the application of coatings. The combination of iron, polyethylene glycol and gentamicin sulfate as a drug appears to be promising because gentamicin sulfate, as an aminoglycoside antibiotic, is mainly used to treat bone infections, and the addition of a polymer coating could improve the degradative properties of iron.

In this work, iron-based samples were prepared by cold pressing at a pressure of 600 MPa. A polyethylene glycol (PEG) coating was applied to part of the sintered samples (Fe-PEG samples), and part of the samples were covered with a PEG coating containing gentamicin sulfate (Fe-PEG+Ge samples). Based on the macroscopic images (Figure 1), the primary structure of the prepared samples was observed. In the case of Fe-PEG and Fe-PEG+Ge samples, the presence of a coating was observed. Grooves were observed on the surface of the uncoated Fe samples, which were created by cleaning the sintered samples with sandpaper (Figure 1a).

Figure 17: Macroscopic images of prepared samples at magnifications of 20x, a) Fe, b) Fe-PEG, c) Fe-PEG+Ge.

The presence of a polymeric PEG coating on the surface of Fe-PEG and Fe-PEG-Ge samples was confirmed by infrared spectroscopy by the presence of a triple peak of C - C and C - O valence vibrations in the range from 1000 to 1200 cm^{-1}. These vibrations are proof of the existence of a crystalline phase and were detected in the spectrum of pure PEG and in the spectrum of Fe-PEG and Fe-PEG-Ge samples [3]. In the spectrum of the Fe-PEG+Ge sample, the peaks characteristic of polyethylene glycol prevailed due to the low content of gentamicin on the sample surface.

The degradation properties were studied electrochemically by the electrochemical impedance spectroscopy (EIS) method. Measurements were made after immersing the samples in Hanks' solution for 60 minutes and then also after

corrosion of the samples. Nyquist diagrams showed higher resistance to charge transfer in uncoated Fe samples compared to coated Fe-PEG and Fe-PEG+Ge samples. The Nyquist plots of the uncoated and coated samples were modeled using the equivalent circuit shown in Figure 2. In this circuit, R_s represents the resistance of the solution, R_c represents the resistance of the polymer layer, R_{ct} represents the charge transfer resistance, and C_1, C_2 are the constant phase elements.

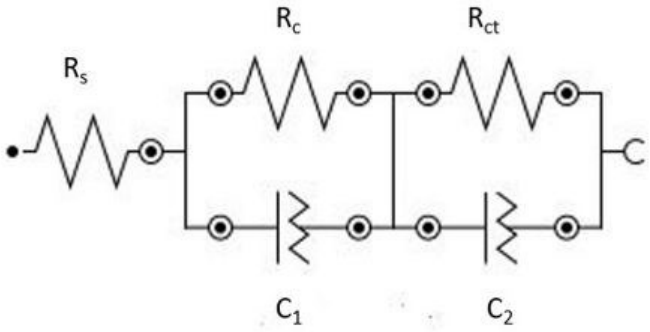

Figure 2: Equivalent circuit - R_s - solution resistance, R_c - polymer layer resistance, R_{ct} - charge transfer resistance, C_1, C_2 - elements of a constant phase.

Acknowledgements
This work was supported by the project APVV-20-0278 of the Slovak Research and Development Agency.

References

[1] J.B. Park, *Biomaterials: An Introduction, 3rd ed;* in: *Springer New York, New York, NY*, 574 p.
[2] F. Ordikhani, F. Mohandes, A. Simchi, Nanobiomaterials Science, Development and Evaluation (2017) 191–210.
[3] X. Fu, W. Kong, Y. Zhang, L. Jiang, J. Wang, J. Lei, RSC Advance, **5** (2015) 68881–68889.

Preparation of Fe-Ni Foam Catalysts Using Replication Method

M. Petráková[a]*, R. Oriňaková[a], A. Gubóová[a]

[a] Department of Physical Chemistry, Faculty of Science, P.J. Šafarik University in Košice, Moyzesova 11, 041 54, Košice
*martina.petrakova@student.upjs.sk

Pressing need for clean and renewable energy source stems from far-reaching environmental issues caused by fast fossil fuel consumption and use of non-renewable energy sources. Pollution of environment caused by excessive consumption of energy is inevitable issue that needs to be promptly addressed by development of clean and suitable energy sources [1]. One of the most compelling alternatives to fossil fuels is hydrogen because of its high energy density and non-polluting properties [2]. Hydrogen is great pure chemical fuel alternative to supply steady and renewable energy [3].

At present, steam reforming of natural gas, partial oxidation of hydrocarbons and gasification of coal are the most economical and widespread technologies to produce hydrogen as a raw material, especially for the chemical and petrochemical industries. As these technologies do not use electricity to produce hydrogen, they do not represent a viable option for the conversion and storage of energy from intermittent renewable energy sources (RES). In addition, all these technologies depend on fossil fuel and emit CO_2 [4].

An alternative technology for hydrogen production is water electrolysis. This is a natural possibility of energy conversion. The CO_2 footprint of water electrolysis is directly related to the source of the electricity used to power it. Therefore, in combination with RES, it offers a clean alternative to the aforementioned technologies.

Carbonyl iron and nickel in powder form were used as base material to prepare foams in various molar ratios starting with an iron: nickel ratio of 1:0 and ending at 0:1 (to prepare pure iron and pure nickel foam for comparison). Gelatine was dissolved in distilled water and used as a polymer binder to facilitate easy and even distribution of metal suspension on the polyurethane foam. Both gelatine and polyurethane foam were later removed by sintering.

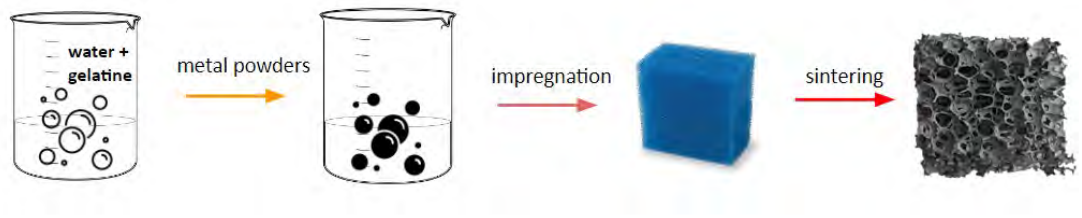

Figure 18: Schematic picture of sample preparation.

Metal porous foams were prepared by the matrix replication method. The process is described as follows: gelatine is dispersed in distilled water, then metal powders are mixed in. Polyurethane foam, which acts as matrix, is cut into specific samples, and impregnated by metal-gelatine suspension. Samples are then dried and sintered in nitrogen and hydrogen atmospheres to achieve desired structure.

Long-term stability is one of the most important parameters for catalysts. Testing by chronopotentiometric test (i-t curve) (Fig. 2) allowed to visualize the behavior of the two best samples (Fe10Ni90 and Ni100) in terms of stability over a longer time interval. The long-term stability test demonstrated the resistance of the samples and their ability to

maintain their activity for at least 22 hours. Samples with maintained a linear shape throughout the measurement, confirming remarkable stability.

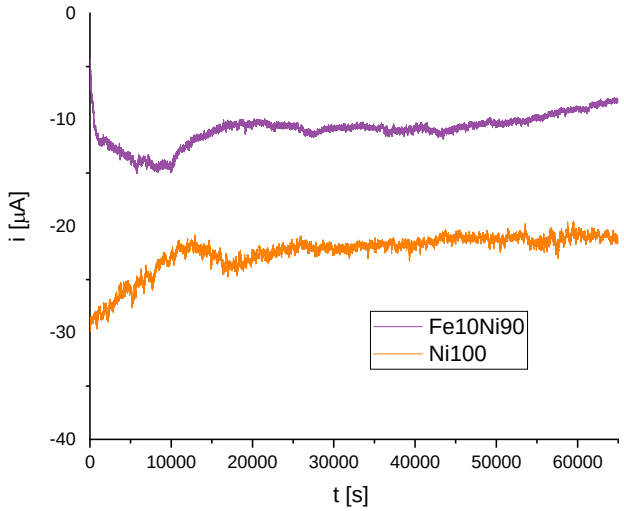

Figure 19: Long-term stability measurements for the best performing samples Fe10Ni90 and Ni100.

Acknowledgements
This work was supported by Slovak Research and Development Agency under the contract no. APVV-20-0299 and Grant Agency of Slovak Academy of Sciences, project no. VEGA 1/0095/21.

References

[1] S. Hussain, et al., Journal of Alloys and Compounds, **788** (2019) 267-276.
[2] J. Zhou et al., Applied Catalysis B: Environmental, **288** (2021) 1-9.
[3] H. Fayaz, et al., Renew Sustain Energy Rev, **16** (2012) 5511-5528.
[4] M. Balat, Int. J. Hydrogen Energy, **33** (2008) 4013-4029.

Low-cost Bimetallic Phosphide as a Catalyst for Alkali Water Electrolysis

O. Petruš[a]*, M. Strečková[a]

[a] Institute of Materials Research, Slovak Academy of Sciences, Watsonova 47, 040 01 Kosice, Slovak Republic
*opetrus@saske.sk

High energy consumption by mankind and the fact of fosil fuel scarcity, it is necessary to find the alternative energy sources comming from renewables. Hydrogen is widely recognized as a substitute for fossil fuels on account of its cleanliness, renewability, and high energy-density. Nowadays, the hydrogen is produced mainly from the natural gas, oil, and coal and only 4% are produced by electrolysis. Forecast for the year 2050 shows, that the 22% of hydrogen will be produced by water electrolysis [1]. For the above reasons, it is necessary to develop new types of catalysts that will be able to replace the currently used Pt and IrO_2. Currently the most research focus on study a non-noble metal hydrogen catalyst with good stability and low overpotential. Transition metals such as Mo, Fe, Ni, Co was found as the sources elements for constructing excellent electrocatalysts compounds due to low price, good electrical conductivity and comparable electrocatalytic performance. Transition-metal phosphates (TMPs) have exhibited remarkable HER performance with the merits of various structures, excellent electronic properties, and remarkable electrical conductivity [2]. In the present study we synthesized MoFeP by wet chemical route followed by precise "time temperature reduction schedule". The citric acid as a complexing agent was used. Two different sintering temperatures (550°C and 700°C) for decarboxidation of organic residues was performed. It was found that the carbonisation temperature used after the synthesis of MoFeP alter the surface morphology while the bulk crystal structure confirmed by XRD remain unaffected (Fig. 1). To evaluate the catalytic effectivity, both catalysts were studied in 0.1 M KOH in three electrode cell. LSV curves shown confirmed that the overpotential of the MoFeP sintered at 550°C manifests improved hydrogen evolution activity with overpotential 340 mV at current density 10 $mA.cm^{-2}$. On the other hand, in case of the MoFeP sintered at 700°C increase the overpotential to 415 mV at current density 10 $mA.cm^{-2}$. As a LSV curves indicated, the MoFeP sintered at lower temperature has similar slope as a reference Pt, which indicates the potential application in alkaline water electrolysis.

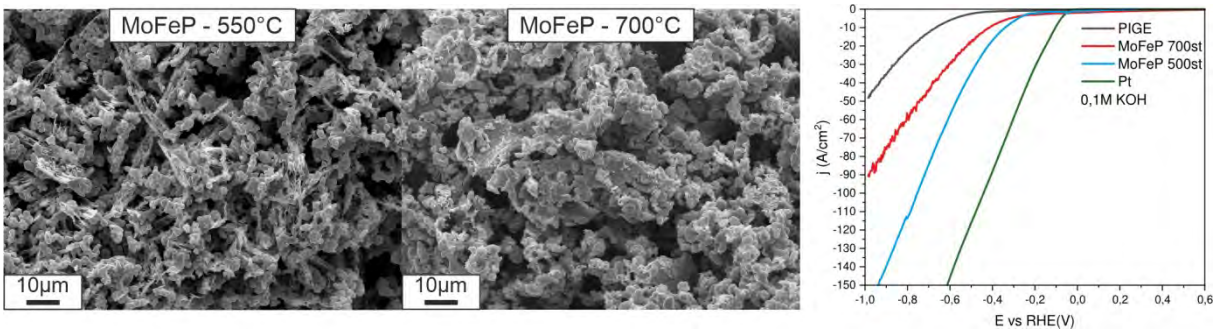

Figure 20: SEM images of MoFeP catalysts sintered at different temperatures and LSV curve in 0.1M KOH compared to Pt and bare PIGE electrode.

Acknowledgements
This work was supported by Slovak Research and Development Agency under the contract no. APVV-20-0229 and Grant Agency of Slovak Academy of Sciences, projects No. VEGA 2/ 0036/20

References
[1] M.N. Udin, V.V. Nageshkar, R. Asmatulu, Energy Ecol. Environ. **5** (2020) 108-117.
[2] J. Li, H. Zheng, Ch. Xu, Z. Su, X. Li, J. Sun, Inorg. Chem. **6** (2021) 1624-1630.

Study of Catalyst for Heterogeneous Catalytic CO_2 Conversion Using Computational Simulations

N. Podrojková[*a], M. Zanatta[b], A. Oriňak[a], V. Sans[b]

[a] Department of Physical Chemistry, Moyzesova 11, Košice 04001, Slovenská republika
[b] Institute of Advanced Materials (INAM), Universitat Jaume I, Castelló 12006, Španielsko
*5157301@upjs.sk

The main cause of global warming is the constant increase in the concentration of CO_2 in the atmosphere in recent decades. Human activity has become the main reason for this increase. In 2018, approximately 33.89 billion tons of CO_2 were released into the atmosphere, and in 2019, the global concentration of CO_2 in the atmosphere reached 407.65 ppm, which represents an increase of approx. 20% in the last 40 years [1]. A partial solution may be the conversion of CO_2 from a waste gas to economic profit in the form of various chemical raw materials, since CO_2 is a cheap, non-toxic, and abundant source of C1. In this context, extensive studies are being carried out with the aim of transforming CO_2 into valuable compounds, mainly through the thermochemical process of CO_2 hydrogenation and CO_2 cycloaddition. The cycloaddition of CO_2 into the structure of epoxides is particularly promising in the case of "green chemistry" because CO_2 is incorporated into epoxides without the formation of by-products. However, the thermodynamically stable and kinetically inert properties of CO_2 make its activation difficult, and therefore, to overcome this problem, many catalysts have been developed that support the CO_2 cycloaddition reaction. Although homogeneous catalysts cause more efficient transfer of mass and heat their use leads to problems such as complex separation of products, difficult cleaning, and difficult recovery of the catalyst. The enormous energy consumption during the separation process prevents the development of homogeneous catalysts in industry [2]. As a result, heterogeneous catalysts for the CO_2 cycloaddition reaction have gradually received more attention in recent years. Traditional heterogeneous catalysts can be easily separated from the products, but the catalytic efficiency is still relatively low under mild conditions. For this reason, ionic liquids (ILs) appear as promising catalysts in the process of CO_2 cycloaddition to cyclic carbonates. ILs can also be encapsulated in porous materials to form ILs on carriers to overcome limitations such as high cost and difficulty in separation and transportation. In contrast to purely solid catalysts, supported ILs can be described as a "solid-liquid" catalyst. Although supported ILs serve as heterogeneous catalysts, the actual catalytically active components of supported ILs are given in liquid form on the inner surface of the pores of the solid support. Due to these unique properties, supported ILs provide the same advantages as homogeneous catalysts.

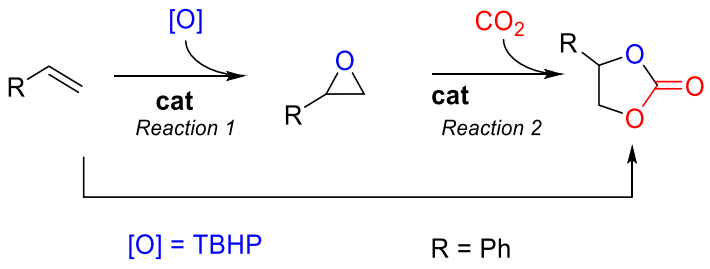

Figure 21: Reaction scheme of studied effect of IL catalyst.

Therefore, the work deals with the computational simulation of CO_2 cycloaddition to the structure of styrene oxide using IL 1-(2-hydroxy-3-methoxy-3-oxopropyl)-3-methylimidazolium bromide which will be used in experimental studies. Subsequently, the work deals with computational simulation of CO_2 epoxidation with the same IL to determine if the process can take place in one-step synthesis (figure 1).

The simulation measurements were calculated on the Shirka computing cluster at the Jaume I University in Spain. Computational simulations were performed using the DFT method with PBE functional and SCF calculation. The PWscf code (pw.x) offered by the Quantum ESPRESSO software was used to perform the calculations. The systems were visualized using various graphics packages, primarily the VESTA package and the UCSF ChimeraX package. Reaction mechanisms and activation energy were analysed with the MechaSVG program.

Calculations led to two reaction pathways, which showed the importance of the modification of the structure of the IL with -OH group and with halogen ions, especially in the first transition state, when the epoxide ring opens. The results showed that reaction pathway 2 has the lowest activation energy at TS1, namely 26.0 kcal/mol (figure 2). Calculations while monitoring the influence of the -OH group showed differences in the reaction energies and activation energies in the sense of lower energy values for the ionic liquid with the -OH group in the structure. The presence of a good nucleophile is also important to achieve complete conversion which is shown by monitoring the effect of halogen ions by DFT simulations. In this case, bromide ion as a stronger nucleophile compared to chloride ion led to lower values of activation energy and interaction energies of the system throughout the reaction. Theoretical calculations of the epoxidation reaction for the one-step synthesis of styrene carbonate showed that the reaction can take place via three reaction pathways, with the most preferable reaction the formation of a diol with an activation energy of 12 kcal/mol (Figure 3). The obtained values show that the one-step synthesis of styrene carbonate using the prepared IL will not lead to the required high conversion values.

The obtained theoretical results and knowledge represent an ecological example of the catalytic conversion of carbon dioxide into value-added chemicals using simple ILs as catalysts, and further study of this system may yield even more interesting results.

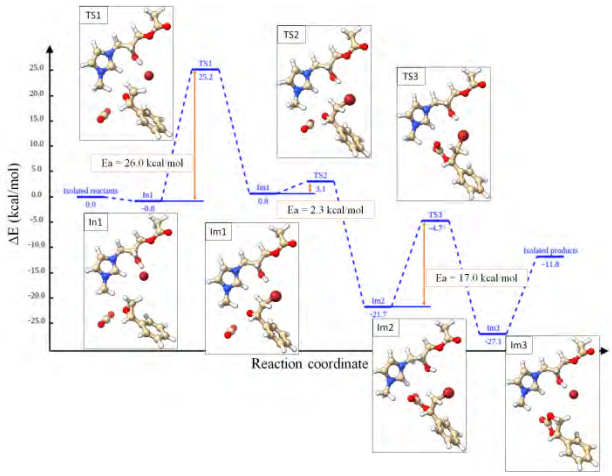

Figure 22: Reaction coordinate with transition states for reaction pathway 2.

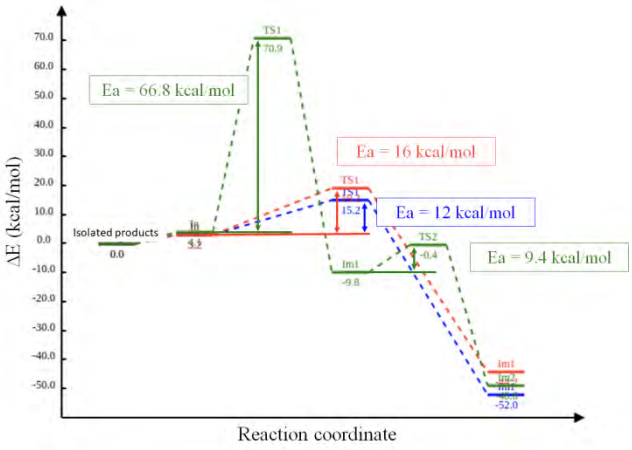

Figure 23: Comparison of reaction coordinates for different reaction pathways of styrene epoxidation with tercbutylhydroperoxide.

Acknowledgements

This work was supported by UJI-B2019-40 and UJI-B2020-44 (Pla de Promoció de la Investigació de la Universitat Jaume I) and RTI2018-098233-B-C22 y C21 (FEDER/ /Ministerio de Ciencia e Innovación – Agencia Estatal de Investigación). MZ and VS thank the funding received from the European Union's Horizon 2020 research and innovation programme under the Marie Skłodowska-Curie Individual Fellowships (GA no. 101026335). VS thanks Generalitat Valenciana (CIDEGENT 2018/036) for funding. The authors are grateful to the SCIC of the Universitat Jaume I for technical support.

References

[1] X. Jiang et al., Chem. Rev. **120** (2020) 7984-8034.
[2] Z. J. Li et al., ChemCatChem **13** (2021) 1848-1866.

Lithium-Ion NMC Batteries: Chemical Toxicity Reflection of Wastewater and Scrap

A. Pražanová[a]*, D. Pilnaj[a, b], M. H. Míka[c], V. Knap[a]

[a] Department of Electrotechnology, Faculty of Electrical Engineering, Czech Technical University in Prague, Technická 1902/2, 16627 Prague, Czech Republic
[b] Department of Environmental Chemistry and Technology, Faculty of Environment, Jan Evangelista Purkyně University in Ústí nad Labem, Pasteurova 3632/15, 400 96 Ústí nad Labem, Czech Republic
[c] Department of Glass and Ceramics, University of Chemistry and Technology, Technická 5, 166 28 Prague, Czech Republic
*anna.prazanova@cvut.cz

Abstract
The ever-increasing requirements for global carbon dioxide CO_2 emission reduction decrease the production of new internal combustion engine vehicles (ICEVs). On the contrary, the demand for electric vehicles (EVs) increases along with the number of spent lithium-ion batteries (LIBs). Recycling LIBs seems to be one of the most promising options for end-of-life (EOL) treatment solutions; however, many process effects of currently used battery compounds are still being addressed, e.g., the safety and potential risks of wastewater, battery scrap, or leaks into the air. In this work, the LIB nickel-manganese-cobalt (NMC) cell electrolyte was characterized in wastewater using gas chromatography with mass spectrometry (GC-MS), inductively coupled plasma with optical emission spectrometer (ICP-OES), and the residues of toxic substances bound to nm-µm valuable metal particles in battery scrap were determined by x-ray fluorescence (XRF).

Introduction

The ever-increasing requirements for global carbon dioxide CO_2 emission reduction resulted in decreased production of new internal combustion engine vehicles (ICEVs) and increased demand for electric vehicles (EVs) [1]. The EU responded to this fundamental change in the automotive industry by introducing new emission-free standards and regulations considering the waste treatment solutions, including the collection targets for portable waste batteries or recycling efficiencies for lithium-ion batteries (LIBs) reaching 65 % by 2025 and 70 % by 2030 [2].

The EVs' LIBs are typically based on valuable metals such as cobalt (Co), manganese (Mn), nickel (Ni), and lithium (Li) in the cathode, graphite (C) in the anode, and other essential materials such as aluminum (Al) and copper (Co) in packaging and electronic components. Lithium hexafluorophosphate ($LiPF_6$) based on toxic phosphorus (P) or fluorine (F) is commonly used as an electrolyte [3]. Further, the battery cell consists of organic polymers, binders, and other adhesives. Although recycling LIBs increases the raw materials saving and reduces the energy and environmental impacts of their mining, the effects of the entire process are still being addressed, such as the safety and potential risks [3,4].

The LIBs electrolyte consists of highly volatile and reactive compounds, resulting in highly toxic products, e.g., widely used $LiPF_6$ salt hydrolyses and evaporates solvents and HF. Many of these substances are released and taken away in wastewater; other residues then remain in a scrap of battery materials (pre-step of black mass production) and are released into the air [4].

This work is devoted to the first part of the characterization of LIB nickel-manganese-cobalt (NMC) cell electrolyte released in wastewater using gas chromatography with mass spectrometry (GC-MS). Major organic solvents were identified and relatively quantified by this technique. Inductively coupled plasma with an optical emission spectrometer (ICP-OES) was used for absolute quantification of selected elements eluted into water (Li, P, Ni, Mn, Co, Cu, Al). The residues of toxic substances such as P or F bound to nm-µm valuable metal particles in battery scrap using x-ray fluorescence (XRF). In addition, the residual proportion of substances after flushing was analyzed. According to the results, most of the electrolyte was released immediately upon breaking the cell cover; its share was already reduced to less than 10 % of total content during the first flush.

Methodology

This work used a deeply discharged NMC (712) pouch LIB cell with a nominal voltage of 3.65 V and 78 Ah capacity for laboratory treatment. This type of cell represents the building element of the Modular electric drive matrix (MEB) platform widely used in electric vehicles, e.g., Volkswagen, SEAT, Audi, or ŠKODA AUTO.

The proportion of valuable metals (Ni, Mn, and Co), covering materials (Cu and Al), and released cell's $LiPF_6$ electrolyte (monitoring by Li and P ratio) within the liquid medium (wastewater) was analyzed. Furthermore, the residual portion of toxic substances, focusing on P and F, in the waste scrap further processed into a black mass was determined. In addition, the reduction of these substances during repeated water-flushing was observed.

Experiment procedure

After immersing the battery cell in a liquid (tap water), the Al cover was cut off (*cell opening*); individual layers were separated (*cell to layers*) and further crushed (*crushing*). After 30 minutes of rest at laboratory room temperature (23 °C), the solid phase was removed from the liquid (*solids removal*) and immersed in a new water bath. The flushing was repeated, overall, four times. The individual experiment steps are illustrated in Figure 1.

Chemical toxicity reflection

Gas chromatography with mass spectrometry (GC-MS) was utilized to identify major organic components released into wastewater. The applied method included Thermo Scientific Trace 1310 GC coupled to ISQ 7000 MS with the extraction of solvent from headspace over aqueous sample by acrylate SPME arrow performed by RSH autosampler. Incubation of samples was performed under 80 °C for 30 minutes. Extraction on the acrylate arrow ran for 5 minutes, thermal desorption in PTV inlet for 1 minute at 200 °C followed by chromatographic separation on TG-5SilMS column (30 m, 0,25 mm, 0,25 µm) with helium flow at 1,2 ml/min. The temperature program started at 40 °C and was held for 1 minute, followed by a linear temperature gradient of 5 °C/min up to 280 °C. The mass spectrometer was set to a 5 Hz scan rate with a range of 35-650 amu. To quantify selected elements released into the water, ICP-OES Perkin Elmer Optima 8000 was used. The samples were diluted 10x into 5% HNO3 and quantified towards 3-point calibration on Astasol multi-component standard. Samples over the linear range were further diluted in one order of magnitude. The nm-µm scale particles of material of thin layers on Cu and Al metal sheets were analyzed using the x-ray fluorescence (XRF) by the Philips PANAlytical spectrometer.

Results

The work analyzed the proportion of individual metals released into water, as shown in Figure 1 (a). When the cell was opened, the electrolyte was mainly released (characterized by the proportion of Li and P), its permissible exposure limit was set to 2.5 [mg/m^3] due to its high environmental and health risks as high acute toxicity, severe burns to skin and eyes. Repeated rinsing reduced its share to less than 1 % (0.7 for Li and 0.2 for P), as illustrated in Table 1. The metal release proportion depends on the individual layers' mechanical damage. At maximum comminution, the maximum release occurred. Flushing reduced the proportion of these materials in wastewater down to 5 %.

Metal emission into the air is expected to be negligible and is mainly present in the aqueous solution and solid parts. A low concentration of Co (less than 1 %) released into the water after the first flush shows its stability in the solid phase during the process; therefore, it possesses a minor risk for an aqueous environment. Cu is dissociating from the electrode into the solution at higher levels. Toxicity for higher mammals is low at these levels, but it may pose a threat to aquatic life. Background trace concentration of Co from tap water pipelines was observed. The detailed analysis of the obtained waste battery scrap characterizing the residues of P and F, as well as the valuable metals, will be covered in a full version of the manuscript.

Main hazards are induced by volatile organic solvents, especially fluorobenzene, esters of carbonic acid, and dioxolanone. They pose a threat due to high flammability, toxicity to aquatic life with long-lasting effects, eye/skin/respiratory irritation, or specific target organ toxicity. Long-term exposure to one of the main solvents, dimethyl ester of carbonic acid, was found to cause weight loss, altered sex ratio, increased number of stunted fetuses,

and fetal malformations for rats at a level of 3000 ppm in air. Precautionary measures are therefore necessary for safe handling during recycling. An overview on these solvents is shown in Figure 1 (b). The substances were evaluated according to their hazard identification, including the GHS statements and LD50.

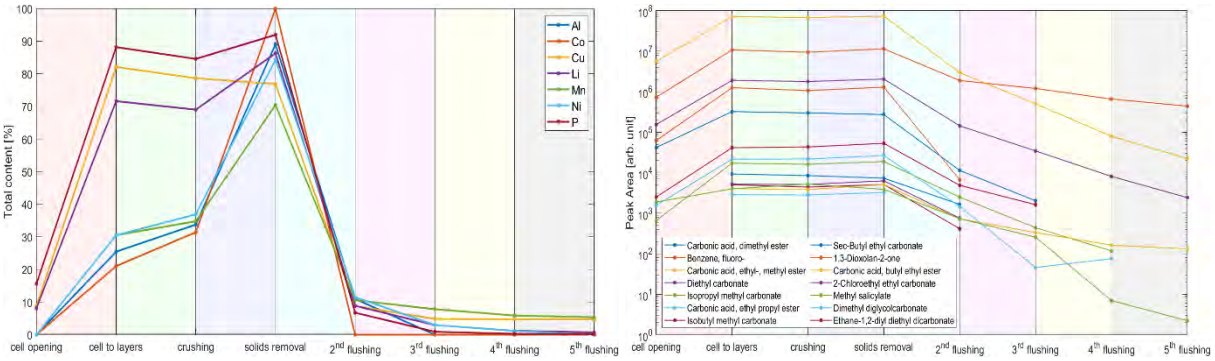

(a) (b)

Figure 24: Results: (a) wastewater analysis of metals in % of a total content, (b) volatile solvents released from wastewater.

Table 1: The concentration of target LIB cell elements released in wastewater.

Concentration (mg/l)	Al	Co	Cu	Li	Mn	Ni	P
cell opening	0.00	0.00	2.01	12.53	0.00	0.00	764.77
cell to layers	2.45	0.05	18.77	110.48	0.34	0.41	4316.84
crushing	3.25	0.08	17.99	106.44	0.39	0.50	4139.83
solids removal	8.58	0.25	17.57	133.13	0.79	1.15	4501.07
2. flushing	1.05	0.00	2.01	13.65	0.12	0.16	329.42
3. flushing	0.00	0.00	1.11	4.54	0.09	0.04	43.83
4. flushing	0.00	0.00	1.09	1.83	0.07	0.02	13.06
5. flushing	0.00	0.00	1.09	1.09	0.06	0.00	7.30
Sum	9.63	0.25	22.87	154.24	1.12	1.36	4894.68

Conclusion

Although recycling spent LIBs from EVs is considered one of the most promising EOL methods, the safety and potential hazards of wastewater, battery scrap, or leaks into the air are being necessarily addressed. Thus, this work characterized the release of a $LiPF_6$ electrolyte by determination of the lithium and phosphorus ratio in wastewater and battery scrap after detecting toxic phosphorus and fluorine. The results show that the electrolyte is dominantly released when opening the battery cell and it is almost fully taken away with water during the first flushing. According to the GC-MS, highly hazardous volatile organic solvents in the wastewater were detected; they were evaluated according to hazard identification, including the GHS statements and LD50. In future work, technological pathways for the purification of this water and material recovery will be proposed. This process's overall risks will be primarily characterized by respiratory exposure to dangerous substances. Based on our results, precautionary measures are necessary to implement for leaks into the air as well as proper liquid treatment and recycling of the solid metals.

Acknowledgements

Special thanks to ŠKODA AUTO, a.s. for the support.

References

[1] L. Lander, T. Cleaver, M. A. Rajaeifar, V. Nguyen-Tien, R. J. R. Elliott, O. Heidrich, E. Kendrick, J. S. Edge, and G. Offer, IScience **24**, (2021).
[2] European Commission, Clim. Action (2019).
[3] A. Pražanová, V. Knap, and D.-I. Stroe, Energies 2022, Vol. 15, Page 1086 **15**, (2022) 1086.
[4] N. Lebedeva and L. Boon-Brett, J. Electrochem. Soc. **163**, (2016).

Engineered Nanoparticles for Imaging of Drug Distribution in Lungs by Magnetic Resonance

R. Sobotova[a,b], M. Koneracka[a], V. Zavisova[a], M. Kubovcikova[a], I. Antal[a], I. Khmara[a], O. Strbak[c], P. Mikolka[c]

[a] Institute of Experimental Physics SAS, Watsonova 47, 04001 Košice, Slovakia
[c]Faculty of Materials, Metallurgy and Recycling of the Technical University of Kosice, Letna 9, 040 01 Kosice, Slovakia
[b] Biomedical Centre Martin, Jessenius Faculty of Medicine in Martin, Comenius University in Bratislava, Mala Hora 4, 03601 Martin, Slovakia
*konerack@saske.sk

The era of Covid-19 reminds us how difficult it is to treat patients with acute respiratory distress syndrome (ARDS) therefore monitoring of the spatial distribution of the directly administrated drug to the lungs is very demanded.

In this work, we focused on the synthesis, functionalization of magnetic nanoparticles, N-acetylcysteine conjugation to magnetic nanoparticles and on the study of drug distribution in the lungs in the aforementioned ARDS by magnetic resonance imaging (MRI). N-acetylcysteine (ACC) is a mucolytic drug commonly used in the treatment of the respiratory tract. The drug dissolves all the components that cause mucus to become viscous and thus promotes expectoration. The first step was the preparation of a conjugate consisting of magnetic nanoparticles modified with functional groups suitable for drug conjugation. Nanoparticle functionalization and drug conjugation were optimized and studied by different physicochemical methods such as SEM and TEM microscopy, Dynamic Light Scattering (DLS), Electrophoretic Light Scattering, UV/VIS, or magnetic measurements to obtain information about morphology, size distribution, surface charge, drug and magnetite concentrations and, last but not least, information about magnetic properties. In the next phase, the stability of the selected conjugate with optimum properties was monitored by DLS and zeta potential measurements in different biological media.

We managed to prepare conjugate with the optimal ACC loading concentration of 1.2 mg/ml which corresponds to ACC/MNPs w/w ratio = 5. The same optimal value was obtained from zeta potential measurements as a function of pH for samples with different ACC loading concentrations. The results indicate a shift of the isoelectric point of unconjugated magnetite (IEP=8.5) towards a more acidic pH, which is an indication of ACC adsorption since the IEP of pure ACC = 2.4 (Fig. 1b). The inset in the figure showed a spherical shape of optimized ACC conjugated nanoparticles with an average mean diameter of 100 nm.

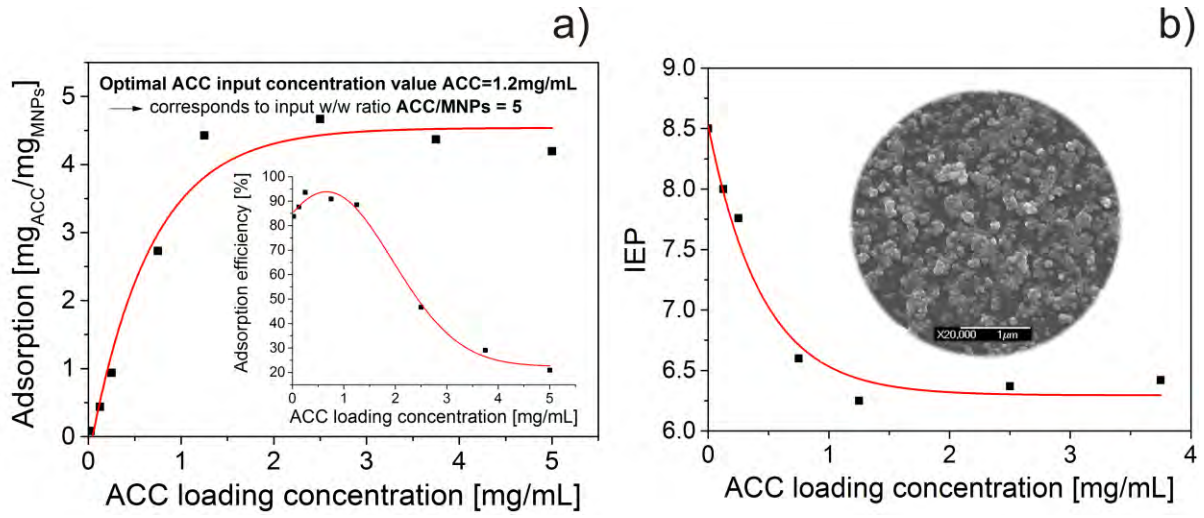

Figure 1: (a) Effect of different initial ACC concentration on adsorption. Inset: Effect of different initial ACC concentration with regart to ACC adsorption efficiency. (b) The IEP dependence in relation with various ACC theoretical concentration. Inset: SEM image of ACC conjugated nanoparticles with the ACC optimal loading concentration of 1.2 mg/ml.

In the next research the selected conjugate will be analyzed by MRI and compared with the properties of commercially available MRI contrast agents and the spatial distribution of the drug in the lungs in ARDS will be studied as well.

Acknowledgement

The work was supported by the Operational Programme Integrated Infrastructure, project "BIOVID", ITMS 313011AVG3 co-funded by ERDF. The work was also supported by the Slovak Research and Development Agency under contracts Nos. APVV-14-0120, APVV-SK-SRB-18-0055, APVV-DS-FR-19-0052, by the Slovak Science Grant Agency VEGA - Project No. 2/0033/19.

Glycerol-Citrate Polymer Incorporation into Calcium Phosphate Cements

T. Sopcak[a]*, L. Medvecky[a], M. Giretova[a], R. Stulajterova[a], J. Brus[b], M. Urbanova[b], F. Kromka[a], M. Podobova[a], M. Faberova[a]

[a]Institute of Materials Research of SAS, Watsonova 47, 04001 Kosice, Slovak Republic
[b]Institute of Macromolecular Chemistry of the Czech Academy of Sciences, Heyrovskeho nam. 2, 162 06, Prague 6, Czech Republic
*tsopcak@saske.sk

Research and development of biomaterials has made enormous progress over the last decades with the effort to find a good healing material that imitates the structure and properties of bone tissue. Because of the composite nature of natural bone, that is composed of the inorganic calcium deficient hydroxyapatite (Hap) reinforced with the polymeric collagen fibrils, there is an increasing demand to explore polymer modified biomaterials with mechanical and biological properties comparable to the hard tissue counterparts [1].

The calcium phosphate cements (CPC) represent a class of self-setting bioactive materials consisting of one or more calcium phosphate powders that upon mixing with water solution form a paste like consistency- easily applicable to the defect site, that is able to harden and form a bone bond [2]. Despite of many advantages, one of the main problems of CPCs is their lower mechanical strength, which hamper their use in high-bearing regions [3]. To overcome the above drawback, some recent studies have introduced biodegradable thermoplastic polymers into CPCs, such as poly(lactic-L-acid; PLLA), poly(L-lactic-co-glycolic acid; PLGA) and poly(ε-caprolactone; PCL), but in many cases the effect of those polymers on mechanical strength enhancement was very low [4]. Recently, a thermosetting polymers known as polyol carboxylates has been synthesized by esterification of alcohols, such as glycerol (G) with carboxylic acid (citric acid, C) to produce inexpensive and biodegradable polymers with improved processability and mechanical properties in comparison with the thermoplastic polyesters [5]. Changing the reaction conditions e.g. type and molar ratio of reactants, polymerization temperature and the use of catalyst allow to effectively control the cross-linking degree, molecular weight and degradation rate as well as mechanical properties of polyol carboxylates [6].

Despite of the increasing number of published works, there has been no study conducting on polyol carboxylate polymers incorporated in the CPCs. Motivated by this fact, therefore our research group tried to develop a glycerol-citrate (G-C) polymer modified tricalcium phosphate (TCP) cements. Firstly, the G-C polymer was synthesized by mixing and esterification of an equimolar molar ratio of glycerol:citric acid blends under heating and polymerization at 135°C for 1.5 h without using any catalyst. Then, the TCP/G-C composites containing various amounts of G-C (2.5, 5 and 10wt%) were prepared by the polymer infiltration into TCP cement matrix by dissolution G-C polymer in ethanol under heating and admixing of TCP powder to the G-C/ethanol solution. After evaporation of ethanol, the composite cement pastes were prepared by mixing the composite powders with the liquid phase (2.5 wt% NaH_2PO_4) at required powder to liquid ratios and the pressed samples (6 x 12 mm dimension) were incubated in phosphate-buffered saline (PBS) solution during 7 days of soaking. Careful structural and chemical characterization was conducted on composite cements in order to investigate the effect of polymer addition on phase changes, microstructural and mechanical properties as well as in vitro cellular response of the TCP/G-C composite cements.

The results showed the formation of a thin and uniform polymer coatings on the surface of TCP/2.5G-C and TCP/5G-C cement particles, which did not hinder the hydration and transformation of phases in comparison with undoped TCP cement. The mechanical properties such as compressive, diametral tensile and bending strengths were considerably improved in composite cements up to 5 wt% of G-C content probably as a result of a reinforcing effect of the polymer coating, which resulted in more compact and denser microstructure. Furthermore, the additional strong interaction between the residual COOH groups of G-C polyester with the surface phosphate groups through the hydrogen bonds could also contribute to the enhancement of mechanical properties of composites. The in-vitro tests of cytotoxicity in cement extracts revealed a high proliferation activity of osteoblastic cells in all of the tested composites that showed a promising potential for use in regenerative medicine.

Acknowledgements
This work was supported by the Slovak Grant Agency of the Ministry of Education of the Slovak Republic and the Slovak Academy of Sciences, Project No. 2/0034/21, by the Slovak Research and Development Agency under contract No. APVV-20-0184, APVV-20-0299 and APVV-20-0278 and by the Slovak - Hungarian bilateral cooperation NKM2018_103 "Low-temperature electrohydrodynamic techniques used for the preparation of bioceramic coatings project".

References
[1] R.A. Perez, H.W. Kim, M.P. Ginebra, J. Tissue Eng. **3** (2012) 2041731412439555.
[2] A. Sugawara, K. Asaoka, S.J. Ding, J. Mater. Chem. B **1** (2013) 1081-1089.
[3] J.T. Zhang, W.Z. Liu, V. Schnitzler, F. Tancret, J.M. Bouler, Acta Biomater **10** (2014)1035–1049
[4] S.H. Huang, T.T. Hsu, T.H. Huang, C.Y. Lin, M.Y. Shie, J. Dent. Sci. **12** (2017) 33-43.
[5] R.T Tran, J. Yang, G.A. Ameer, Annu. Rev. Mater. Res. **45** (2015) 277–310.
[6] B. Tisserat, R.H. O'kuru, H. Hwang, A.A. Mohamed, R. Holser, J. Appl. Polym. Sci. **125** (2012) 3429-3437.

New Sulfur Based Composite Materials as Cathodes for Li-S Batteries with Improved Stability

A. Straková Fedorková[a*], V. Niščáková[a], D. Capková[a], R. Oriňaková[a], E. Shembel[b], T. Kazda[c]

[a] Department of Physical Chemistry, Faculty of Science, Pavol Jozef Safarik University in Košice, Moyzesova 11, 040 01 Košice, Slovakia

[b] Scientific Research Laboratory of Chemical Power Sources of Ukrainian State University of Chemical Technology, Dnipro, 49005, Ukraine

[c] Brno University of Technology, Faculty of Electrical Engineering and Communication, Technicka 10, 61600 Brno, Czech Republic

*andrea.fedorkova@upjs.sk

Introduction

Lithium-sulfur batteries (Li-S) belong to new class energy storage systems which are based on intercalation reaction. Their high theoretical energy density, cost effectiveness and non-toxicity of sulfur is very interesting for practical applications in different fields. Li-S batteries are rechargeable devices and consist of a sulfur-based cathode, binder, separator, organic liquid electrolyte, lithium anode and current collector. Process of conversion is based on reaction of lithium and sulfur to lithium sulfide:

$$16Li + S_8 \rightarrow 8Li_2S \quad (1)$$

The electrodes in this cell (Fig. 1) mainly consist of metallic lithium (negative electrode, anode during discharging) and sulfur (positive electrode, cathode during discharging). During discharge lithium is oxidized, the Li+ ions are dissolved in the solvent and move towards the cathode. There, they react with reduced sulfur to finally produce Li_2S via several intermediates (the polysulfides).

$$S_8 \rightarrow Li_2S_8 \rightarrow Li_2S_6 \rightarrow Li_2S_4 \rightarrow Li_2S_3 \rightarrow Li_2S_2 \rightarrow Li_2S \quad (2)$$

Theoretically, for every gram of sulfur in the cathode, 433 mg of lithium is required for the reaction in equation 16 to go to completion. Therefore, the theoretical gravimetric capacity of the lithium-sulfur battery with respect to the combined mass of sulfur and lithium is 1167 mAh/g. With an average discharge voltage of approximately 2.2 V, the energy density of the battery is 2567 mWh/g [1]. Fig. 1 Schematic diagram of Li-S battery [3]

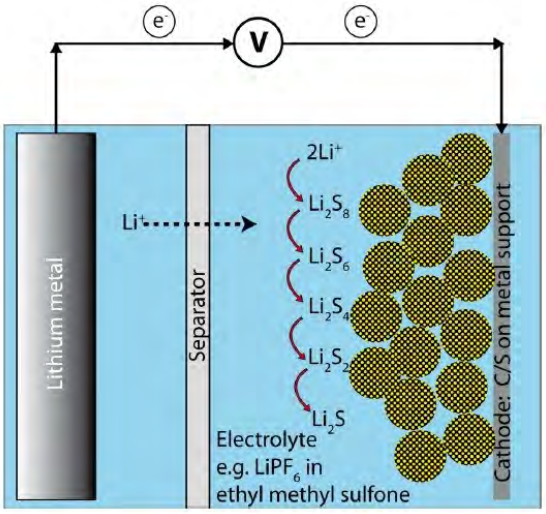

Figure 1: Schematic representation of Li-S battery [2].

Results and discussion

During cycling and conversion reaction new electrochemical compounds are formed what can cause some scientific problems [3, 4]. Various forms of sulfur, called polysulfides (PS), are produced during discharging and show poor ionic and electronic conductivity. The next problem is related to the volume change of the sulfur cathode. Sulphur can change its volume of about 79%, what can cause the structure change and decrease the conductivity and stability of cathode material. The drastic volume variation of the electrodes can lead to serious safety problems [6, 7].

The cathodes have been made according to the technology of saturation of the carbon matrix with the sulfur that has been soluble in the aprotic solvent that has low evaporating temperature. The cathode composition includes the following: sulfur 70%, carbon black 27%, F4-D 3%. Substrate - stainless steel mesh. The area of the sulfur electrode is equal to the area of the lithium electrode and is 2 cm^2. Temperature was 25 °C. Electrolyte composition: DME, DOL (2:1), 0.7 M LiTFSI and 0.25 M $LiNO_3$.

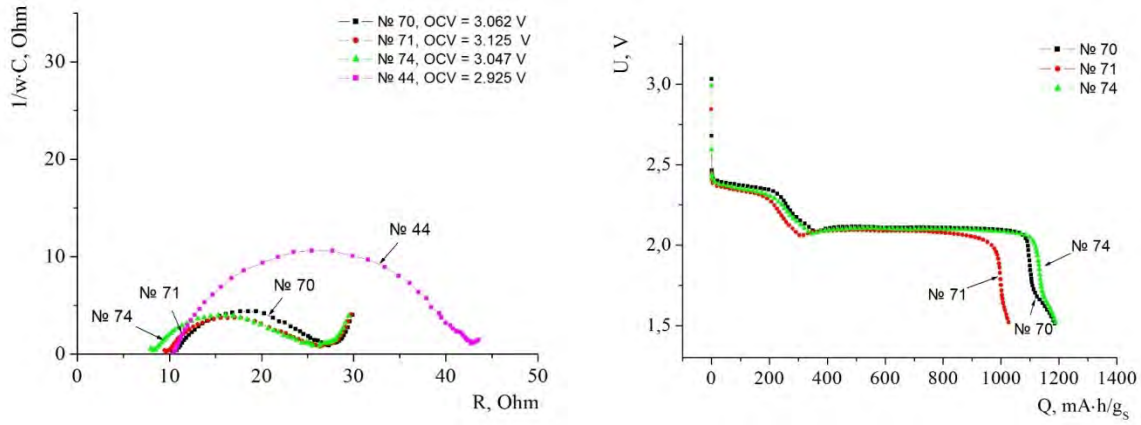

Figure 2: EIS spectra and discharge curves of Li-S carbon composites. The numbers on the curves are cell numbers.

Cell No. 70, 71 and 74 - carbon matrix material – carbon black that was calcined at 1000 °C for 10 hours in dry argon atmosphere. Cell No. 44 - the carbon matrix material is carbon black, treatment at a temperature of 250 °C for 3 hours. Primary discharge characteristics of sulfur electrodes are shown on Fig. 2 right. The carbon black that was calcined at 1000 °C for 10 hours in dry argon atmosphere was used as the carbon matrix. The discharge current is 0.1 C (based on the expected capacity of 1000 mAh/g). Discharge currents: 70 – 0,77 mA, 74 – 0,99 mA, 71 – 1,29 mA. High initial discharge capacities were obtained for samples with calcination treatment as for example 1200 mAh/g_S.

Conclusions

- Li-S-carbon composite cathode materials were prepared by saturation of a porous carbon matrix with sulfur using the dissolution of sulfur in a low boiling organic solvent.
- Electrochemical impedance spectroscopy, galvanostatic charge/discharge and other techniques were used for characterization of as prepared samples.
- A higher initial discharge capacity of 1200 mAh/g was achieved.

– Stability of carbon matrix was improved by calcination process, and it was confirmed by EIS measurements.

Acknowledgement

This work was supported by projects APVV-20-0138 and APVV-20-0111 and by the Operational program Integrated Infrastructure within the project: Innovative Solutions for Propulsion, Power and Safety Components of Transport Vehicles, 313011V334, co-financed by the European Regional Development Fund.

References

[1] Y. Jung, Int. J. Electrochem. Sci. **3** (2008) 566.
[2] J. D. Schuster, Morphology Control of Ordered Mesoporous Carbons for High Capacity Lithium Sulfur Batteries, dissertation thesis (2011), München
[3] A. Strakova Fedorkova, T. Kazda, K. Gavalierova et al., Int. J. Electrochem. Sci. **13** (2018) 551.
[4] X. Zhang, B. Jin, L. Lin et al., J. Electrochem. Chem. **26**, (2016) 780.
[5] D. Capková, T. Kazda, A. Straková Fedorková et al., ECS Transactions **95** (2019) 19.
[6] H.D. Yoo, E. Markevich, G. Salitra et al., Materials Today **17** (2014) 110.

Transition Bimetallic Phosphides for Electrocatalytic Water Decomposition

M. Strečková [a]*, O. Petruš [a], C. Bera [a], A. Gubóová [b], R. Oriňáková [b]

[a] Institute of Materials Research, Slovak Academy of Sciences, Watsonova 47, 040 01 Kosice, Slovak Republic
[b] Institute of Chemistry, Faculty of Science, P.J. Safarik University, Moyzesova 11, 040 01 Kosice, Slovak Republic
*mstreckova@saske.sk

Due to the global warming and its negative impacts on the environmental situation, as well as due to the urgent need of the developed economies to become independent of the fossil fuels originating in the politically unstable regions, the future of energy supply is shifting from fossil fuels to renewables. Hydrogen as the product of water electrolysis using renewable electricity represents a flexible and clean energy carrier. It not only offers the prospect of large, short as well as long term energy storage capacities, but also a spectrum of the other options for industry decarbonisation. However, currently only 4% of globally produced hydrogen originates from electrolysis sources. It is mainly due to the economic issues. A promising way to increase competitiveness of this technology represents enhancement of the both, HER as well as OER reaction by means of a suitable electrocatalyst. Today, platinum group metals such as Pt, RuO_2 and IrO_2 are considered as the state- of-the-art electrocatalysts due to a high intrinsic activity and stability. Due to their scarcity and related high price, the scientific community around the globe strives to find an adequate alternative from the family of non-noble metals while maintaining all exceptional electrochemical properties and excellent stability.

Transition metal phosphides (TMPs) have been recognized as the best non-noble electrocatalysts in recent years because of their distinct physicochemical properties. Numerous studies have shown that TMPs based on Ni, Co or Fe may display significantly improved electrochemical activity for catalysis of both OER and HER in comparison with the constituting pure metals and in the case of some authors even in comparison with iridium and platinum [1-3]. NiCoP bimetallic phosphide nanoparticles incorporated into the carbon fibres (CF) were evaluated in this work as the most active materials within the investigated trinity NiCoP CF, FeNiP CF and FeCoP CF. An important part of the catalyst represents suitable support. It primarily allows high degree of catalyst utilisation due to the existence of a high concentration of the nucleation centres during the synthesis and at the same time fixing catalyst itself in the formation position while minimising danger of its larger agglomeration.

It is tempting to conjecture that synergetic interaction of the catalyst material with the support improves catalyst activity. One of the most widespread type of the active support in electrochemistry represents carbon fibers. In this work, the electrospinning was implemented as low cost, large-scale and versatile production technology for carbon fibers preparation modified with TMP_S. The design of modified carbon fibers (TMPs CF) for overall water splitting are regarded as a type of functional materials with exceptional stability, conductivity, modulated porosity and unique three-dimensional architectures (Fig.1). Three different composition of TMPs CF was developed as a novel, economically viable electrode material suitable for performing water electrolysis process both in PEM and alkaline environment. The final transition metal phosphide carbon fibres (TMP CF) were prepared in a form of the felt sheets suitable for direct implementation in the cell. The electrocatalytic activity of the electrodes produced was compared with the state-of-art electrocatalysts, i.e., Pt/C for HER and IrO_2 for OER process.

NiCoP CF as breakthrough bifunctional catalyst was studied in 1 M KOH as well as 0.5 M H_2SO_4 solutions simulating environments of alkaline and proton exchange membrane (PEM) electrolysis, respectively. High electrocatalytic activity was detected for material prepared in both environments, resulting in cell voltage at the current density of 10 mA/cm^{-2} as low as 1.71 V and 1.51 V in KOH and H_2SO_4 solution, respectively. Corresponding overvoltage has reached 257 mV for HER and 300 mV for OER, whereby the respective Tafel slopes acquire the values of 38.6 mV/dec for HER and 81 mV/dec for OER, respectively. An excellent stability in acidic environment was proven indicating high material potential for a practical utilization of these materials in water electrolysis energy conversion processes.

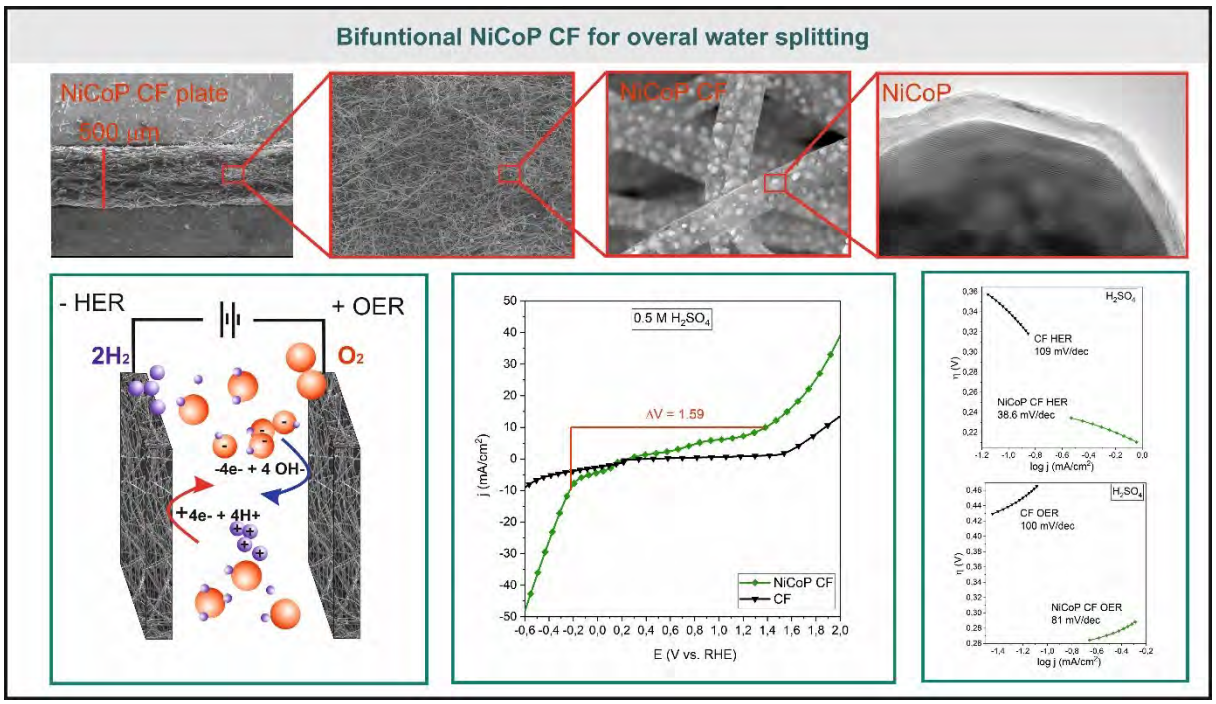

Figure 1: The morphology of NiCoP CF and electrochemical characterization in two-electrode system in 0,5M H_2SO_4. The Tafel slopes for HER and OER.

Acknowledgements

This work was supported by Slovak Research and Development Agency under the contract no. APVV-20-0229 and Scinetific Grant Agency of Ministry of Education , Science, Research and Sport of Slovak Republic and Slovak Academy of Sciences, projects No. VEGA 2/ 0036/20 and VEGA 1/0095/21.

References

[1] J.F. Callejas, C.G. Read, C.W. Roske, N.S. Lewis, R.E. Schaak, Chem. Mater. **28** (2016) 6017–6044.

[2] X. Wang, W. Li, D. Xiong, D.Y. Petrovykh, L. Liu, Adv. Funct. Mater. **26** (2016) 4067–4077.

[3] J. Kibsgaard, C. Tsai, K. Chan, J.D. Benck, J.K. Nørskov, F. Abild-Pedersen, T.F. Jaramillo, Energy Environ. Sci. **8** (2015) 3022–3029.

Laboratory for Advanced Materials at Comenius University (ERA Chairs project)

M. Sýkora[a*]

[a]Laboratory for Advanced Materials, Faculty of Natural Sciences, Comenius University, 842 15 Bratislava, Slovakia
*sykoram@uniba.sk

Laboratory for Advanced Materials (LAM) is a newly established research laboratory at the Faculty of Natural Sciences at Comenius University in Bratislava, Slovakia, supported by the European Commission (EC) under the Horizon 2020 program, the ERA Chairs scheme. According to the EC definition:[1]

ERA Chairs stand for bringing excellence to institutions. ERA Chairs projects bring outstanding academics, with proven research excellence and management skills, to universities and research institutions in Widening countries with potential for research excellence. They aim to attract and maintain high quality human resources under the direction of an outstanding researcher (the 'ERA Chair' holder) while at the same time implementing structural changes necessary to achieve excellence on a sustainable basis.

In 2018 Comenius University was successful in winning the prestigious ERA Chairs grant to recruit an internationally recognized scientist and to establish a new laboratory for materials research. This was a second ERA Chairs grant ever awarded to a Slovak research institution. The project, funded for five and half years will be completed in Spring of 2024. Following an international search, I was selected for the position of the ERA chair and a director of newly established laboratory, with my official start on February 1, 2019. In my presentation I will summarize the progress we have made in the last approximately three and half years in establishing the laboratory and the challenges we encountered in the process. I will also provide a short overview of the research topics in which the members of LAM are currently engaged.

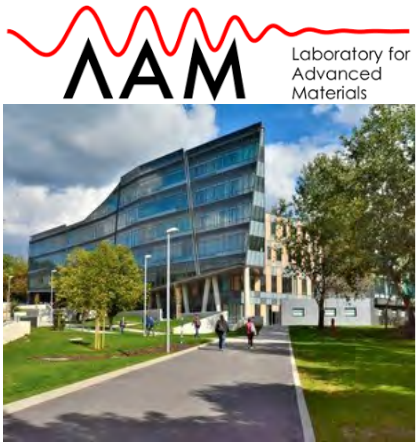

https://fns.uniba.sk/lam/
http://www.lam.sk

Figure 25: Logo, location and websites links for Laboratory for Advanced Materials.

Acknowledgements

The work presented was financially supported by the European Union's Horizon 2020 research and innovation programme under grant agreement No. 810701, Slovak Research and Development Agency under grant agreement No. APVV-19-410 and Slovak Ministry of education under grant agreement No. 1/0892/21.

References

[1] https://wayback.archive-it.org/12090/20220124151655/https://ec.europa.eu/programmes/horizon2020/en/h2020-section/era-chairs

How Can External Mechanical Load Help in EV Battery

M Šedina[a]*, T. Kazda[a]

[a] Department of Electrical and Electronic Technology, Faculty of Electrical Engineering and Communication, Brno University of Technology, Technická 10, 616 00 Brno, Czech Republic
*xsedin00@vut.cz

Abstract
The article briefly describes the background of the electrification of the European car market with the prediction of the sales by power train. There is mention of trends in research of batteries for the automotive sector and high-power applications. The last part is focused on research on how external force can affect batteries and how this can be used in EVs.

Introduction

European show plan called The European Green Deal. The goals are to reduce CO_2 by 55 % by 2030 and from 2050 achieved zero net emissions [1]. These goals will touch all parts of our lives and one of the most transforming is personal transporting (cars, public transport, etc.). Automotive is transforming toward greener ways of power trains as electricity and fuel cells (hydrogen for now), as you can see in Fig.1. Data on Fig.1 could change due to banning cars with internal combustion engines since 2035 in all EU countries.

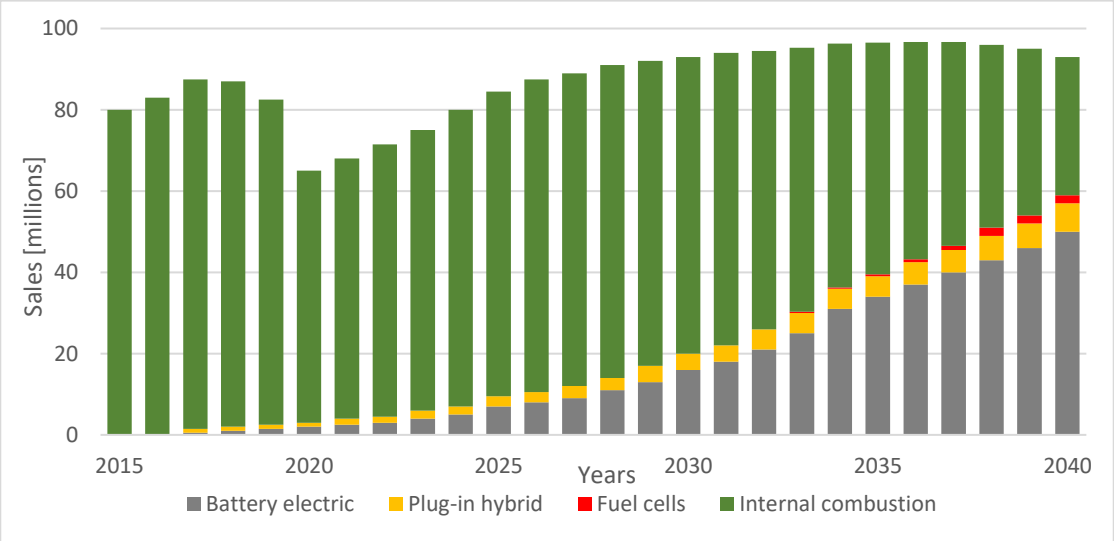

Figure 1: Global annual passenger vehicle sales by drivetrain [2].

This transformation speeds up research in the battery field and automotive companies are trying to offer cheaper, faster, safer, and more powerful batteries. There are several technologies which are in the later stages of development as Li-ion with silicone anode, Li-ion with solid-state electrolyte or Li-S batteries. All these technologies have one common negative behaviour and that is inflation of the battery. In connection with the construction of the battery modules in modern EVs, is possible that there will be some pressure interaction between batteries in a battery module. [3][4]

Experiment

An experiment is focused on measuring batteries under constant mechanical load. As I mentioned above with future battery technologies, there is the possibility of some pressure effect in the battery module. This experiment used batteries from EV Škoda Enyaq. It is an LG Chem E78 battery with a capacity of 78 Ah and it is a pouch cell. The goal of the experiment is how external load affects the battery or if can this load improve battery parameters.

For the moderating force is used clamp with eight springs with a maximal load of 50 kg on each spring (see Fig.2). In the experiment are used loads of 5, 10, and 20 kg were developed on each spring.

At this moment I am using four pouch cells, one is used for uncompressed measurement and one for each force. The battery is compressed during the cycling and measuring electrochemical impedance spectroscopy and then is uncompressed and run the parametric test.

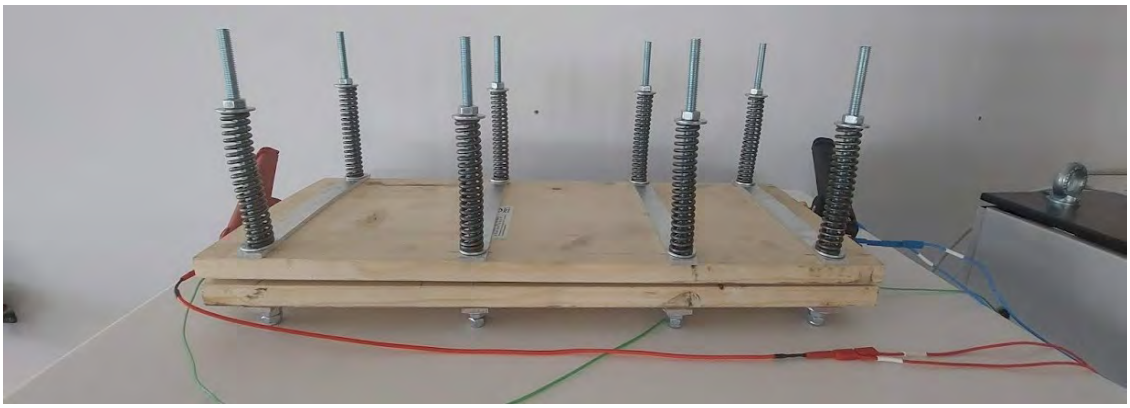

Figure 2: Battery during the measurement drivetrain.

Conclusion

New battery technologies are appearing on the market. These new technologies bring new challenges, such as a larger change in battery volume. It is necessary to find out how these volume changes will affect the functioning of the batteries, for example in automotive, where there is not much space for the batteries to be inflated and external forces will be applied to the batteries.

Acknowledgements

This work was supported by the specific graduate research of the Brno University of Technology No. FEKT-S-20-6206 and EIT Urban Mobility project SEVES (No.22041). This work was supported by Škoda Auto a.s.

References

[1] "Zelená dohoda pro Evropu", Evropská komise, 02019.
[2] Intelligence in Mobile Battery Applications (D5.1 Desk Research & Data Analysis IMBA – Release 1). 2019.
[3] W. Zhang et al., J Mat ChemA, **5** (2017) 9929-9936.
[4] V. Müller et al., J Electrochem Soc, **166** (2019) A3796-A3805.

Preparation, Characterization and Electrochemical Behavior of Ciprofloxacin Modified Polymer Coated Biodegradable Metallic Material

I. Šišoláková[a]*, R. Gorejová[a], K. Özaltin[b], R. Oriňaková[a]

[a] Department of Physical Chemistry, Faculty of Science, P.J. Šafárik University in Košice, Moyzesova 11, 041 01, Košice, Slovak Republic

[b]Centre of Polymer Systems, University Institute, Tomas Bata University in Zlín, Třída Tomáše Bati 5678, 76001 Zlín, Czech Republic

*ivana.sisolakova@upjs.sk

Zinc-based biodegradable metals represent a new group of promising scaffold materials intended for use in bone healing applications [1]. Various methods can be used for their preparation including replication methods, infiltration casting or additive manufacturing, e.g. Due to the low strength of pure zinc, alloying with other metals are commonly employed to enhance its mechanical properties [2]. Moreover, surface modification of zinc alloys may result in improved corrosion and biological performance. Polymeric coatings are commonly used due to their flexibility and ability to be loaded with several biologically active species (anticoagulants, antibiotics, e.g.) [2]. Zinc (Zn) and iron (Fe) powders were used as raw materials for sample preparation. Powders were homogenized in a laboratory mixer for 1 h prior to the next step. Two grams of the mixture were cold-pressed to form green compacts in a form of pellets with a diameter of 12 mm, and with a composition of 98 wt% zinc - 2 wt% iron (Zn-2Fe). Samples were further sintered, and radio frequency air plasma was applied to activate their surface. Two types of polymeric coatings (polyethyleneimine, PEI, 10 wt/v% and poly(lactic acid), PLA, 2.5 wt/v%) were prepared and deposited onto the metallic surface by dip-coating. The second coating composed of antibiotic ciprofloxacin (CPR) loaded fucoidan (FU) (0.1 wt% of CPR) was further applied. Scanning electron microscopy (SEM) and Fourier-transformed Infrared Spectroscopy (FTIR) was employed to study coating morphology and chemical composition. Cyclic voltammetry was used to study the ciprofloxacin electrochemical behaviour in the PBS solution using nickel modified screen-printed electrodes (NiSPEs). Thick PLA layer with the wavy pattern was observed (Fig. 1a) while rather non-homogeneous polymer distribution with visible cracks (Fig. 1b) was found on the PEI-coated samples. Successful polymer and FU/CPR deposition was confirmed by the FT-IR (Fig. 1c). Ciprofloxacin (CPR), chosen as an analyte, was electrochemically determined in the PBS solution simulated human body conditions. Cyclic voltammograms (CV) for various CPR concentrations on NiSPCE are shown in Fig. 1d. Based on obtained CV analytical characteristics of NiSPCE were calculated. The modified carbon electrode displayed a wide linear range from 50 μM to 500 μM, a low limit of detection of 43 μM, and a high sensitivity of 3.71 μA/μM. The above results show the high promise of this electrode for detecting CPR in clinical samples.

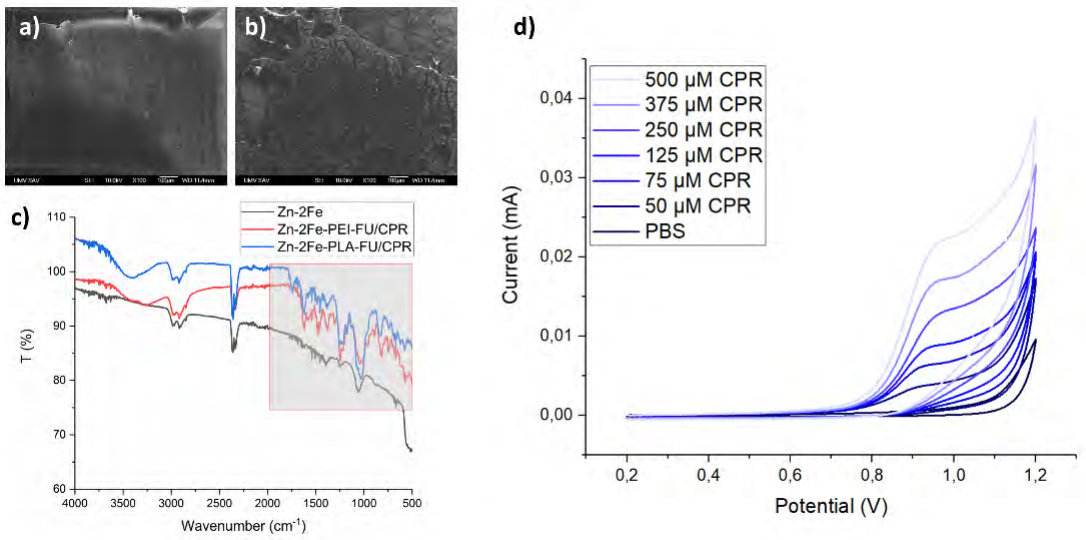

Figure 1: SEM images of Zn-2Fe-PLA-FU/CPR (a) and Zn-2Fe-PEI-FU/CPR (b) surfaces. FTIR spectrum of polymer coated materials modified by the ciprofloxacin (CPR) /fucoidan (FU) (c). Cyclic voltammograms of ciprofloxacin on NiSPCE determined in the PBS solution (d).

Acknowledgments
This work was supported by the Slovak Research and Development Agency (project no. APVV-20-0278).

References

[1] G. K. Levy, J. Goldman, E. Aghion. Metals. **7(10)** (2017) 402.
[2] H. Yang et al. Nat. Commun. **11(1)** (2020) 1-16.
[3] R. Oriňaková et al. Coatings. **10(9)** (2020) 819.

Novel synthesis approach for the preparation of chalcogenide Perovskites

S.K. Tiwari[a], R. Bystrický [a,b], P. Hutár [a,c], M. Sykora[a]*

[a]Laboratory for Advanced Materials, Faculty of Natural Sciences, Comenius University, Ilkovičova 6, 842 15 Bratislava, Slovakia,

[b]Institute of Inorganic Chemistry, Slovak Academy of Sciences, Dúbravská cesta 9, 845 36 Bratislava, Slovakia,

[c]Institute of Electrical Engineering, Slovak Academy of Sciences, Dúbravská cesta 9, 841 04 Bratislava, Slovakia

*sykoram@uniba.sk

Introduction

Organic-inorganic hybrid perovskites (OIHPs) have attracted significant interests in recent years primarily due to their extraordinary performance as active components of solar cells, rapidly reaching and even exceeding the performance of much more mature Crystalline-Silicon technologies [1]. Although OIHPs have excellent photophysical properties and impressive performance in devices, they suffer from poor ambient stability, rapidly degrading in the presence of Oxygen, humidity, or high temperature. Therefore, there is a great deal of interest in identifying alternative chemically and thermally stable materials with optical and electrical properties similar to the OIHPs. One group of materials that has been recently suggested as a promising alternative are chalcogenide perovskites (CPs), crystaline materials with composition ABX_3, where A, B are cations and X = S, Se [2]. CPs offer number of important advantages, as they can be prepared from non-toxic and abundant elements. Many recent computational studies suggest that CPs are likely to have similar or even more appealing electronic properties for application in Photovoltaics (PV) than OIHPs [3].

CPs are structurally related to previously extensively studied oxide perovskites with general formula ABO_3 (Figure 1). While these materials are known for their good thermal and chemical stability and methods for preparation of oxide PSs are available in literature, these materials are not suitable for application in PV because of their large bandgaps, typically extending to UV portion of the solar spectrum. The larger energy differences between the transition metal d-orbital conduction band and O2p orbital valance band typically leads for larger bandgaps. By replacing Oxygen from ABO_3 with S, Se we can move the valance band composed of mainly chalcogen (S, Se) 3p or 4p orbital higher and decrease the bandgap to visible-NIR range. CPs are theoretically predicted to retain many of the chemical properties of oxides, but at the same time have narrower electronic bandgap suitable for application in PVs and possess many appealing properties of OIHPs (Fig. 1b).

One of the main barriers to studies and development of CP applications is the lack of convenient, reliable and commercially appealing methods for preparation of pure CPs. The known methods are based on high-temperature (>1000 °C) solid-state syntheses. Synthesis techniques based on sulfurization of oxide precursors with CS_2, H_2S requires use of toxic and highly flammable gases, which decompose at high reaction temperatures, often yielding contaminated products. Synthesis by using highly reactive precursors like elements and binary sulfides also often yield contaminated products, because of the high susceptibility of the starting materials to oxidation.

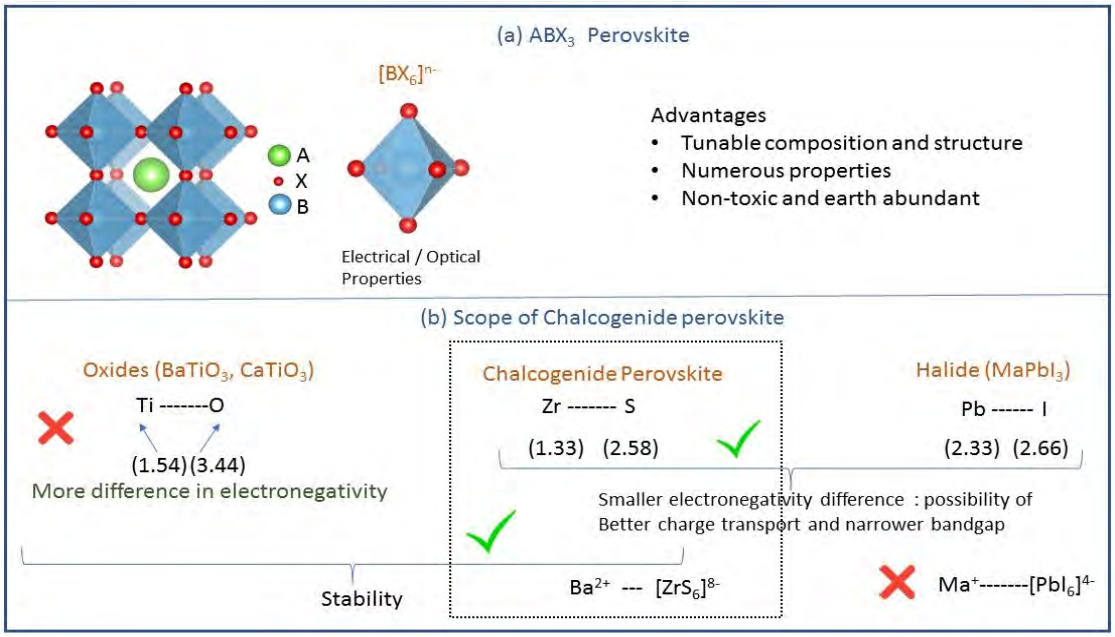

Figure 1: (a) Structure of a PS. (b) Schematic comparison of the properties of oxide, halide and chalcogenide PSs.

Results

In this work we developed a new method for preparation of sulfide CP's by solid state reaction of stable ternary oxides with boron and sulfur (Fig. 2). By this approach we can prepare the samples in ambient condition which is more convenient and reliable. The starting precursors are stable so that they do not need to be stored in inert conditions. In a typical reaction, ternary oxide was taken as a staring precursor and mixed with stoichiometric amount of sulfur and boron (10% molar excess) sealed under vacuum ($<10^{-2}$ mbar) in a quartz tube. The ampules are then heated in a high-temperature furnace up to 1000 °C for ≤36 h for full conversion into sulfide CP's. The high effectivity of gaseous boron sulfides as sulfurizing agents for oxides is, in part due to a large difference in the thermodynamic stability of the byproduct B_2O_3 ($\Delta G_f^{\circ,298}$= -1192.3 kJ/mol) and B_2S_3 ($\Delta G_f^{\circ\ 298}$= -247.6 kJ/mol) and BS_2 ($\Delta G_f^{\circ,298}$= -120 kJ/mol). Thus, boron sulfides serve not only as a source of sulfur but also as an effective "oxygen" trap. Purification of all synthesized samples were done by sonicating the powders in 20 ml HPLC grade methanol and vacuum filtering by Buchner funnel to wash the byproduct B_2O_3.

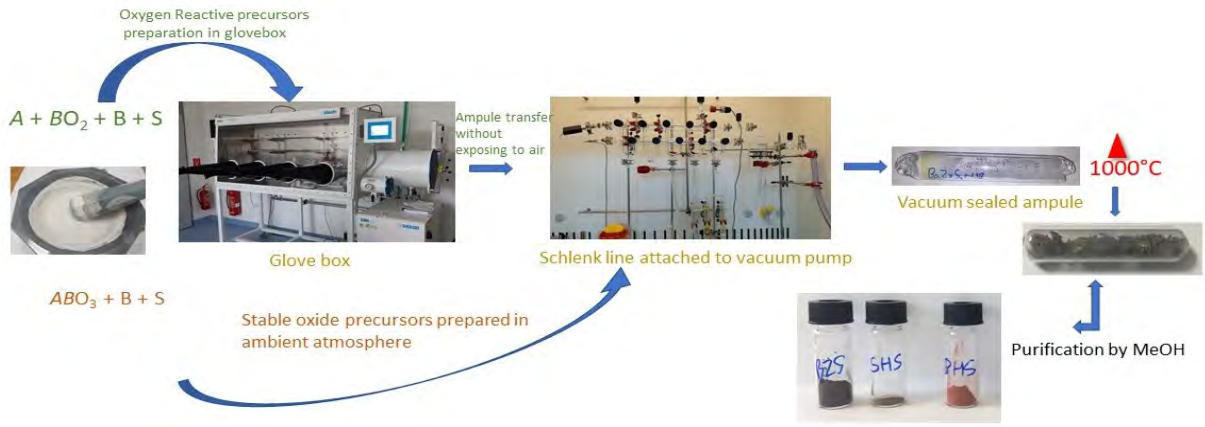

Figure 2: Pictorial representation of how the synthesis approch of CP's starting from ternary oxides (general formula ABO_3 where A = Ba^{2+}, Sr^{2+} and B = Zr^{+4}, Hf^{+4}). Letters B and S represent elemental Boron and Sulfur.

The as-synthesized materials $BaZrS_3$, β-$SrZrS_3$, $BaHfS_3$, $SrHfS_3$ were characterized by X-ray diffraction. The results show that all materials contain pure single phase of $GdFeO_3$ structure validating the formation of CP's. The product lattice parameters were in good agreement with the literature values, indicating the formation of pure phases. The shape of the diffraction peaks and flat background indicate good crystallinity of the products.

Acknowledgements

This work was supported by the European Union's Horizon 2020 research and innovation programme under grant agreement no. 810701 and by the Slovak Research and Development Agency under grant agreement no. APVV-19-410.

References

[1] A. Kojima, K. Teshima, Y. Shirai and T. Miyasaka J. Am. Chem. Soc **1** (2009) 6050.
[2] V. Pecunia, L. G. Occhipinti, A. Chakraborty, Y. Pan, Y Peng. APL Mater. **8** (2020) 10091.
[3] P. Basera, S. Bhattacharya J. Phys. Chem. Lett. (2022) 6439–6446.

Nanocarriers as Drug Delivery Systems

V. Závišová[a]*, M. Kubovčíková[a], I. Antal[a], I. Khara[a], A. Juríková[a], R. Sobotová[a,b], M. Koneracká[a]

[a] Institute of Experimental Physics, Slovak Academy of Sciences, Watsonova 47, 040 01 Košice, Slovakia
[b] Faculty of Materials, Metallurgy and Recycling of the Technical University of Košice, Letná 9, Slovakia
*zavisova@saske.sk

Nanocarriers, colloidal drug carrier systems, showed great promise in the area of drug delivery. The overall goal of utilizing nanocarriers in drug delivery is to treat a disease effectively with minimum side effects [1]. Nanocarriers, owing to their high surface area to volume ratio, have the ability to alter basic properties and bioactivity of drugs. Improved pharmacokinetics and biodistribution, decreased toxicities, improved solubility and stability, controlled release and site-specific delivery of therapeutic agents are some of the features that nanocarriers can incorporate in drug delivery systems [1,2]. Moreover, the physiochemical properties of nanocarriers can be tuned by altering their compositions, sizes, shapes and surface properties. Surface properties i. e. surface charge and functional groups are mainly influenced by compound used for nanoparticles coating.

In the present study, three types of drug immobilization are described. The first type is drug conjugation via physical adsorption, the second one is covalent binding and the third one is polymer entrapment. The immobilization processes are schematically depicted in Fig. 1.

The physical adsorption method is defined as one of the straightforward methods of reversible immobilization that involves the biologically active material being physically adsorbed or attached to the support material. Adsorption can occur through weak non-specific forces such as van der Waals, hydrophobic interactions and hydrogen bonds, whereas in ionic bonding the biologically active material is bound through salt linkages. The reversibly immobilized enzymes can be removed from the support under gentle conditions.

The covalent binding was performed using 1-ethyl-3-(3-dimethylaminopropyl) carbodiimide (EDC). EDC reacts with carboxylic acid groups to form an active O-acylisourea intermediate that is easily displaced by nucleophilic attack from primary amino groups in the reaction mixture. The primary amine forms an amide bond with the original carboxyl group, and an EDC by-product is released as a soluble urea derivative. In our experiment enzyme conjugation was conducted by reaction of the enzyme carboxyl groups with amines via EDC catalysed amidation, when EDC type activation agent was used.

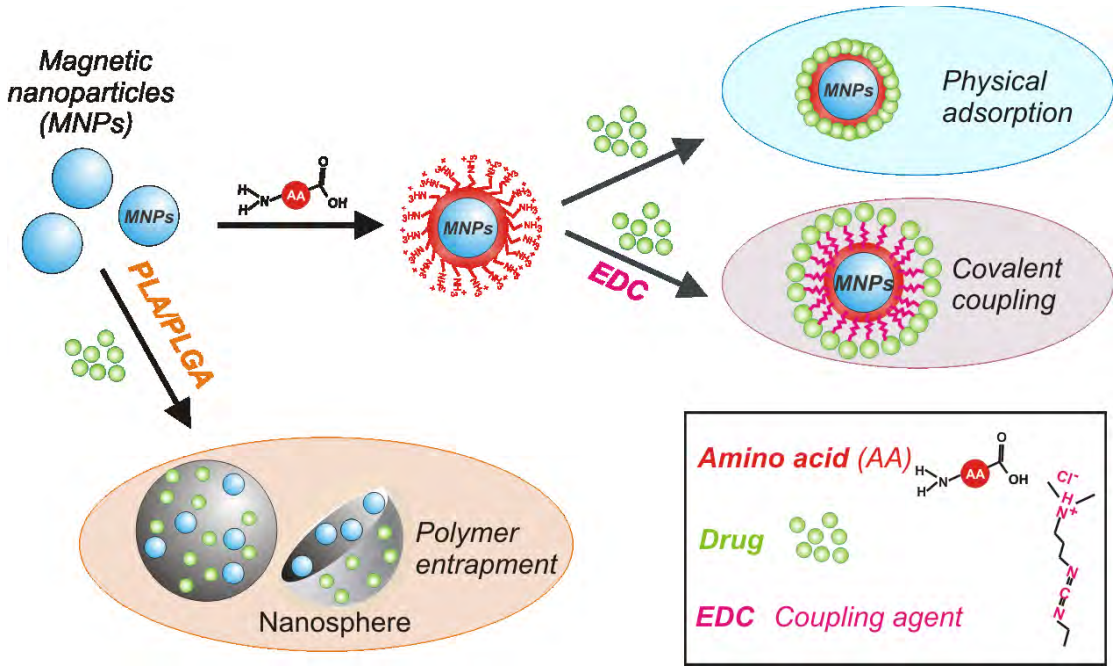

Figure 1: Drug immobiliation processes.

The polymer entrapment was used as the next immobilization technique to entrap drugs in a biodegradable polymer matrix e.g. polylactic acid (PLA), poly(D,L-lactide-*co*-glycolide) (PLGA). In recent years, biodegradable polymeric nanoparticles have attracted considerable attention because of their ability to avoid being quickly taken up by the reticuloendothelial system, prolonged circulation time in the blood, target drugs to specific sites and reduce side effects. Both mentioned polymers are routinely used in medicine as the main component of biodegradable screws and nails for bone fixation or absorbable fibres. Monomers of lactic and glycolic acids are non-toxic and are incorporated into biocompatible metabolic (glycolytic) pathways. So far we have immobilized *Taxol* - anticancer drug [3], *Indometacine* – antiinflammatory drug [4], and *Aliskiren* – used for essential (primary) hypertension [5]. As a model drug for COVID-19 treatment drug *Prednisone* was chosen. *Prednisone* – is in a class of medications called corticosteroids and is used alone or with other medications to treat the symptoms of low corticosteroid levels (lack of certain substances that are usually produced by the body and are needed for normal body functioning). Prednisone is also used to treat other conditions in patients with normal corticosteroid levels. These conditions include certain types of arthritis; severe allergic reactions; multiple sclerosis (a disease in which the nerves do not function properly); lupus (a disease in which the body attacks many of its own organs); and certain conditions that affect the lungs, skin, eyes, kidneys blood, thyroid, stomach, and intestines. Prednisone is also sometimes used to treat the symptoms of certain types of cancer.

The preparation of polymer nanospheres was optimized, polymer concentration in the organic phase was changed, while the concentration of the other components was kept constant. Furthermore, the surfactant and drug concentration was optimized. The appropriate analytical method (UV spectrophotometry) was used for determination of the drug loading content and entrapment efficiency. According to the results of encapsulation efficiency, the process of preparation of drug loaded MNPs was optimized. By the dynamic light scattering (DLS) method, transmission electron microscopy (Fig. 2a), and scanning electron microscopy (Fig. 2b) were obtained information on the particle and nanosphere size distributions. Nanoparticle and nanosphere surface charge were investigated by zeta potential measurements. Zeta potential served us not only as an indicator of the interaction between nanoparticles and drugs but also provided us with information regarding the stability.

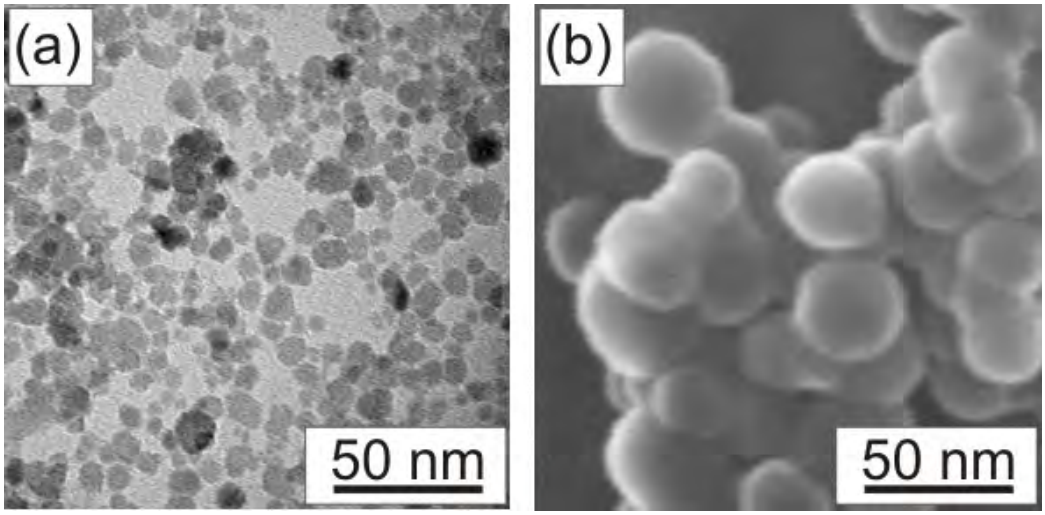

Figure 2: Magnetic nanoparticles coated by amino acid Cysteine observed by Transmisssion electron microscopy (a) and polymer nanospheres with encapsulated drug observed by Scanning electron microscopy (b).

Drug immobilized on nanoparticles has potential for their utilization in drug targeting, magnetic hyperthermia treatment or magnetic resonance imaging. The specific drug immobilization will make the targeted delivery of drug much easier and can guide researchers in the development of new methods for the prevention, diagnosis, and treatment of COVID-19.

Acknowledgements

This work was funded by the Operational Programme Integrated Infrastructure, the project "BIOVID", ITMS: 313011AVG3 co-funded by ERDF. The work was also supported by the Slovak Research and Development Agency under contracts Nos. APVV-14-0120, APVV-SK-SRB-18-0055, APVV-DS-FR-19-0052, by the Slovak Science Grant Agency VEGA - Project No. 2/0033/19.

References

[1] B. Mishra, B.B. Patel, S. Tiwari, Nanomedicine **6** (2010) 1, 9.
[2] C.W. How, A. Rasedee, S. Manickam, R. Rosli. Colloids Surf B Biointerfaces **112** (2013) 393.
[3] V. Závišová, M. Koneracká, M. Múčková, et. al., J. Magn. Magn. Mater. **321**(2009)1613–1616.
[4] V. Zavisova, M. Koneracká, O. Štrbák, et. al., J. Magn. Magn. Mater. **311** (2007) 379–382.
[5] O. Pechanova, A. Barta, M. Koneracka, et al. Molecules **24** (2019) 2710.

Preparation of MoS_2 Nanocrystals by Colloidal Methods Using Nontoxic Precursors

F. Zechel[a], P. Hutár[a,b], A. Haque[a], M. Sýkora[a]*

[a]Laboratory for Advanced Materials, Faculty of Natural Sciences, Comenius University, Ilkovičova 8, 841 04 Bratislava, Slovakia

[b]Institute of Electrical Engineering SAS, Slovak Academy of Sciences, Dúbravská cesta 9, 841 04 Bratislava, Slovakia

*sykoram@uniba.sk

Introduction

Bulk MoS_2 has recently attracted a significant interest because of its unusual electronic, optical, and catalytic properties [1]. The MoS_2 layered crystal structure is composed of trigonal prismatic $\{MoS_6\}$ units forming planes connected by interlayer Van der Waals interactions (Fig. 1.a) [2]. One interesting observation associated with this material is the transition from indirect-bandgap of bulk MoS_2 (Fig. 1.b) to direct-bandgap in a single-monolayer thick MoS_2 (Fig. 1.c) [2]. Preparation of single-monolayer MoS_2 was previously achieved by exfoliation methods or CVD [3]. Size- and thickness-controlled synthesis of MoS_2 nanoplatelets (*NPLs*) was also achieved by chemical methods, mostly based on colloidal synthesis [3,4]. All the approaches reported previously for the colloidal synthesis of MoS_2 *NPLs* utilize toxic chemicals, such as $[Mo(CO)_6]$, or thioacetamide. With the goal to help facilitate preparation and use of MoS_2 *NPLs* in commercial applications we have pursued the development of synthetic procedures for preparation of MoS_2 *NPLs* utilizing less toxic or nontoxic, "green" chemical precursors.

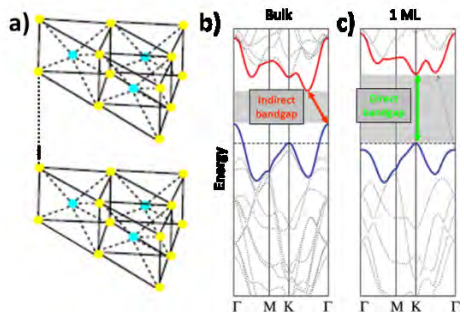

Figure 1: a) Crystal structure of MoS_2 [1]. Band-structure diagrams of: b) bulk c) single-layer MoS_2 [5].

Experimental section

The synthetic approach employed in our work is shown in Fig. 2a. In the scheme OLAM = Oleyl amine, TOPO = Trioctylphosphine-oxide. All reagents were purchased commercially. Oleylamine was used in technical purity (80-90 %). TOPO (99 %) and other reagents reagent grade purity without any purifications. Inert atmosphere was provided by argon (purity 99,999 %). The list of the experimentally investigated Sulphur precursors and their degree of toxicity are summarzied in Fig. 2b. Reactions were carried out in inert argon atmosphere using greaseless Schlenk-line techniques. The reaction temperature was controlled using commercial temperature controller. Small aliquots extracted from reaction mixture at regular time intervals to observe the formation of the nanocrystals (*NCs*). The aliquots were cooled by rapid dilution in hexane and the absorption spectra of the obtained solutions were collected. The reaction products prepared with the tested precursors were purified from the excess of ligands by procedure described previously [3] and subsequently dispersed in hexane. The electronic absorption spectra of the hexane solutions were measured using an Agilent 8453 diode array absorption spectrometer. Electronic emission and Raman spectra were collected using Olympus FV1200 WITec Alpha 300R.

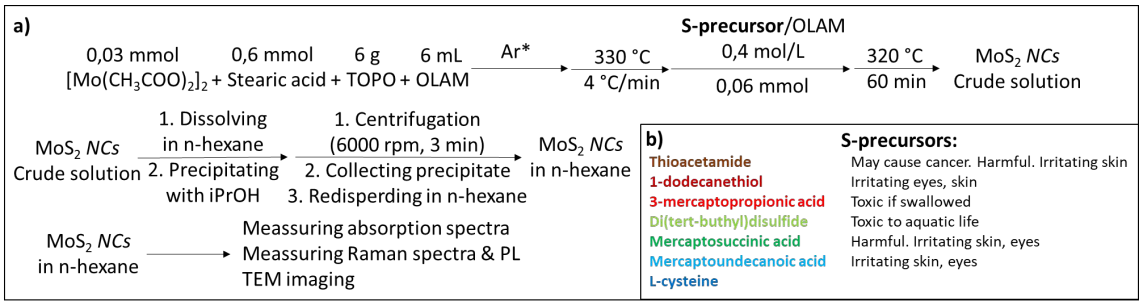

Figure 2: a) Synthetical method. b) Used sulphur sources.

Results

The materials prepared by the new, nontoxic synthetic approach developed here were characterterized by electronic absorption, photoluminescence (PL) and Raman spectroscopies. The results are summarized in Figure 3. Panels "a" and "b" show the comparison of the electronic absorption spectra of MoS_2 *NPLs* reported by Yang *et al.* [3] and those prepared in this work, respectively. Absorption features noted as A (approx. 650 nm) and B (approx. 600 nm) correspond to band edge K-point transitions (see Fig. 1). Strong absorption feature marked as C (approx. at 400 nm) corresponds to the transitions between higher density of state regions [3]. The transitions do not show significant dependence on MoS_2 NCs thickness or lateral size. Accordingly, the electronic absorption spectra generally do not provide information about the size and shape of the NCs, only a confiration that the MoS_2 *NCs* were formed.

The absorption measurements of reaction aliquotes revealed that for certain types of precursors (generally those with short hydrocarbon chain, such as di(tert-buthyl)-disulfide), the formation of MoS_2 *NCs* took place quickly (after 10 minutes), for the other group of precursors (generally those with longer hydrocarbon chain, such as 11-mercaptoundecanoic acid or dodecanethiol) the formation of MoS_2 *NCs* was observed after longer time (above 30 minutes). Electron microscopy and other optical studies are currently in porogress, to more quantitatively classify the sulphur sources accroding to their reactivity.

The synthesized MoS_2 *NCs* were further characterized by Raman and PL spectroscopies. The results of the electronic absorption, Raman and PL characterization of the MoS_2 *NCs* prepared by 3-mercaptopropionic acid as the S-source are summarzied in Fig. 3 c-e. Typical Raman spectra of MoS_2 *NCs* possess two fingerprint phonon modes: out-of-plane vibrations annotated as A_{1g} (at approx. 410 cm^{-1}) and in-plane vibrations annotated as E^1_{2g} (at approx. 380 cm^{-1}) [6]. This is consistent with our observations shown in Fig. 3d.The most direct optical method for prooving the formation of single-layer MoS_2 is photoluminescence (PL). The energy of the PL maximum and the PL intensity are both strongly dependent on the thickness of the MoS_2. With increasing thickness the PL intensity decreases and the PL maximum shifts to lower energy. For the MoS_2 *NCs* with small lateral sizes (from 2,0 nm to 7,0 nm) in lateral-confinement regime, the PL energy is strongly dependent on the lateral size. Correspondingly, the PL peak red-shifts from 430 nm for the smallest MoS_2 *NCs* to 610 nm for the largest MoS_2 *NCs* [8]. In contrast ot this, the PL spectrum of mechanically exfoliated MoS2 *NPLs* possess only one narrow feature at appprox. 650 nm [1]. In the products developed here, we observed PL peak position at approx. 580 nm (Fig. 3d), which suggests the presence of small, single-layer MoS_2 flakes, with lateral sizes in the ~4-6 nm range. The NCs in this size range are also called MoS_2 *quantum dots*. Additional studies of the prepared MoS_2 NCs using TEM imaging and SAXS are currently in progress.

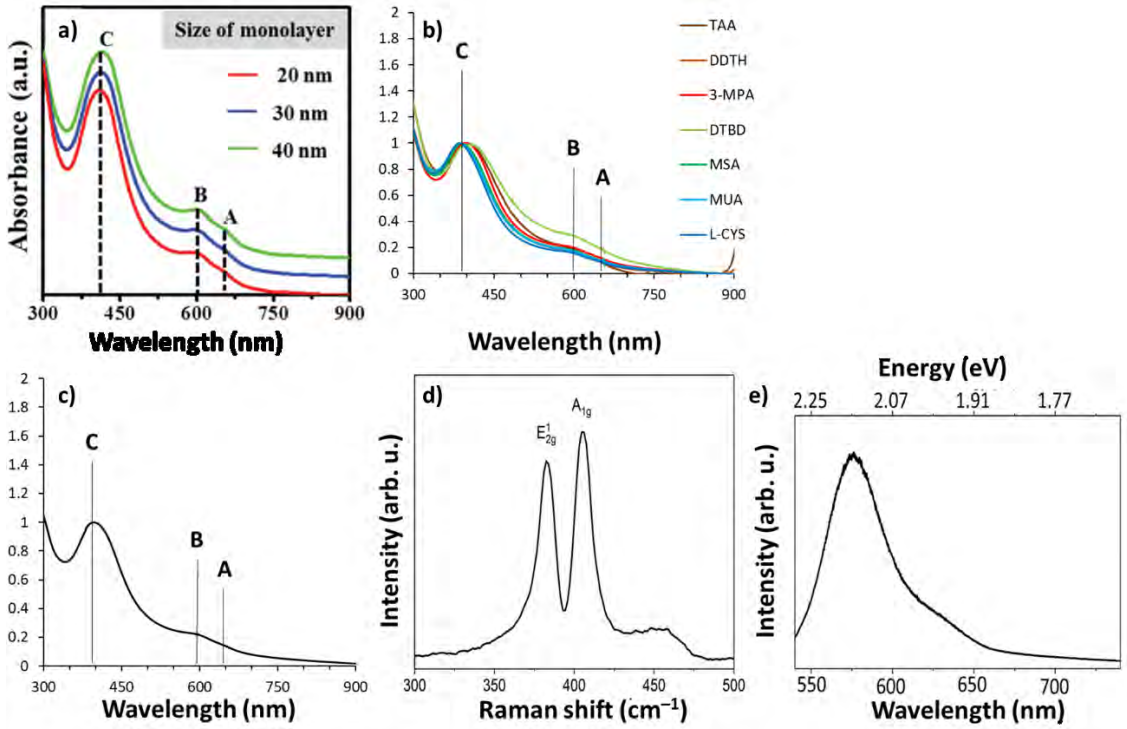

Figure 3: a) Absorption spectrum of MoS_2 *NPLs* from literature [3]. b) Absorption spectra of MoS_2 *NCs* obtained with different S-sources. Optical characterization of MoS_2 *NCs* prepared using 3-mercaptopropionic acid as S-source: c) Absorption spectra. d) Raman spectra. e) Photoluminescence spectra.

Conclusion

Our results show that we have successfully prepared MoS_2 *NCs* using new colloidal synthesis method utilizing low toxicity chemical precursors. The initial optical characterization shows features characteristic of single-layer thick MoS_2 nanocrystals. Further studies aimed on the determination of the exact lateral sizes of the prpared NCs are currently in progress.

Acknowledgements

This work was supported by the European Union's Horizon 2020 research and innovation programme under grant agreement No. 810701 and by the Slovak Research and Development Agency under grant agreement No. APVV-19-0410 and the Slovak Ministry of Education Grant. No. VEGA 1/0892/21 and by UK grant No. UK/266/2022.

References

[1] K. F. Mak, C. Lee, J. Hone, J. Shan, T. F. Heinz. Phys. Rev. Lett. **105** (2010) 136805-136808.
[1] P. Miró, M. Audiffred, T. Heine. Chem. Soc. Rev. **43** (2014) 6537-6554.
[1] M. Zhou, Z. Zhang, K. Huang, Z. Shi, R. Xie, W. Yang. Nanoscale. **8** (2016) 15262-15272.
[1] K.-N. Lee, D. Y. Park, G. Choi, D. A. Nguyen, Y. C. Choi, M. S. Jeong. ACS Appl. Mater. Interfaces. **12** (2020) 35716-35724.
[1] A. Splendiani, L. Sun, Y. Zhang, T. Li, J. Kim, C.-Y. Chim, G. Galli, F. Wang. Nano Lett. **10** (2010) 1271-1275.
[1] H. Lin, C. Wang, J. Wu, Z. Xu, Y. Huang, C. Zhang. New J. Chem. **39** (2015) 8492-8497.

Reactor for studies of photocatalytic activity of quantum-confined nanocrystals

D. Zinoviev[a], M. Sýkora[a*]

[a]Laboratory for advanced materials, Faculty of Natural Sciences, Comenius University, 842 15 Bratislava, Slovakia
[*]sykoram@uniba.sk

Introduction

Photocatalysis using inorganic quantum-confined nanocrystals (NCs) has over the last decade attracted an increased level of interest [1-3]. One of the important tools for these types of reactions is a suitable photoreactor. Although, many reactor designs have been described in the literature, majority of them are economically prohibitive for use in academic laboratories [4]. Because of the longstanding interest of our team in investigation of photocatalysis, we designed and developed a cost effective photoreactor suitable for studies of the photocatalytic activity of quantum-confined inorganic NCs, with the flexibility of providing excitation light at multiple wavelengths. The described design was inspired by the recent report of Weix and co-workers [5].

Results

A photograph of the constructed reactor and the schematic of the electrical circuit are shown in Fig. 1. The reactor consists of three separate parts: power source, cooling system and a set of light source units. The main advantages of the design are its low cost and flexibility. As the light source units, we use 4-8 LED crystals attached to passive cooling radiators. Each light source unit can be easily disconnected, and a unit with different wavelength can be used with the same power source and cooling system. Also, the reactor can be easily modified to simultaneously use light sources with two or more wavelengths. In the presented design, the LEDs with four different excitation wavelengths are available: 400, 450, 530 nanometers and simulated sunlight 5700K. The design also allows for the use of UV light source with quartz glass cuvettes. The standard reactor volume is 4x 3mL, but larger reaction volumes are possible.

In the evaluation of the performance of the reactor, temperature measurements were done in various configurations of the cooling system. Tests were performed with and without thermal paste, active cooling, radiators on LEDs and extra radiators under the emissive part. During the experiments the temperature of water in vial was monitored for period of 15 minutes of irradiation. The control samples were measured after 15 minutes and for 1 hour, giving consistent results. Best configuration included passive radiators on LED crystals, high performance processor thermal paste and PC 140mm fan above the emissive component. The power source consists of transformer, on/off indicator, grounding, and several connectors for safety reasons and easy connection to the light sources and electrical outlet.

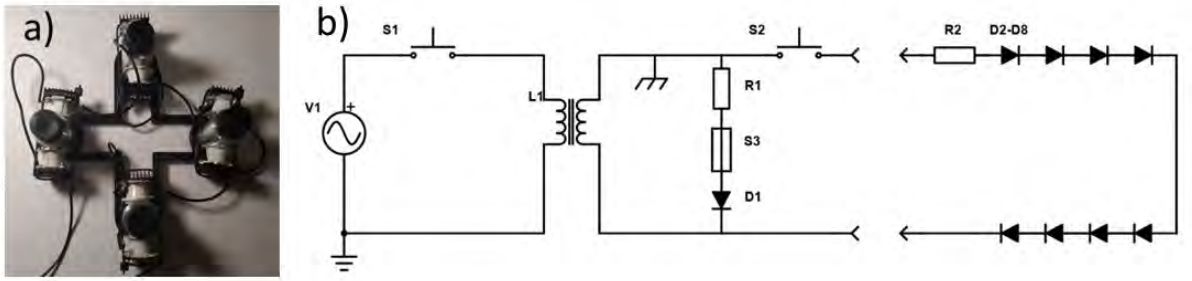

Figure 1: (a) Photograph of the assembled photoreactor; (b) Scheme of the electrical circuit including the power source and light emitting diodes.

Conclusions

We have constructed and tested a simple and economic photoreactor for studies of catalytic reactions with monochromatic and polychromatic light sources.

Acknowledgements
This work was supported by the European Union's Horizon 2020 research and innovation programme under grant agreement No. 810701 and by the Slovak Research and Development Agency under grant agreement No. APVV-19-0410 and the Slovak Ministry of Education Grant. No. VEGA 1/0892/21.

References
[1] H. De Lasa, B. Serrano, M. Salaices, *The Energy Efficiency Factors in Photocatalytic Processes;* in *Photocatalytic Reaction Engineering*. Springer New York, New York, 119-131.
[2] F. E. Osterloh, Chem. Soc. Rev. **42** (2013) 2294-2320.
[3] L. E. Brus, J. Chem. Phys, **80** (1984) 4403-4409.
[4] L. M. Zhao, Q. Y. Meng, X. B. Fan, C. Ye, X. B. Li, B. Chen, V. Ramamurthy, C. H. Tung, L. Z. Wu, Angew. Chem. Int. Ed. **56** (2017) 3020-3024.
[5] J. A. Caputo, L. C. Frenette, N. Zhao, K. L. Sowers, T. D. Krauss, D. J. Weix, J. Am. Chem. Soc. **139** (2017) 4250-4253.

The 6th International Conference on Nanomaterials: Fundamentals and Applications
Book of Abstracts

Edited by: RNDr. Jana Shepa, PhD.

Publisher: Pavol Jozef Šafárik University in Košice
Publishing ŠafárikPress

Year: 2022
Pages: 147
Author's sheets: 8,66
Edition: first

ISBN 978-80-574-0127-8 (e-publication)